SKB

TECHNICAL REPORT 90-40

Distinct element modelling of the rock mass response to glaciation at Finnsjön, central Sweden

Lars Rosengren[1], Ove Stephansson[2]

[1] Itasca Geomekanik AB, Falun, Sweden
[2] Division of Rock Mechanics, Luleå University of Technology, Luleå, Sweden

December 1990

SVENSK KÄRNBRÄNSLEHANTERING AB
SWEDISH NUCLEAR FUEL AND WASTE MANAGEMENT CO

BOX 5864 S-102 48 STOCKHOLM

TEL 08-665 28 00 TELEX 13108 SKB S
TELEFAX 08-661 57 19

DISTINCT ELEMENT MODELLING OF THE ROCK MASS RESPONSE TO GLACIATION AT FINNSJÖN, CENTRAL SWEDEN

Lars Rosengren[1], Ove Stephansson[2]

1 Itasca Geomekanik AB, Falun, Sweden
2 Division of Rock Mechanics, Luleå University of Technology, Luleå, Sweden

December 1990

DISTINCT ELEMENT MODELLING OF THE ROCK MASS RESPONSE TO GLACIATION AT FINNSJÖN, CENTRAL SWEDEN

Lars Rosengren
Itasca Geomekanik AB
Falun, Sweden

Ove Stephansson
Division of Rock Mechanics
Luleå University of Technology
Luleå, Sweden

December 1990

SUMMARY

Six rock mechanics models of a cross section of the Finnsjön test site have been simulated by means of distinct element analysis and the computer code UDEC. The rock mass response to glaciation, deglaciation, isostatic movements and water pressure from an ice lake have been simulated.

Four of the models (Model 1-4) use a boundary condition with boundary elements at the bottom and sides of the model. This gives a state of stress inside the model which agrees well with the analytical solution where the horizontal and vertical stresses are almost similar. Roller boundaries were applied to two models (Model 5 and 6). This boundary condition cause zero lateral displacement at the model boundaries and the horizontal stress are always less than the vertical stress. Isostatic movements were simulated in one model (Model 5).

Two different geometries of fracture Zone 2 were simulated. Results from modelling the two different geometries show minor changes in stresses, displacements and failure of fracture zones.

Under normal pore pressure conditions in the rock mass the weight of the ice load increases the vertical stress in proportion to the thickness of the ice sheet. The horizontal stresses in the models differ depending on the boundary condition. An ice thickness of 3 km and 1 km and an ice wedge of 1 km thickness covering half the top surface of the model have been simulated. For each loading sequence of the six models a complete set of data about normal stress, stress profiles along selected sections, displacements and failure of fracture zones are presented.

Major stress discontinuities exist in the vicinity of the fracture zones and fracture Zone 2 in particular. When the pore pressure from an ice lake is simulated in the models the effective stresses acting in the models tend to make the stress state more isotropic and the stress discontinuities of the fracture zones diminish.

The strength of the fracture zones are evaluated based on the Coulomb slip criterion. Models with boundary elements (Model 1-4) showed minor failure along the steeply dipping fracture zones.

Simulation of isostatic movements in combination with ice loading and melting gave several interesting results. Stress discontinuities and large displacements appear at the major fracture zones. Major changes in failure appear when ice thickness is reduced. Fracture Zone 2 fails and other failures are located to the uppermost ~1000 m of the crust.

Based on the results of this study a protection zone of ~100 m width from the outer boundary of stress discontinuity to the repository location is suggested. This value is based on the result that the stress disturbance diminishes at this distance from the outer boundary of the discontinuity. Further, a repository located between the steeply dipping fracture Zones 1, 14 and 5 should be located below fracture Zone 2 at a depth of about 600-650 m. This value will be less (i.e. 500-550 m) if the interpretation of a horizontal fracture Zone 2 is accepted.

TABLE OF CONTENTS

1 INTRODUCTION

An understanding of the stability of the bedrock of Fennoscandia is of utmost importance to existing ideas about final storage of spent nuclear fuel in granitic rocks. The problem of longterm stability of the crust with special emphasis on waste isolation has been addressed in the research plan of the Swedish Nuclear Fuel and Waste Management Company (1986) for the time period 1987-1992. As a part of the research program, long term rock stability modelling of the response of rock masses to external loads from earthquakes, glaciation and glacial rebound have been conducted, Stephansson (1987), and Stephansson and Shen (1990). The neotectonics at Lansjärv, Northern Sweden with clear evidences of late-glacial movements have been studied in detail, Bäckblom and Stanfors (1990). Although the results are specific for Northern Fennoscandia they are of major importance for the understanding of possible rock deformation in the crust in conjunction with future deglaciations.

As an integrated study of the ongoing program for research and development within SKB an integrated safety analysis called SKB-91 will be conducted, Swedish Nuclear Fuel and Waste Management Company (1989). The analysis will pay specific attention to the glaciation scenario and related phenomena. Therefore, SKB of Sweden and TVO of Finland in co-operation have initiated studies of the World's ice ages and changing environments and their importance for future glaciations in Fennoscandia, Eronen and Olander (1990) and Björk (written communication). The integrated safety analysis of SKB-91 will be applied to the Finnsjön site of Central Sweden. The objective of the study reported here is to illustrate quantitatively possible rock mass deformations due to glaciation with special emphasis on a future repository located at Finnsjön.

In modelling the curstal rock mechanics of a vault subjected to glaciation and deglaciation one must know the geometric structure and geomechanical properties of large rock masses and the boundary conditions which might be applied to the models. In Chapter 2 the glaciological aspects of waste disposal in Fennoscandia are presented and the modelling sequences and the related glaciological phenomena are discussed. Chapter 3 gives a description of the Finnsjön site and the assumptions about its geomechanics properties. The numerical modelling method using distinct elements to simulate the rock mass response is presented in Chapter 4. The modelling approach and the sequences of ice loading, unloading with the effect of different pore pressure assumptions in the fracture zones are described in Chapter 5. Results of modelling are presented in Chapter 6. A discussion of the results are presented in Chapter 7 and the conclusions are drawn in Chapter 8.

2 STRATEGY OF MODELLING GLACIOLOGICAL ASPECTS OF VAULT STABILITY IN FENNOSCANDIA

It is recognized that the location of a nuclear waste vault in the Fenno-scandian bedrock will be affected by large ice sheets in the future. A proper crustal rock mechanics model should treat this problem on a global scale assuming the rigid crust supported by the visco-elastic sub-stratum of the earth's mantle. Dealing with the stability and integrity of a restricted waste disposal area located less than one kilometer deep down in the crust, the time-dependent properties of the crust and mantle can be omitted. This does not mean that the crust is not sub-jected to visco-elastic deformations. However, the limited size of the area under study, 2.5 by 2.5 km in plan and 2 km in depth in the case of Finnsjön, means that the crust can be treated as a non-linear elastic material where the stability is governed by the strength of the fracture zones.

Problems concerning vault integrity under a thick ice sheet have been discussed by Koerner (1984), and Stephansson (1987), and these are as follows:

(i) Erosion of the vault roof by the ice sheet

(ii) Increased availability of water and increased water pressure under the ice sheet

(iii) Excess stresses on the rock produced by the weight of the overlying ice sheet

(iv) Stress relief during deglaciation and cyclic opening and closing of fractures due to repeated glaciations and deglaciations

2.1 EROSION UNDER AN ICE SHEET

The general concensus among earth sicentists is that ice sheet flow will produce very little erosion relative to the subairial and fluvial mecha-nisms. In the most recent reviews of the problem Koerner (op. cit.) arrives at an erosion rate of 15 m in 1 Ma. The traditional view of the Finnish geologist is that the resulting erosion of Northern Europe during the latest glaciations was of a few metres, Eronen and Olander (1990). The present conclusion is that glacial erosion does not con-stitute a threat to a repository situated deeper than a couple of hundred metres. The effects of erosion need not therefore be simulated in the numerical modelling of crustal rock mechanics.

2.2 WATER PRESSURE UNDER THE ICE

One of the principal sources of uncertainly in the storage of high-level radioactive waste in the bedrock of Fennoscandia arises from the effects of increased water availability and water pressures associated with large ice sheets. In a review of the literature about present-day ice sheets Eronen and Olander (1990) claim that the ice sheets are of cold-based type and therefore saline groundwater can accumulate beneath it. Koerner (1984) presents evidence that the rock surface will have a

water interface for most of the time when it is covered with an ice sheet. This will result in a development of excess pore-water pressure and the volume of water flow above a repository could be at least 3 to 6 times greater than it is at present for the same depth. The hydrostatic pressure at the interface could be sufficiently high for water to penetrate new or old fractures in the bedrock. It might also be possible that the excess water pressure could cause hydraulic fracturing of the surface bedrock as has been suggested by Muir Wood (1989) among others. The details of the modelling approach are demonstrated in Chapter 5 and the results from modelling the fractures with and without the increase of pore pressure due to an ice lake are presented in Chapter 6.

There is no general agreement on the precise location of the water table within an ice sheet. Vonhof (1984) claims that the ice surface can not be considered equivalent to a zero potential surface. For tempered glaciers it is likely that water can flow through the ice and become coupled with the ordinary groundwater. An elevated ice lake also can be interconnected with the groundwater level at lower attitudes. Finally, there is a general concensus that high water pressures can develop in the ablation zone.

In conclusion, in the simulation of rock mass displacement and stress changes under glacial loading, changes of pore water pressure in the bedrock due to changes in the water table of the ice sheet should be considered and they are considered in this report.

2.3 GLACIALLY INDUCED STRESS AND STRAIN CHANGES

Any increase in thickness that takes place in a major ice sheet will cause depression of the earth's crust beneath it. Given densities of approximately 0.9 tons/m^3 for the ice and 2.7 tons/m^3 for the underlying bedrock, a continental ice sheet 3 km thick could in theory depress the earth's crust by about 1 km (Eronen and Olander, 1990) and deformations of this order have indeed been detected in Fennoscandia.

The extension of the Late Weichselian ice cap during the last glacial maximum, about 18,000 B.P. is given by the heavy line in Figure 2.1. Contours of the total absolute uplift and subsidence in metres are shown in the same figure (Mörner, 1979). Kakkuri (1986) calculates from gravity anomaly data that 100-150 m of uplift still remains at the centre of Fennoscandia before the crust returns to a state of isostatic equilibrium.

In modelling the crustal response to ice loading two assumptions can be made about the bottom boundary of the model. The first assumption is a zero vertical displacement of the bottom edge of the model. Any point along the bottom boundary is allowed to translate laterally. The other boundary condition takes into account the vertical displacements caused by the ice load and the uplift from melting of the ice. The situation for Fennoscandia between two interglacial equilibria is illustrated in Figure 2.2. When the ice sheet starts to grow and reaches its maximum thickness of 3 km during Late Weichselian (18,000 B.P.) the crust will subside about 1 km in the center of Fennoscandia. The shear strain, γ, in the earth's crust is governed by

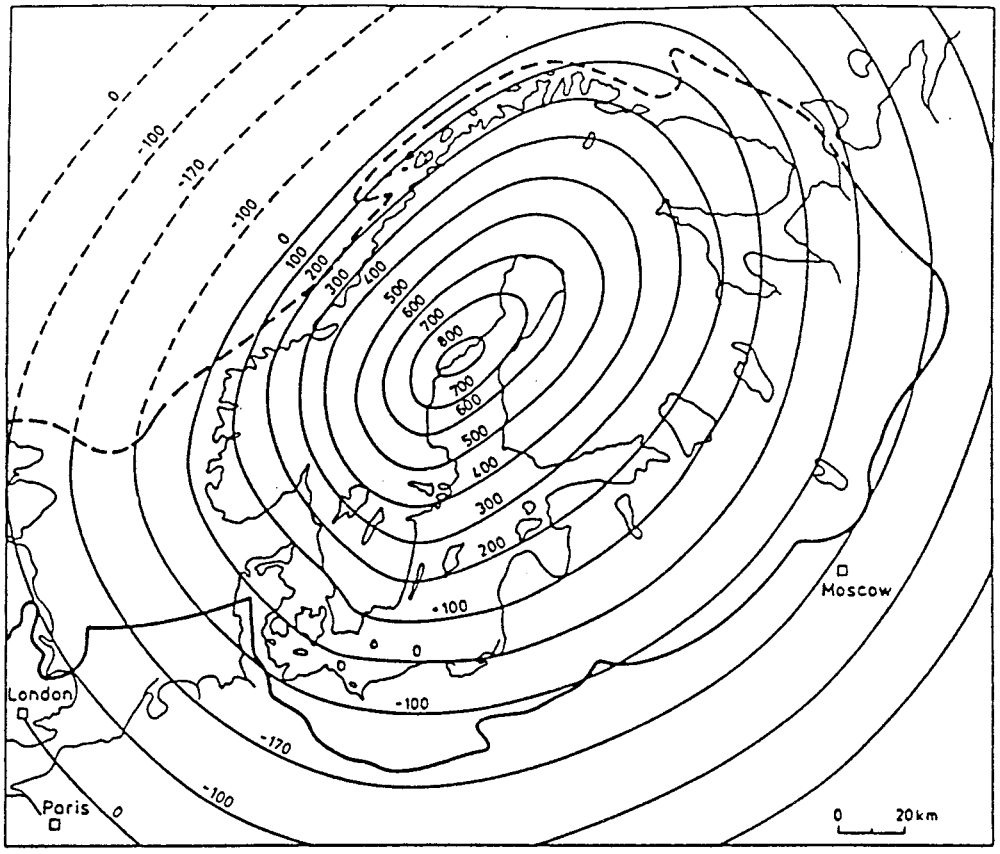

Figure 2.1 Contours of the total absolute uplift in relation to the last glaciation of Fennoscandia and surroundings. The extension of the Late Weichselian ice cap is illustrated by the heavy line. After Mörner (1979).

$$\gamma=\frac{\Delta l}{l}=\frac{1}{1000}=10^{-3} \qquad (2.1)$$

where Δl is the subsidence and l is the redius of the deflection (cf. Figure 2.1). Modelling the response of the bedrock at Finnsjön to a future ice load one has to investigate the effect of the subsidence together with the loading from the weight of the ice sheet. For a numerical model with the length of 2 km the vertical displacement is given by applying eq. (2.1)

$$\Delta l=\gamma\cdot l=10^{-3}\cdot 2=2\cdot 10^{-3}km=2m$$

In the distinct element approach of modelling the rock mass response to glaciation and deglaciation at Finnsjön the two different boundary conditions for strain are investigated. The effects of a moving inflexion point and forebulge as the ice sheet is building up and melting are not condsidered in this study.

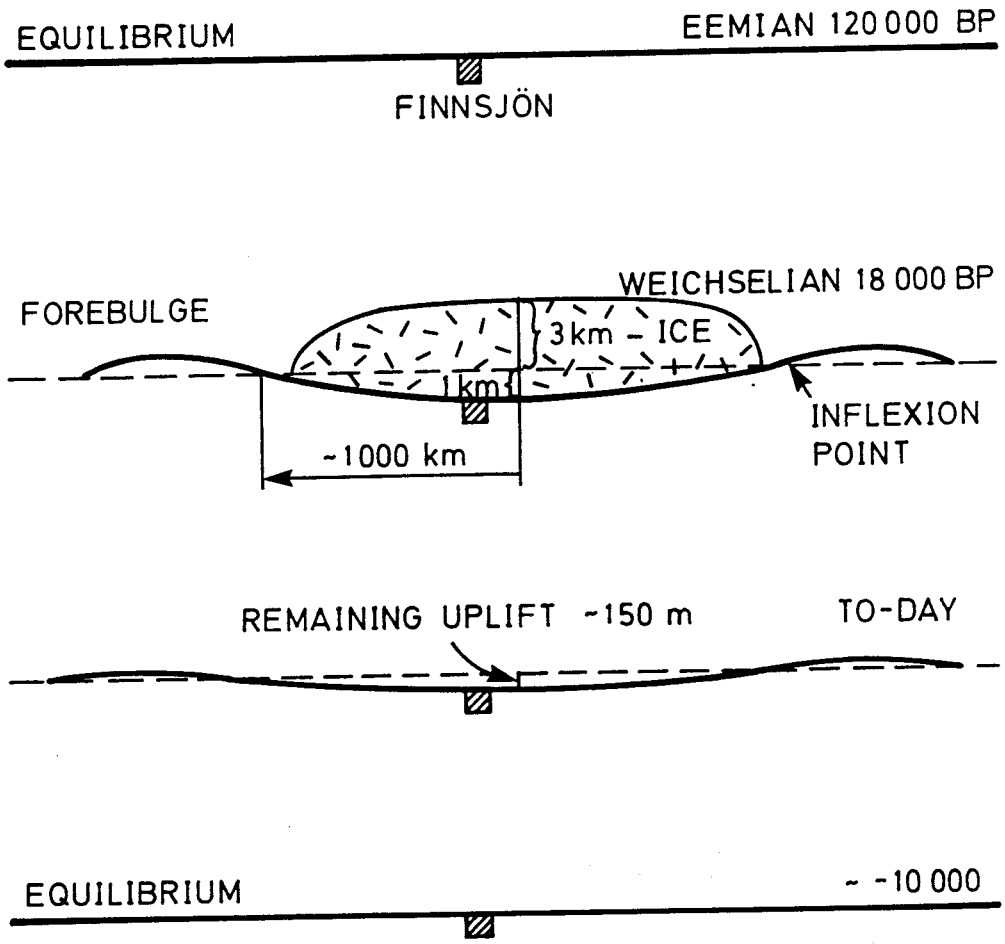

Figure 2.2 Principal vertical crustal deformation in Fennoscandia from Eemian interglacial 120,000 B.P. to the new equilibrium about 10,000 years in the future.

An ice sheet produces differential loads over the earth's crust. By assuming an infinite extension of the ice, roller boundaries and linear elastic properties of the crust the theoretical horizontal stress would increase by an amount $\Delta\sigma_H$ given by

$$\Delta\sigma_H = \frac{\nu}{1-\nu}\Delta\sigma_V \qquad (2.2)$$

where ν is the Poisson's ratio and $\Delta\sigma_V$ is the change in overburden load from the ice sheet defined as

$$\Delta\sigma_V = h\rho g \qquad (2.3)$$

where h is the thickness of the ice sheet, ρ the ice density and g is the gravitational acceleration. Modelling the crustal response to glaciation at Finnsjön a maximum ice thickness of 3 km is assumed. However, it is not obvious that the next ice age estimated to come 23,000 years from now will produce that thick ice sheet but a conservative assumption has been used. Since the melting of the ice takes place much quicker than the building up, it is most likely that the melting can cause instabilities in the crust. Therefore the reduction in loading from melting the ice sheet from 3 km to 2 km has been studied.

Recent studies of the neotectonic fault at Lansjärv, Northern Sweden (Bäckblom and Stanfors, 1990) have demonstrated the late-glacial origin of the reverse fault-scarps. The effect of the very late retreat of the ice will be simulated with a triangular ice wedge loading one half of the surface of the model.

2.4 STRESS CONCENTRATION AT THE ROCK-ICE INTERFACE

Stephansson (1987) has reviewed the theory of glacial sliding and listed thirteen parameters and processes that have been thought to influence glacial sliding. The average shear stress at the base of a glacier has been calculated and experimentally confirmed to be of the order of 0.1 MPa. Jing and Stephansson (1988) included the effect of glacial sliding in their generic models of glacial response of faulted rock masses. Superimposing a simple shear stress at the surface of the bedrock to simulate glacial sliding prooved to give only minor disturbances to the rock mass. Therefore simulation of stress concentrations at the rock-ice interface has been omitted in this study.

3 DESCRIPTION OF THE FINNSJÖN SITE

Generic studies of fracture zone were initiated by SKB to further quantify the safety performance of the geosphere barriers. These studies comprise two main projects, characterization of fracture zones in tunnels, and borehole studies of a specific fracture zone at the Finnsjön site, Central Sweden, Ahlbom and Smellie (1989). The Finnsjön site has now been selected as a test site for the on-going integrated safety analysis - SKB-91. This chapter summarizes the geology, hydrology and rock mechanics of the site with special emphasize on background data for the crustal modelling. The data are to a large extent based on the compilation by Ahlbom and Smellie (op. cit.).

3.1 MAIN CHARACTERISTICS

The Finnsjön site is located in the county of Uppland, Central Sweden, about 140 km north of Stockholm, Figure 3.1. The site has a low relief and flat topography with altitude variations less than 15 m. Finnsjön is located about 15 km east of the coastline of the Baltic Sea. The test area is covered to 85 % by Quaternary sediments, mainly till.

3.2 BEDROCK GEOLOGY

Within the Finnsjön area the predominant rock is a greyish, medium-grained and foliated granodiorite dated to about 1.8 Ga (1800 mil. years); minor amounts of pegmatite, metabasite and aplite also occur. Fracture mapping has revealed an orthogonal fracture system with the following fracture sets

N30°-70°W, subvertical
N30°-70°E, subvertical
N45°W, gently dipping SW

The NW-trending fractures are related to the foliation. Logged fractures in drillcores give an average fracture frequence of ~ 1 fracture/m.

Three sets of fracture zones dominate in Finnsjön, these are:

N30°E, steep dipping
N60°W, steep dipping
N20°W, dipping 10°-20°SW

A generalized map of the fracture zones at the level of the ground surface is presented in Figure 3.2 and the characteristics of each individual zones are given in Table 3.1.

A shallow dipping fracture zone (Zone 2) is defined only from borehole data. It is trending north with a dip of 16 degrees to the SW and is located in an area of approximately 500 m x 500 m in the northern part of the Finnsjön area, Figures 3.1 and 3.2. The fracture is almost planar within this area with the upper boundary located between 100 and 200 m below the ground surface. The zone is interpreted to have a width of about 100 m. Fracture frequency in Zone 2 is on average 5 fractures/m

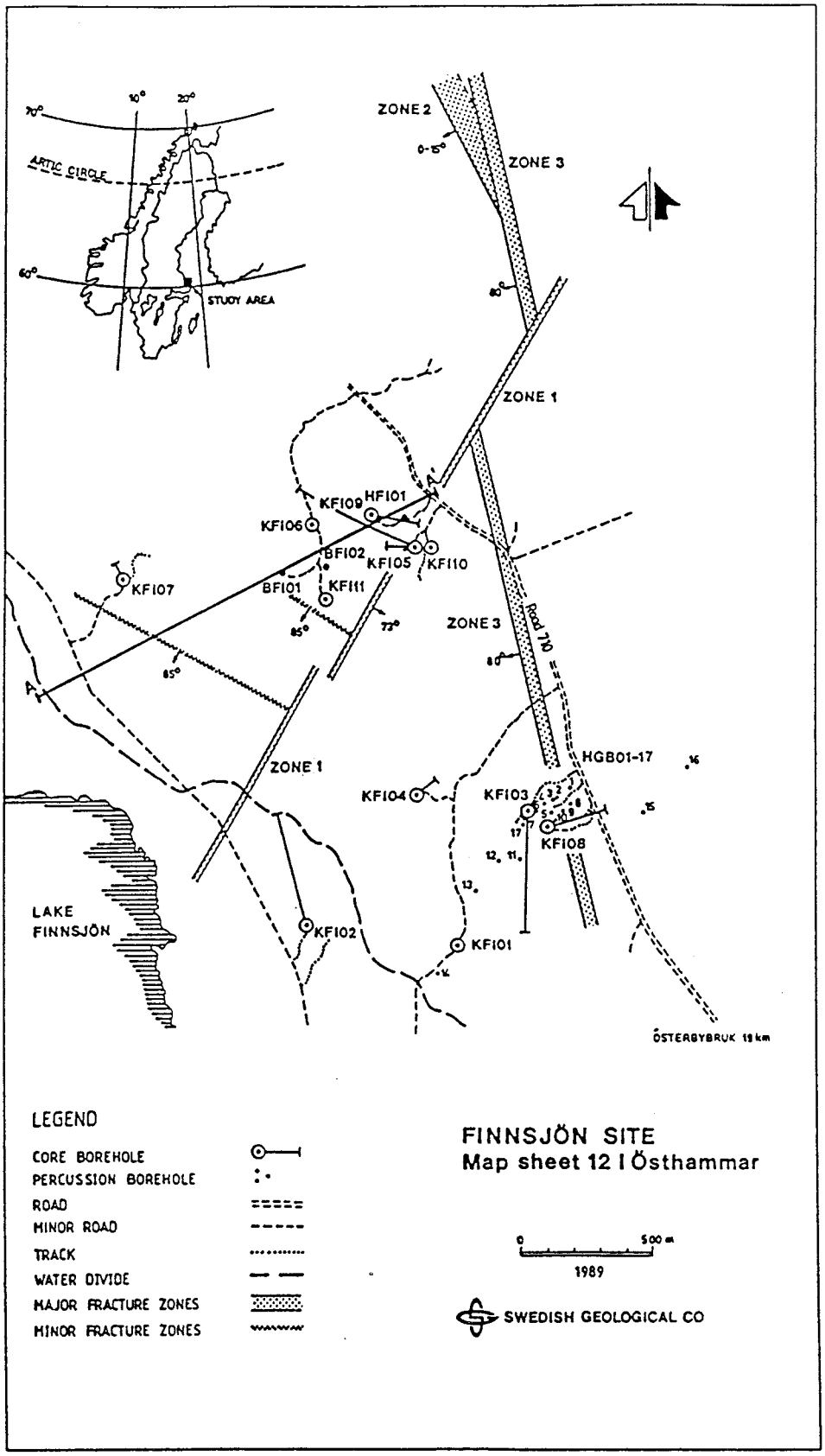

Figure 3.1 Simplified map of the Finnsjön site showing borehole locations and major fracture zones. Section A-A', illustrated in Figure 3.3, is also shown. After Ahlbom and Smellie (1989).

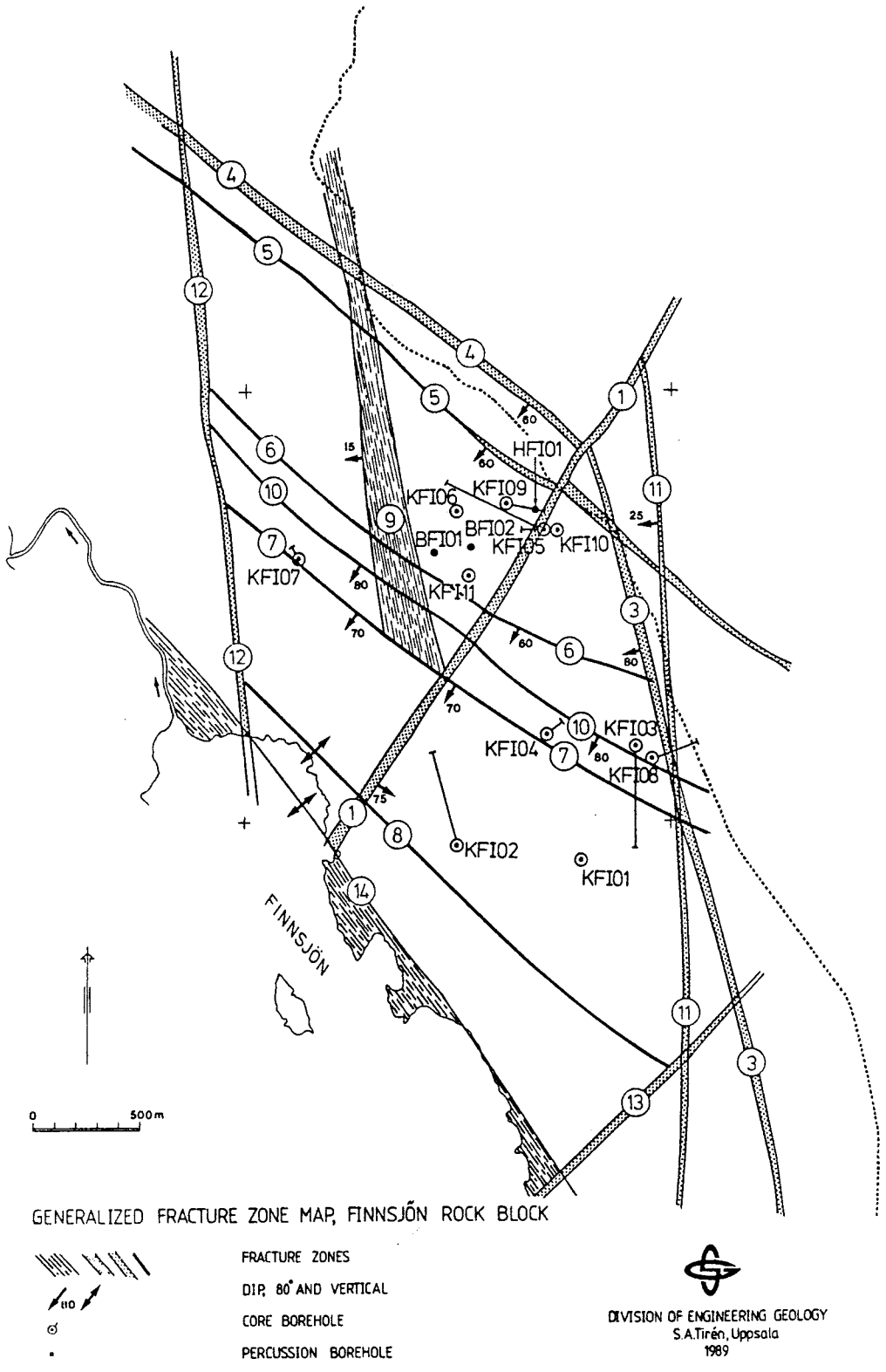

Figure 3.2 Generalized map of fracture zones at the Finnsjön site, ground surface level. After Ahlbom and Tirén (1989).

Table 3.1 Characteristics of fracture zones at Finnsjön site. * After Ahlbom and Smellie (1989).

Zone No.	Orient	Width [m]	Trace length [m]	Fracture frequency range [fr/m]	Remote sensing	Surface mapping	Ground geophysics	Borehole	Borehole radar
1	N30 E/75 SE	20-30	>2 500	20-50	x	x	x		
2	N28 W/16 SW	100-150		<32				Fi 5-7, 10-11, BFi 1-2	Fi 5-7, 10-11, BFi 1-2
3	N26 W/80 W	>25	>3 000		x	x		Fi 8	Fi 8
4	N50 W/80 SW	<20	1 000		x				
5	N60 W/80 SW	<10	800		x				
6	N60 W/80 SW	5	700	0.5-5		x	x	HFi 1	HFi 1
7	N60 W/90		450		x				BFi 1-2
8	N60 W	<10	>900		x	x			
9	N60 W	<10	350		x	x			
10	N60 W/85 S		>1 000		x	x			
11	N60 W		800		x				
12	N30 E/85 NW		400		x	x			BFi 1
13	N23 W/19 S	<5	1 000	<5			x	Fi 6, 11	
14	NS/15 W	<65	>1 600		x	x		Fi 7	
15	NS/15 SW		>1 600		x	x		Fi 7	

* This is an early version of fracture zone characteristics but the numbering differs from data in Figure 3.2.

but sealed fractures with infillings, mostly of hydrothermal origin are numerous. Fractures and their fillings are dated and have ages of 1.6-1.5 Ga.

Major emphasis have been made to characterize the geology and hydrology of fracture Zone 2 cf. Ahlbom and Smellie (1989). The most likely model of a transverse section A-A' in a NE-SW direction over the Finnsjön site is depicted in Figure 3.3. Here Zone 2 has an off-set at the deepest part in the SW corner of the area. However, there are indications that Zone 2 might be continuous forming a planar zone over a part of the Finnsjön area. Therefore it was decided to study two different numerical models of the cross section A-A in Figure 3.3. The geometry of the two models is presented in Chapter 5. A detailed description of the other fracture zones is presented by Ahlbom and Tirén (1989).

3.3 HYDRAULICS AND GROUNDWATER FLOW

A great number of hydraulic tests have been made to characterize the hydraulics and groundwater flow of the Finnsjön site and Zone 2 in particular, Ahlbom and Smellie (1989).

Single-hole injection tests showed a general decrease in hydraulic conductivity with depth including the bedrock above Zone 2. The uppermost boundary of Zone 2 proved to be highly conductive. Towards the bottom of the zone several alternating thin intervals of very high hydraulic conductivity exist while the conductivity is in general low below the zone. In summary fracture Zone 2 can be charcterized as a large-

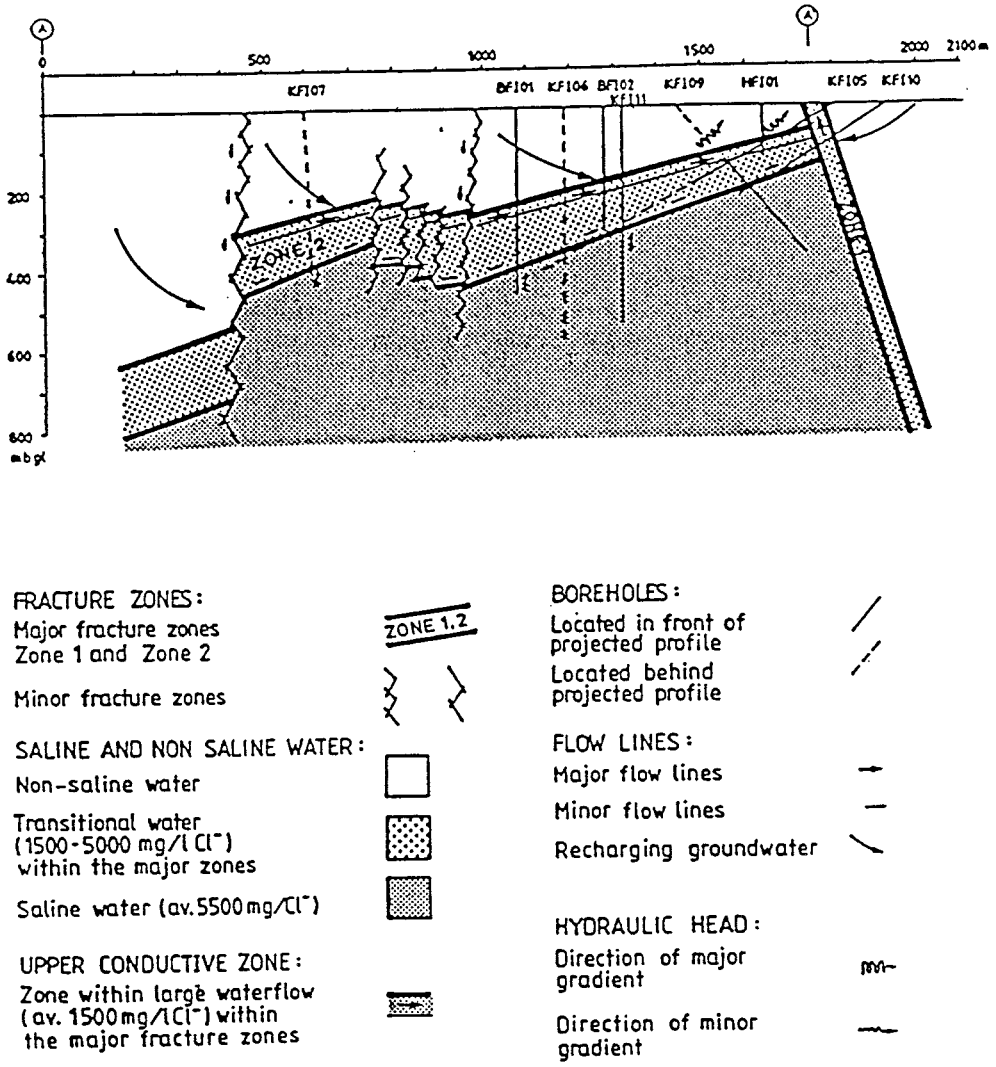

Figure 3.3 Transverse hydrogeological section (A-A') showing a tentative model of groundwater flow during unperturbed conditions. Location of section A-A' is shown in Figure 3.1. After Ahlbom and Smellie (1989).

scale, uniform, and open low angle fracture zone of much greater dimensions and hydraulic potential than could have originally been envisaged.

In support of the hydraulic conductivity values tracer tests and groundwater flow measurements both show a large and rapid movement of groundwater along the upper boundary of Zone 2. Below this boundary measurements indicate more or less stagnant groundwater conditions with old relict saline water at depth, cf. Figure 3.3. The upper boundary of Zone 2 therefore act as an efficient structural/hydraulic boundary to the groundwater flow. In modelling the mechanical response of the fracture zones we are primarily interested in the pore pressure influence on the effective stresses in joints rather than the actual flow rates. Therefore, assumptions were made regarding the steady state pore pressure distribution in the models for each loading step.

3.4 STRESS MEASUREMENTS

Hydraulic fracturing stress measurements have been conducted in the vertical borehole KFI06 (see Figure 3.2) at the eastern part of the extension of fracture Zone 2, Finnsjön study site, Bjarnason and Stephansson (1988). Stress measurements were attempted at 40 different depths in the borehole of which 26 were used for the stress determination.

The maximum horizontal stress, S_H, is larger in magnitude than the estimated vertical stress, S_V, at all depths. The results indicate a stress field with thrust fault conditions ($S_V < S_h < S_H$) from surface down to 500 m. The stress magnitudes at Finnsjön are in general agreement with other stress data of Fennoscandia as recorded in the Fennoscandian Rock Stress Data Base, Stephansson et al. (1986). Regression analysis of stress magnitudes versus depth give:

$$S_V = 0.0265\, z \quad [\text{MPa}] \quad \text{(estimated)} \tag{3.1}$$

$$S_h = 2.6 + 0.0237\, z \quad [\text{MPa}] \quad r = 0.92 \tag{3.2}$$

$$S_{HI} = 6.2 + 0.0416\, z \quad [\text{MPa}] \quad r = 0.85 \tag{3.3}$$

$$S_{HII} = 2.4 + 0.0412\, z \quad [\text{MPa}] \quad r = 0.89 \tag{3.4}$$

where, S_V = estimated vertical stress (overburden pressure)
S_h = minimum horizontal stress
S_{HI} = maximum horizontal stress by the first breakdown method
S_{HII} = maximum horizontal stress by the second breakdown method
z = depth in metres
r = correlation coefficient

Linear regression of the minimum horizontal stress, S_h, above and below Zone 2 indicated a small discontinuity in stress magnitudes of about 3 MPa over the zone. A similar regression analysis for the maximum horizontal stress gave inconclusive results. Therefore it is suggested that the applied in situ stresses to the numerical models vary linearly with depth and in accordance with eqs. (3.1)-(3.4).

Orientations of vertical hydrofractures generated in the borehole wall give a consistent NW-SE orientation of the maximum horizontal stress with one exception at 495 m depth. The average stress orientation above Zone 2 is N45°W but N53°W below the zone. The measured maximum and minimum horizontal stresses are oriented slightly oblique to the strike of fracture Zone 2.

4 DISTINCT ELEMENT MODELLING WITH UDEC

4.1 GENERAL

This study required that specific discontinuity behavior of the rock mass be accounted for in the model analysis. Therefore the distinct element method was used for all computer runs. Although the distinct element method requires more input data than that, for example, for continuum based codes, the method gives a more complete description of the mechanisms involved in the behaviour of faulted rock masses.

The distinct element method is a recognised discontinuum modelling approach for simulating the behavior of jointed and faulted rock masses subjected to quasistatic or dynamic conditions. The method has three distinguishing features which makes it well suited for discontinuum modelling:

1) simulation of the crustal rock mass as an assemblage of blocks which interact through corner-and-edge contacts

2) discontinuities regarded as boundary interactions between these blocks

3) utilization of an explicit timestepping algorithm which allows large displacements and rotations and general non-linear constitutive behavior of the faults.

The distinct element method and UDEC are discribed by Cundall (1971), Cundall (1980), Lemos (1987) and Itasca (1990).

4.2 BLOCK SYSTEM

UDEC requires that the body to be modelled can be divided into blocks which are separated from neighboring blocks by joints, faults or interfaces, Figure 4.1. The blocks may be considered to be rigid or deformable. Deformable blocks are subdivided into triangular finite difference zones for calculation of internal stress and strain. The interfaces may be considered to conform to either a standard Coulumb slip condition or a displacement-weakening model. The system is subjected to static or dynamic boundary conditions and the blocks are allowed to interact with one another across the interfaces.

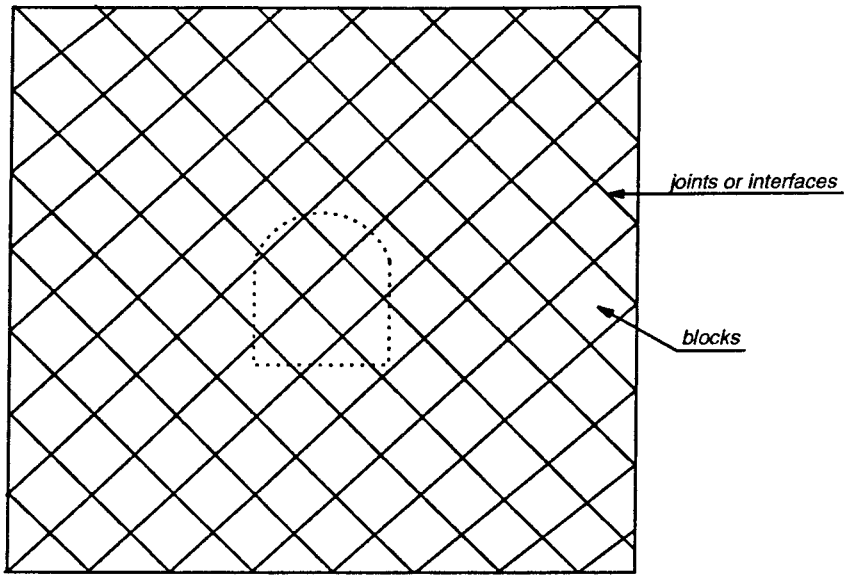

Figure 4.1 Body divided into a system of blocks which may be rigid or fully deformable.

4.3 EXPLICIT SOLUTION PROCEDURE

UDEC uses an explicit solution procedure as opposed to an implicit approach which is most common in finite element or boundary element methods.

In the implicit approach, the equations describing the motion of all elements in the problem are solved simultaneously. For a linear-elastic, static analysis, the implicit solution is performed once but, for non-linear problems, several iterations of the complete set of equations may be required to converge to equilibrium solution state. For non-linear dynamic analysis, the implicit scheme requires convergence to a solution state at each timestep. The timestep can be arbitrarily large with regard to numerical stability, but can still be restricted by the path dependency of the non-linear behavior of the system. The implicit approach is not well suited for problems that involve frequent changes to the connectivity between elements from, for example, highly non-linear behavior or dynamic loading. This is because the stiffness matrix must be reformulated every time a change in connectivity occurs.

In the explicit approach, unknown values of the variables relating to each element in the problem are calculated from known values in that element and its immediate neighbors. The equations relating these values are solved locally for each timestep. This "timestep" may be a physically realistic timestep for dynamic analysis or a calculational increment progressing to an equilibrium state for a static analysis. The equations are solved in the explicit approach by direct intergration using a numerical differencing scheme.

The timestep limitation in the explicit approach restricts the computation efficiency for solving linear problems because many calculational

timesteps may be required to reach the equilibrium state. However, for non-linear analysis with an explicit program, there is little appreciable increase in computer time over the linear analysis, whereas an implicit program becomes much less efficient and may take several iterations to reach the solution, solving the complete system of equations at each step. The explicit approach , in this instance, proves more advantageous.

4.4 GENERAL SOLUTION PROCEDURE IN UDEC

The explicit algorithm used in the UDEC code is based on the use of force-displacement laws which specify the interactions between a block and its surrounding neighbors, and a law of motion which governs the displacements of the block as they are subjected to forces which are not in balance. As described above, the the explicit method requires that a problem be solved in a time- marching procedure in which a calculation cycle is performed for each timestep. The basic mechanical calculation algorithms for rigid and fully deformable (f.d.) blocks are shown in Figures 4.2 and 4.3, respectively. Each of these calculation cycles perform the same basic calculations, the primary difference is that the law of motion is applied to the blocks themselves in the rigid block model, whereas it is applied to the grid points of the finite difference zones in the f.d. blocks. In each case, an initialization procedure is first performed in which the inertial masses of the blocks or grid points and critical timestep are determined. The law of motion is applied to each block (grid point) using known force sums derived from boundary conditions, structural elements, fluid pressures (f.d. blocks), etc., to determine its velocity components. Coordinates of the block corners (rigid) or grid points (f.d.) are updated from the velocities. Since the UDEC code is a large strain model, there is no restriction in the deformation or motion of the blocks.

The normal and shear displacement increments across an interface are computed for each contact point. For f.d. blocks, the increments come from the strain-rates of the contacting grid points. The normal and shear forces across the contacts are detrmined from the joint constitutive law. In this study the normal force is linearly related to the normal displacement, and the shear force is limited by the Coulomb slip condition. These forces are added into the force sums for the blocks or grid points involved in the contact. If f.d. blocks are used (as in this study), the zone stresses are updated based on the constitutive relations for the block (intact) material.

The calculation cycle shown in Figures 4.2 and 4.3 is performed once per timestep. For quasi-static problems, the timestep does not refer to real time, but a calculation increment and is more correctly viewed as a means of "cycling" a problem to the equilibrium or steady state.

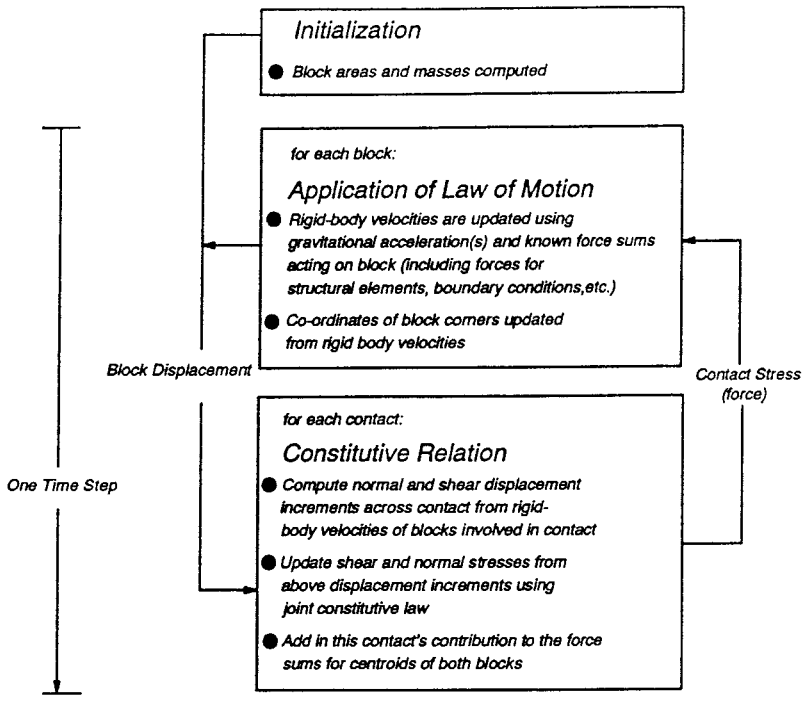

Figure 4.2 Diagram showing the overall calculation flow for the mechanical portion of the UDEC program for rigid blocks. After Board (1989).

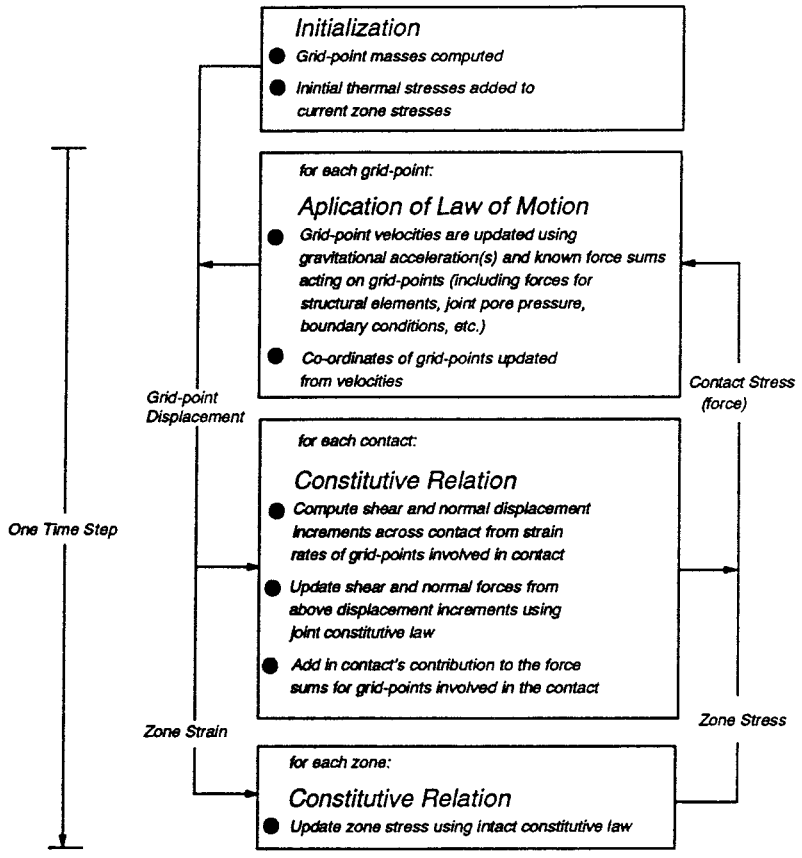

Figure 4.3 Overall calculation flow for the mechanical portion of the UDEC program for fully-deformable blocks. After Board (1989).

5 MODELLING APPROACH AND SIMULATIONS

5.1 GEOMETRY

This study simulates a vertical section which strikes N40°E-S40°W across the Finnsjön site area, Figure 5.1. This section is called "Section A-A" in order to distinguish it from possible other sections to be modelled in the future.

Due to uncertainty about the location of the subhorizontal fracture zone (Zone 2), two different geometries are considered for Zone 2, Figure 5.2. The plots shown in Figure 5.2 are based on Auto Cad-drawings provided by SGAB, Uppsala.

Sections marked with index A-A1 indicates that Zone 2 has the same constant dip throughout the model and is displaced a certain amount by simple shearing along an intersecting fault zone (Zone 6). An index A-A2 indicates that Zone 2 consists of one gently dipping part and one horizontal part separated by Zone 6. Zone 2 is not displaced along Zone 6 for sections A-A2. The two different ways of defining the geometry of Zone 2 represent two different interpretations of core drilling data and hydraulic field testing, see Chapter 3.

The area of interest for modelling the Finnsjön site is about 2.5 km in length and the model depth was choosen to be 2 km. For four of the total six model runs boundary elements were applied at the sides and bottom of the models. The shape and dimension of the entire model and the area of interest is presented in Figure 5.3.

As the computer code UDEC is a two-dimensional representation, but the real problem is three-dimensional in nature it is assumed that all fracture zones are infinitly long and oriented perpendicular to the plane of the analysis. This is a conservative assumption with respect to movement along the fracture zones. In addition, a plane strain condition is assumed, which means that strain perpendicular to the model section is zero.

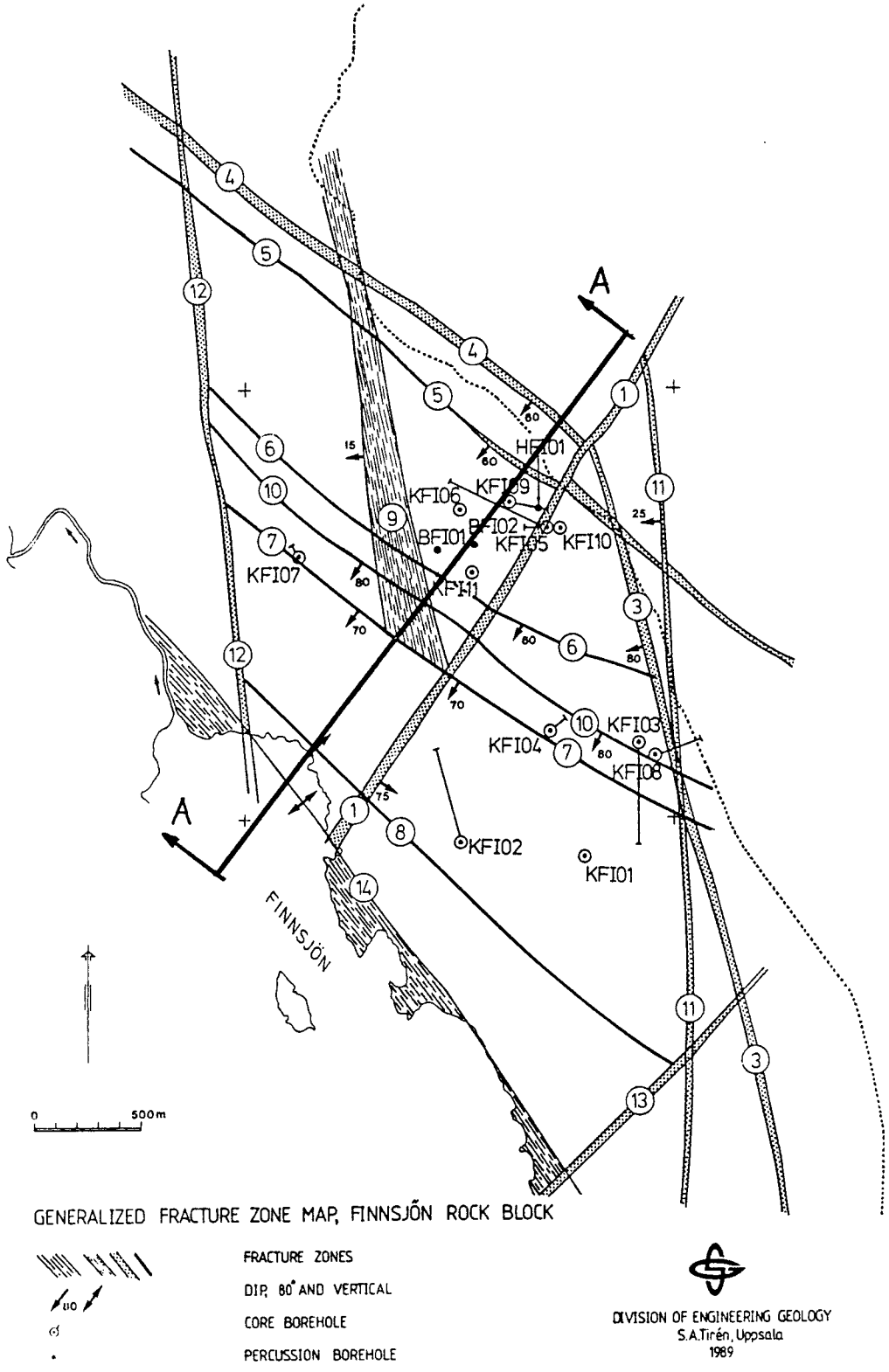

Figure 5.1 Map of the Finnsjön area and the location of section A-A.

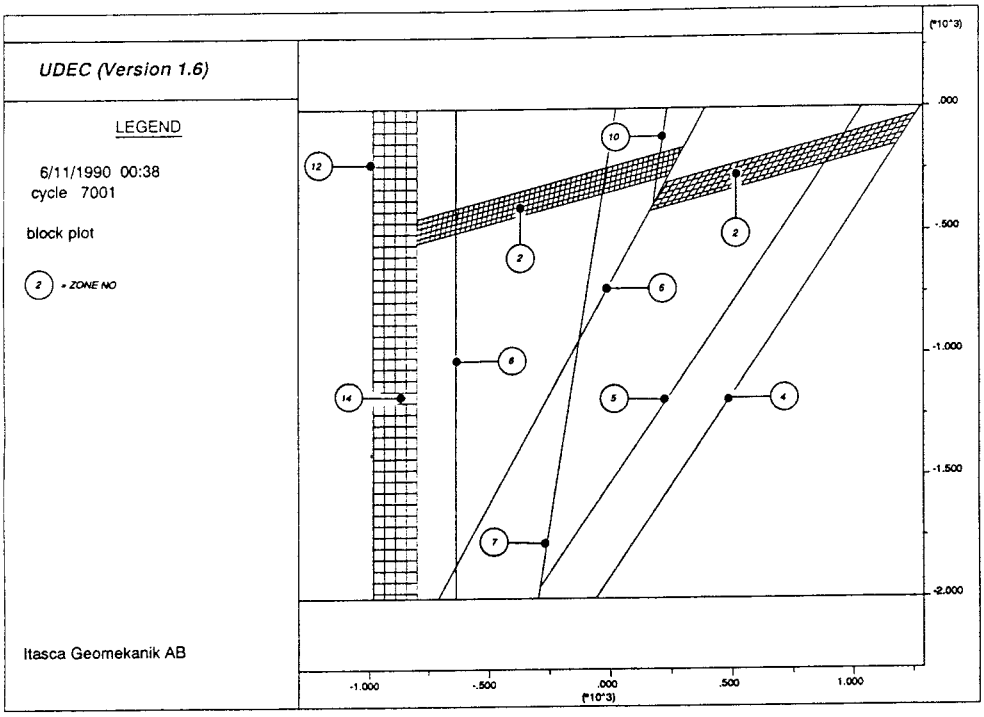

a)

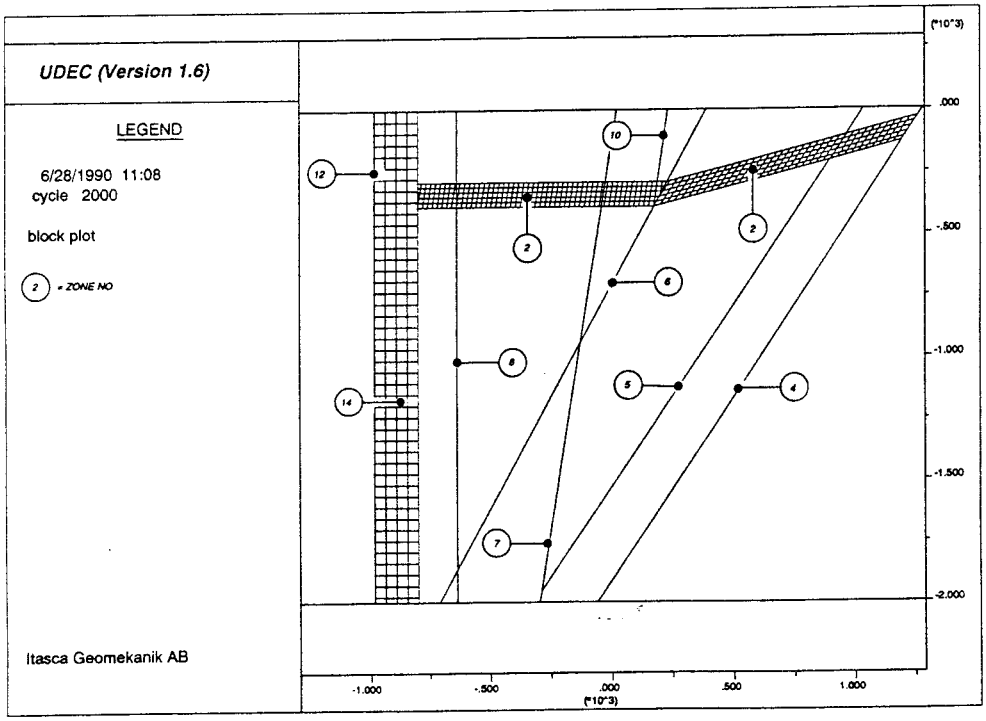

b)

Figure 5.2 Fault geometry for Zone 2. a) off-set of Zone 2, section A-A1, b) continuous Zone 2, section A-A2.

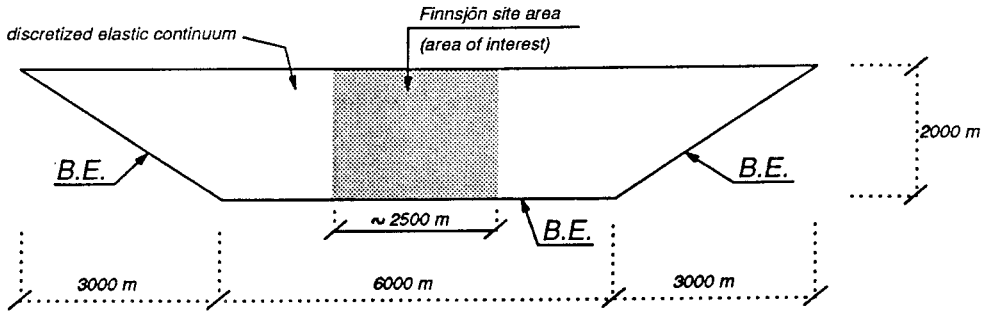

Figure 5.3 Shape and dimensions of the Finnsjön UDEC-models 1-4.

5.2 PROPERTIES OF INTACT ROCK MATERIAL

The intact rock, i.e. the rock material between the discontinuities, is assumed to behave as a linear-elastic, isotropic and homogeneous material. This assumption leads to generation of high stresses in the intact rock blocks and therefore this can be considered as the most conservative situation regarding rock mass stresses.

The properties of the intact rock blocks used for all models are:

Density, ρ [kg/m^3]	2650
Young's modulus, E [GPa]	40
Poisson's ratio, ν	0.2

and the acceleration, g, was set to 10 m/s^2.

5.3 PROPERTIES OF FAULT ZONES

The geometries and orientation of faults used for the UDEC runs (Figure 5.2) are of two different types namely, fault zones that are represented by one single joint (type S) and zones that are represented by a regulary spaced fracture pattern (type F). Fracture zones with a width less than or equal to 50 m are modelled as a single fault zone, i.e. type S, whereas fault zones with greater width are modelled as type F.

To simulate the fracture zones, the following assumptions were made:

- all zones strike perpendicular to the plane of the analysis
- joint properties for each fault zone are in accordance with Table 5.1. All joint properties are hypothetic, i.e. laboratory or field testing have not been conducted
- the location and orientation of the fault zones are in accordance with the Auto Cad drawings provided by SGAB, Uppsala. (Ahlbom, personal communication)

- the strength of the fracture zones are defined by Coulomb slip criterion, Figure 5.4. When shear or tensile strength of the fracture is exceeded it looses its cohesion and tensile strength. The initial tensile strength of the fracture zones is zero.

Table 5.1 Properties of fracture zones presented in Figure 5.1.

Parameter	Fracture zone								
	2	4	5	6	7	8	10	12	14
Normal stiffness, Kn [GPa/m]	1.0	10.0	10.0	10.0	10.0	10.0	10.0	10.0	1.0
Shear stiffness, Ks [GPa/m]	0.33	3.33	3.33	3.33	3.33	3.33	3.33	3.33	0.33
Cohesion, C [MPa]	0.5	1.0	1.0	1.0	1.0	1.0	1.0	1.0	0.5
Friction angle [°]	20	25	25	25	25	25	25	25	20
Tensile strength [MPa]	0	0	0	0	0	0	0	0	0

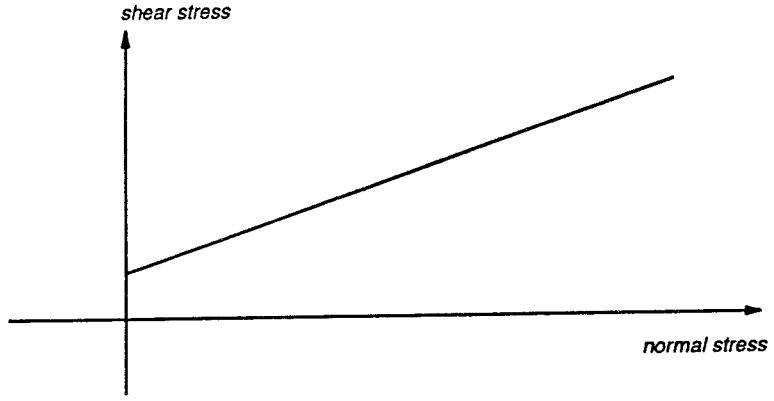

a)

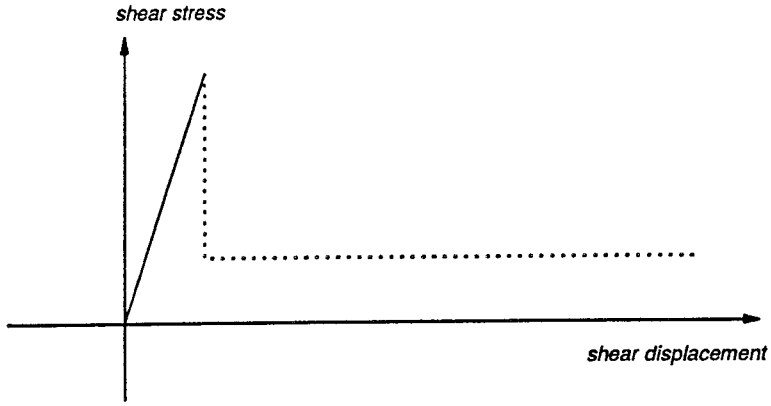

b)

Figure 5.4 Coulomb slip criterion used in this study. a) Shear stress versus normal stress, b) shear stress versus shear displacement.

5.4 IN SITU STRESSES AND BOUNDARY CONDITIONS

In situ stress measurements at the Finnsjön site area were conducted by Luleå University of Technology, Division of Rock Mechanics and are reported by Bjarnason and Stephansson (1988).

The orientation of the minimum horizontal stress is approximately N40°E-S40°W which is parallel to the plane of analysis for models of section A-A. This means that applied in situ stresses for models of section A-A are in accordance with eqs. (3.1) and (3.2) (Chapter 3.4)

During the consolidation of the models all the boundaries, except for the surface, were prevented from displaceing in normal directions. In all subsequent loading steps, fixed boundaries were changed to boundary element for Models 1-4. This means that the force-displacement relation at the boundary is the same as that for a semi-infinite linear-elastic, isotropic and homogeneous material. The elastic properties of the boundary element domain were the same as for the intact rock blocks used in the distinct element modelling.

The use of boundary elements to represent the far field requires that one point in the model has to be fixed, otherwise the entire model will translate when surface loading is applied. In this study the fixed point is located at the center line, and 4000 m below surface. The location of the fixed point does not influence the vertical strain in the model, only the total magnitude of displacements. From a series of test runs, the maximum vertical displacement versus the location of the fixed point below the surface was determined, Figure 5.5.

A boundary element approach provides more accurate representation of the far field stress, but causes some problems to reproduce an accurate displacement field for finite uniform surface loading condition.

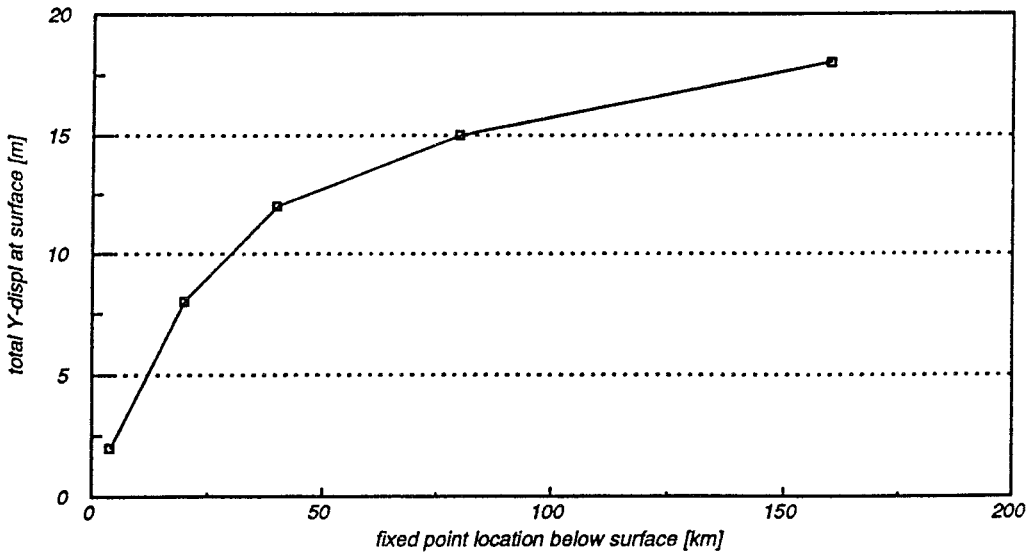

Figure 5.5 Maximum vertical displacement versus fixed point location along the model center line for uniformly distributed load of 27 MPa (= 3 km ice) with an extension of 12 km parallel to the plane of the model as shown in Figure 5.3.

5.5 LOADING CONDITON AND LOADING SEQUENCES

5.5.1 Models 1-4

The ice load was applied on the top boundary as a finite uniformly distributed, static boundary stress, acting vertically. When boundary elements are used this loading condition produces a response in the model that is very similar to a uniformly loaded beam. The magnitude of vertical displacement decreases away from the center line, Figure 5.6

If the load is extended, the vertical displacement contours in the center of the model tend to become less curved, i.e. the horizontal gradient due to the vertical displacements decreases.

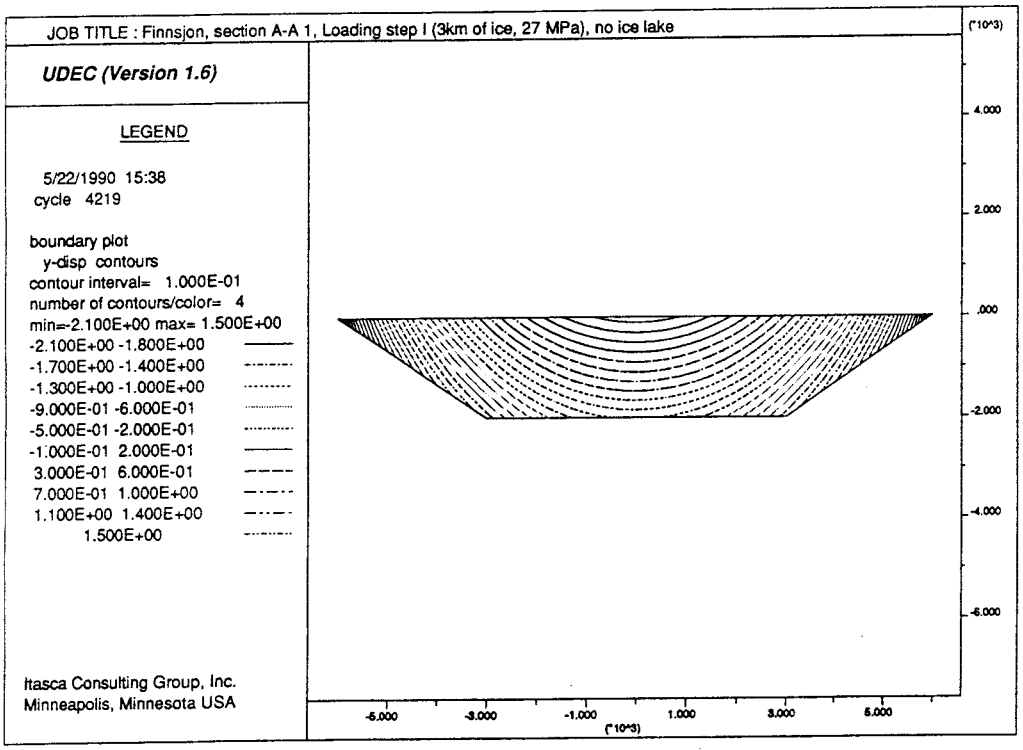

Figure 5.6 Distinct Element - Boundary Element analysis of vertical displacement from a finite uniform vertical load. The fixed point is located 4000 m below surface. Elastic model, no joints, vertical load = 27 MPa.)

In the UDEC code there is no possibility, at present, to specify a load at the boundary of the elements. The model had to be extended laterally in order to get the load as far away from the center as possible and thereby decrease the effect of bending in the area of interest. This was the reason for extending the model outside the area of interest. Theoretically there are no limits how large the model can be except practical limitations. The width of the entire model, exclusive boundary elements, was 12 km at the top (ground suface) and 6 km at the bottom. The reason for having the inverted slopes at the ends was to save the number of zones and thereby save computer time (effective run-time for one model was about two days).

The loading sequence for Model 1-4 was as follow (see Figure 5.7):

Loading step	Loading condition	Model 1,3 (no ice lake) [MPa]	Model 2,4 (ice lake) [MPa]
0	(insitu stress state)	-	-
I	uniform load of 3 km ice	27	30
II	uniform load of 1 km ice	9	10
III	ice wedge	0-9	0-10
IV	no load	-	-

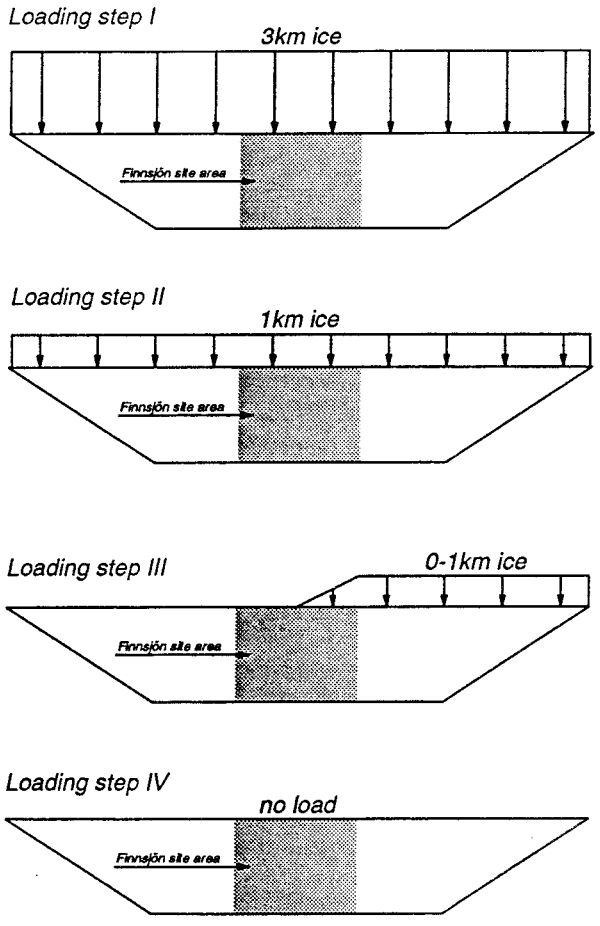

Figure 5.7 Loading sequence for Models 1-4.

5.5.2 Model 5

The purpose of Model 5 was to simulate the effect of a viscous (time dependent) movement of the bottom boundary using a quasistatic approach. This required that the boundary conditions be changed from one loading step to another. Thus, the boundary conditions of the boundary element could not be used to represent the "far-field" stresses. The ice load on the top surface was applied in the same way as for Models 1-4.

The loading sequence for Model 5 is rather complex since the boundary conditions are a part of the loading sequence. Figure 5.8 shows the loading sequence and the change of boundary conditions for the different loading steps.

5.5.3 Model 6

Model 6 simulates the same loading sequences as Models 1-4 but without boundary elements along the vertical sides of teh 2.5 x 2 km model. In that respect Model 6 is similar as Model 5 except the vertical displacements along the bottom and right hand side of the model (cf. Figure 5.8). The main idea with this model is to study the effects of roller boundaries along the vertical sides and bottom of teh model in comparison with boundary element boundary condition.

5.6 HYDRAULIC CONDITIONS

The effect of pore presssure and static water load has been included in all models of this study. For the models where an ice lake is not taken into account (Models 1,3 and 5, 6), the pore pressure distribution was assumed to be hydrostatic, i.e. zero at the ground surface and 20 MPa at the bottom of the model.

Models where an ice lake was simulated (Models 2 and 4), the ice lake was assumed to exist on the top of the ice sheet. The pore pressure in the fault zones was equal to the water head for loading step I and II (3 km and 1 km of ice). A pore pressure gradient in the horizontal direction only exists for the case where the ice load partly cover the surface (loading step III). Here the pore pressure at the surface is zero for the unloaded part and is in accordance with the ice thickness for the loaded part. The horizontal pressure gradient was modelled as a steady state equilibrium pore pressure distribution in the model. The pressure in the model was then held constant during the cycling. The assumed pore pressure distribution is shown in Figure 5.9.

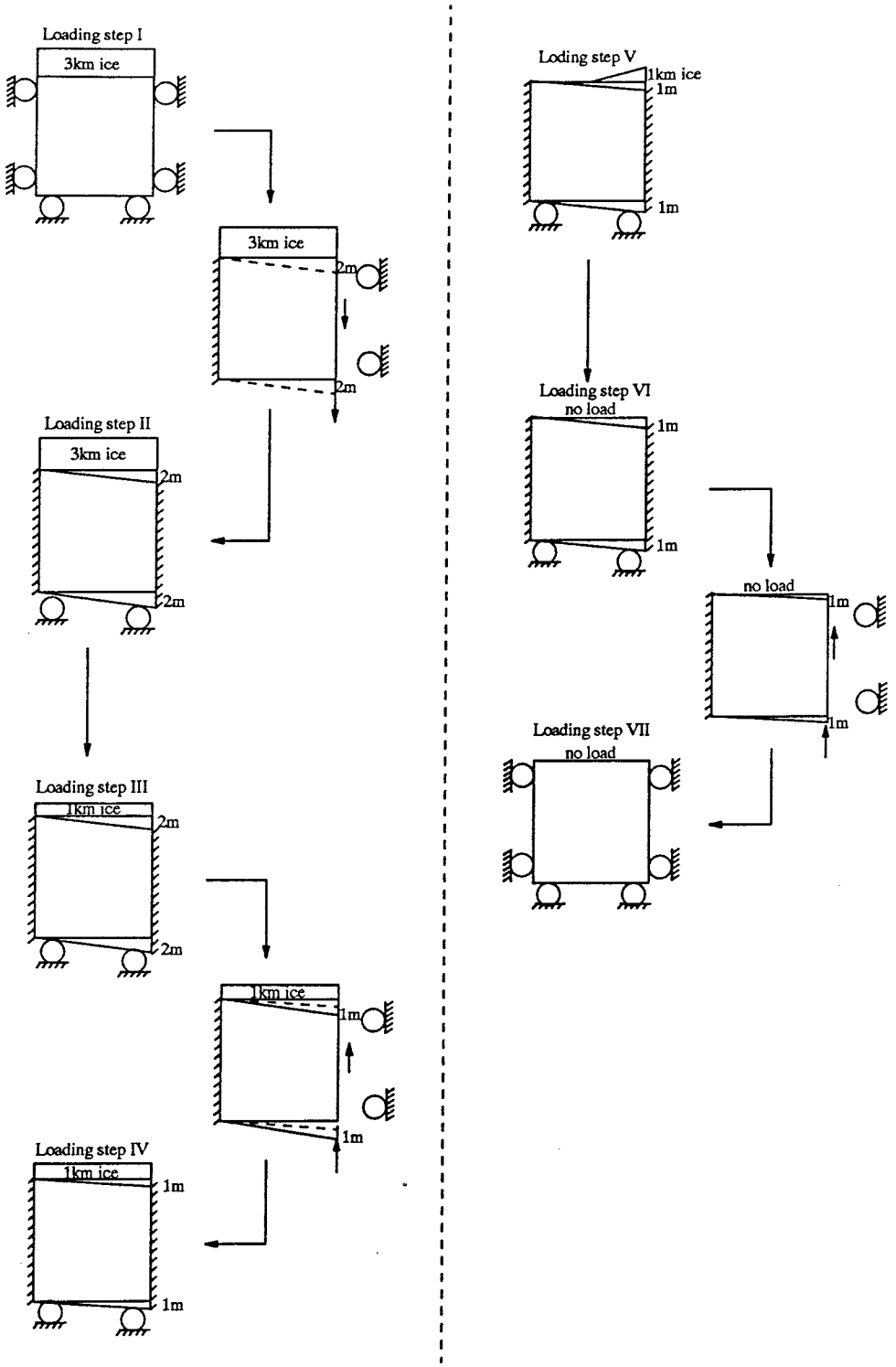

Figure 5.8 Loading and boundary conditions for Model 5. The effect of ground subsidence and rebound is simulated together with the ice loading.

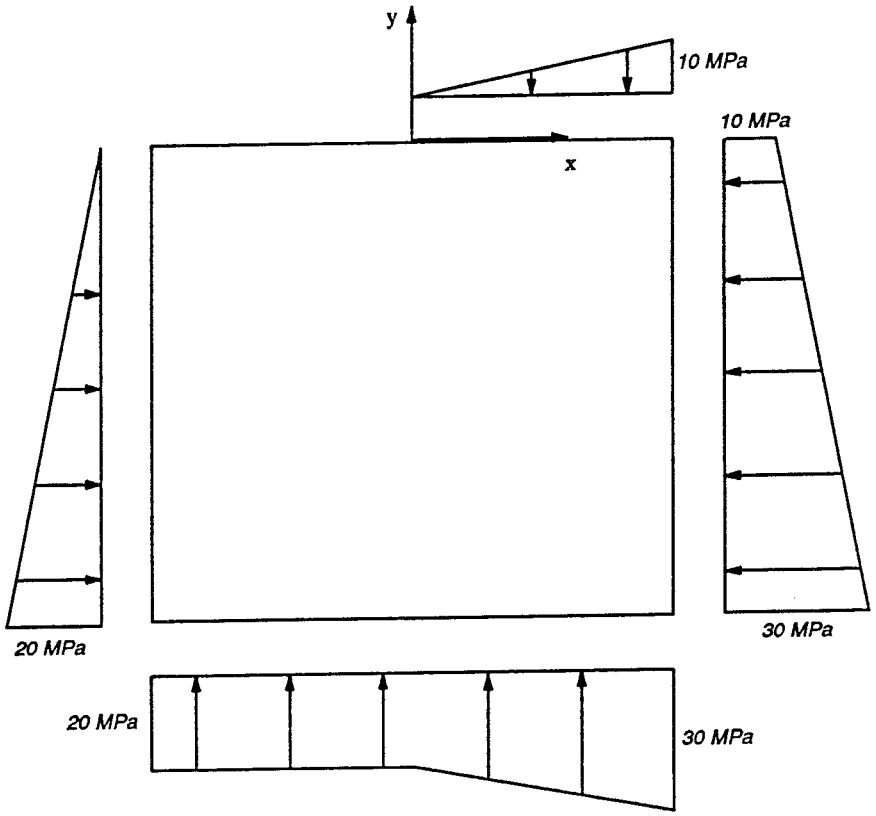

Figure 5.9 Applied steady state, pore pressure for Models 2 and 4, loading step III (ice wedge).

The pore pressure for any point in the models can be calculated from the equations below:

$$PP = (-0.01 * y) \quad \text{for } x < 0, y < 0 \tag{5.1}$$

$$PP = (0.00826 * x) + (-0.01 * y) \quad \text{for } 0 < x < 1210, y < 0 \tag{5.2}$$

$$PP = 10 + (-0.01 * y) \quad \text{for } x > 1210, y < 0 \tag{5.3}$$

The Y-coordinate is defined negative downwards, and $y = 0$ at the ground surface.

Notice that pore pressure in the models can only exist in fault zones since the intact blocks in the UDEC code are considered as impermeable. Density for water was assumed to be 1000 kg/m^3.

This study considered only the mechanical response of the rock mass. Therefore, water flow in fracture zones was not simulated.

5.7 SIMULATIONS

In total six different models were analysed. The same modelling approach has been used for Models 1-4, i.e. the same boundary conditions and loading sequence. The geometry of Zone 2 and the simulation of the ice lake are varied, Table 5.2.

Table 5.2 Specifications for Models 1-4.

Model	Section	Ice lake
1	A-A 1	no
2	A-A 1	yes
3	A-A 2	no
4	A-A 2	yes

Models 5 and 6 have a fault geometry in accordance with section A-A1. The effect of ice lake is not considered in these models and the pore pressure in the fracture zones is assumed to correspond to the hydrostatic pressure, i.e. zero at ground surface and 20 MPa at the bottom of the model. Model 5 considers the vertical displacement due to isostasy and roller boundaries while isostasy is omitted in Model 6.

All simulations in this study were performed using version 1.6-1.63 of the UDEC code. The code was run on a ordinary 386 Personal computer with a RAM memory of 4 Mb with a Weitek 3167 math coprocessor.

6 RESULTS

6.1 PRESENTATION OF RESULTS

Six complete numerical analyses have been conducted, namely four with boundary element boundary conditions (Models 1-4) and one with displacement (velocity) boundaries (Model 5) and one with roller boundaries (Model 6).

The results are presented as plots provided directly from UDEC runs and as post-processed data, e.g. diagrams showing stresses versus depth for selected sections of the models.

For the stress plots (principal stresses and stress components, SXX, SYY, and SXY) with the dimensions 2000 x 2000 m the most interesting parts are presented. Some stress plots with an even smaller area are shown in order to obtain better resolution of interesting parts of the models.

For displacement plots (displacement vectors, displacement contours, and shear displacements on joints) and plots of fractured joints an area of 2580 x 2000 m has been used. This enables complete presentation of all major faults that exist within the Finnsjön site area.

Stresses versus depth are presented for two vertical lines at x = 175 and x = -540 respectively (Figure 6.1). These lines are located at the same co-ordinates for all models.

In addition to regular plots and diagrams of stresses and displacement history plots of stresses and displacements are presented. History plots show the change of stress and displacement caused by changes in the loading conditions. The x-axis (horizontal axis) for all history plots represents fictitious time, i.e. the time step multiplied by the number of cycles of the finite difference procedure in the UDEC code. Table 6.1 and Figure 6.2 present type and locations of history points for the models.

It is not meaningful to present all UDEC plots for every loading step of each model. Therefore, only the most interesting results are selected, compiled and presented. The interested reader can study a complete set of plots from all models and loading steps. The information is stored in a separate volume at SKB.

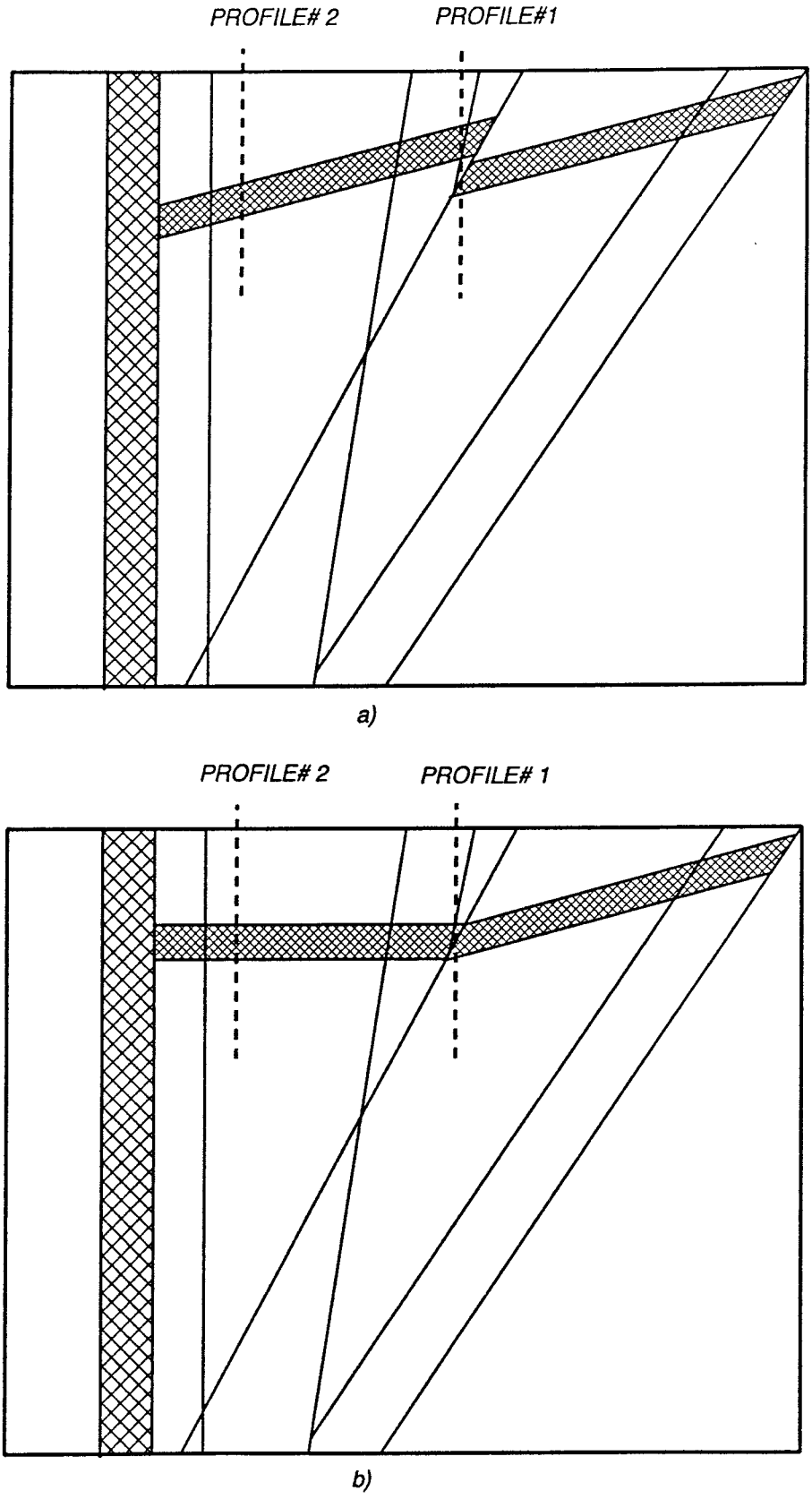

Figure 6.1 Location of two vertical lines in the models along which stress are presented, a) Section A-A 1, b) Section A-A 2.

Table 6.1 Number, type and co-ordinates of history points.

No.	Type	x-co-ordinate	y-co-ordinate
1	max unbal force	--	--
2	y-displ	21	0
3	y-displ	-559.1	-84.6
4	y-displ	-560.1	-183.6
5	y-displ	-559.0	-282.4
6	y-displ	-542.2	-398.1
7	y-displ	-525.5	-506.1
8	y-displ	-568.3	-593.7
9	y-displ	-505.8	-692.2
10	xx-stress	-549.0	-511.2
11	xx-stress	-547.5	-611.2
12	yy-stress	-549.0	-511.2
13	yy-stress	-547.5	-611.2
14	y-displ	161.2	-95.7
15	y-displ	179.3	-190.0
16	y-displ	162.8	-294.3
17	y-displ	171.1	-397.6
18	y-displ	185.9	-504.3
19	y-displ	154.1	-610.1
20	y-displ	171.2	-694.8
21	xx-stress	148.4	-503.3
22	xx-stress	168.1	-589.3
23	yy-stress	148.4	-503.3
24	yy-stress	168.1	-589.3
25	y-displ	-1096.0	0.0
26	y-displ	-890.0	0.0
27	y-displ	-717.5	0.0
28	y-displ	-389.6	0.0
29	y-displ	-225.4	0.0
30	y-displ	126.0	0.0
31	y-displ	309.5	0.0
32	y-displ	631.4	0.0
33	y-displ	793.6	0.0
34	y-displ	1123.0	0.0

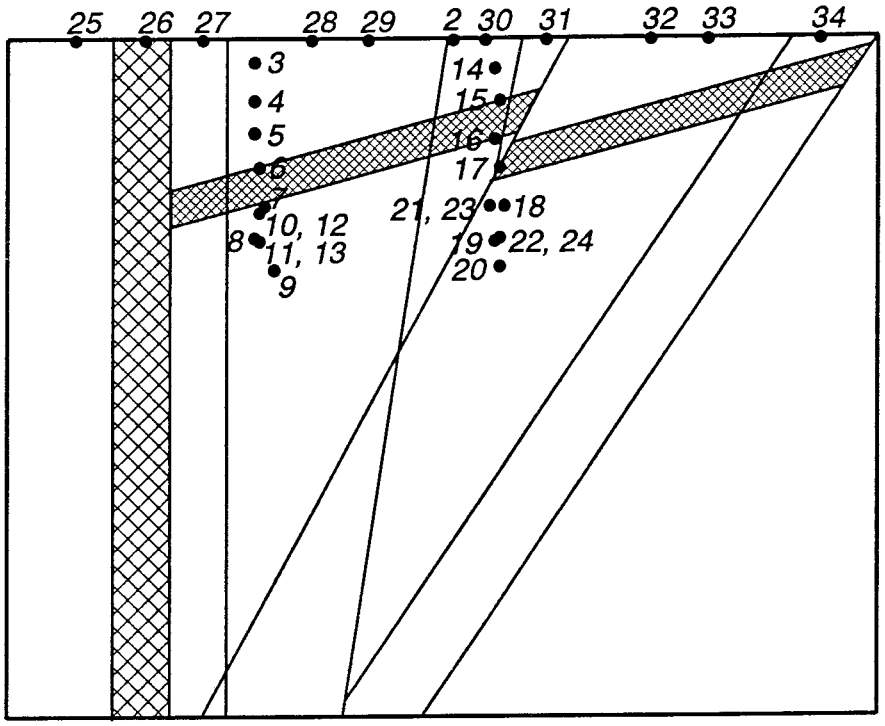

a)

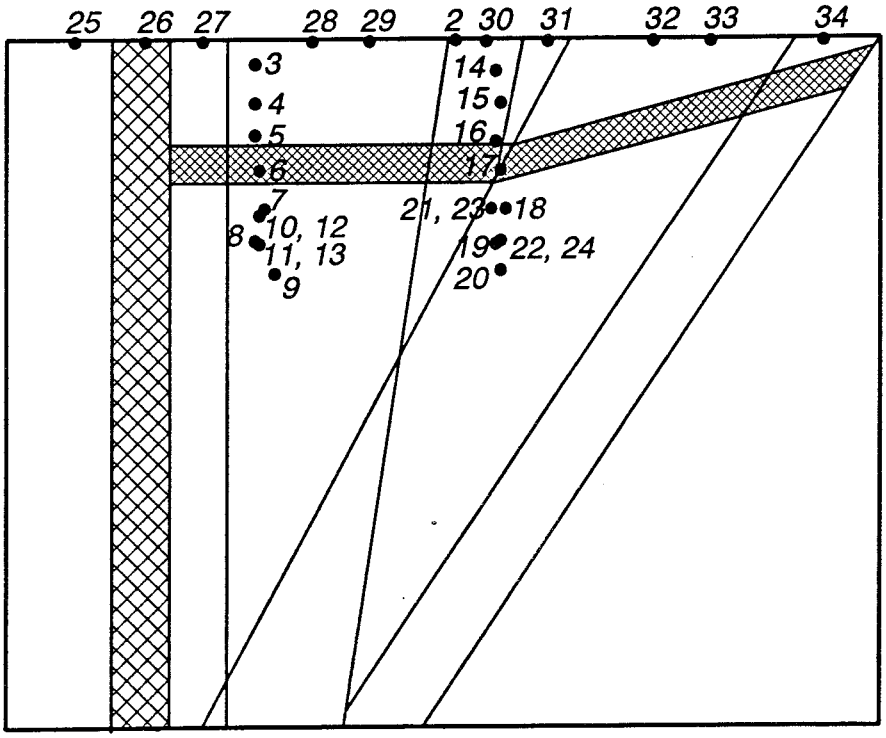

b)

Figure 6.2 Location of history points in the models. Co-ordinates are presented in Table 6.1. a) Section A-A1, b) Section A-A2.

6.2 MODELS 1-4

6.2.1 Stress

No significant difference exists in the stress state for each loading step between section A-A 1 and A-A 2 of the models for identical pore pressure. However, models of the ice lake show a very different stress distribution in comparison with the models where the ice lake is not taken into account. Figures 6.3 and 6.4 show principal stresses for loading step I (3 km ice). Notice that compressive stresses are negative. The principal stress vectors in the vicinity of the sub-horizontal fracture Zone 2 and in the vicinity of Zones 12 and 14 are non-uniform for models without ice lakes.

The random orientation of the stress vectors for the ice lake models are due to a more or less hydrostatic stress state. This appears as a band of rotated stress vectors at a certain level in the models. The magnitude of the the maximum principal stress at each loading step is almost the same for all models.

The difference in stresses between the two models with different pore pressure becomes more clear if the stress components are studied. Figures 6.5 and 6.6 show the horizontal stress, SXX, and vertical stress, SYY, between 50 and 750 m levels below surface, for two profiles of section A-A1. The stress gradients in the ice lake case do not change with depth, whereas for the model without ice lake, drastic change in stress at certain areas can be seen. This stress change occurs at a depth between 100 and 500 m below surface, depending on where the profile intersects the discontinuities. Fracture Zone 2 has the major impact on the stress gradients for the two profiles studied. The magnitude of the stresses is due to the fracture strength and stiffness parameters assigned to the fracture that are intersected by the profiles as shown by Rosengren (1989). However, this is not verified in this study since sensititvity studies have not been performed.

The difference in results between the two models can be explained by the different pore pressure distribution, the effective stresses, and the ability to transmit shear stresses. The pore pressure in the ice lake model is 30 MPa higher than in the model without ice lake, and consequently the effective stresses are lower. A low effective stress in the fracture result in a decreasing ability to transfer shear stresses. In Figure 6.7 are the shear stress contours shown for Model 1, section A-A1, loading step I. It is obvious that the ice lake model can hardly transmit any shear stresses and, thus, only very small shear stresses can be built up. If the shear stresses are zero, then the horizontal and vertical stress components coincide with the principal stresses, both in magnitude and orientation.

To complete the discussion about stresses from 3 km of ice loading contours of the horizontal and vertical stress for section A-A1, loading step I, are shown in Figures 6.8 and 6.9. An ice lake on top of the ice sheet or acting at the rock/ice interface reduce the stress concentrations at Zone 2.

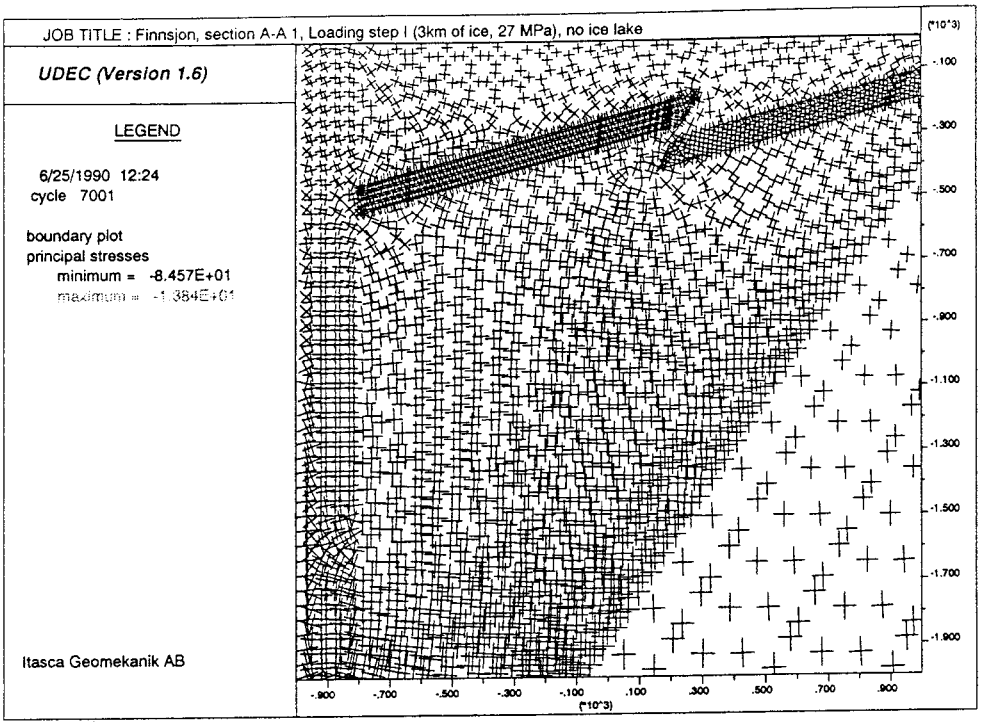

a)

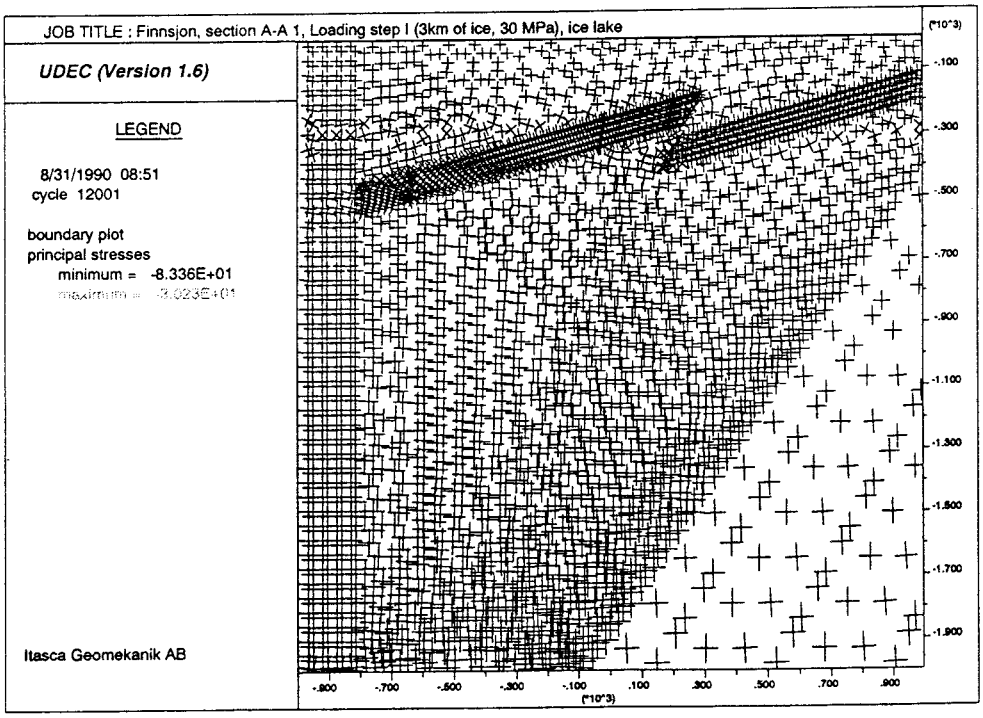

b)

Figure 6.3 Principal stress distribution, loading step I. a) Model 1, b) Model 2.

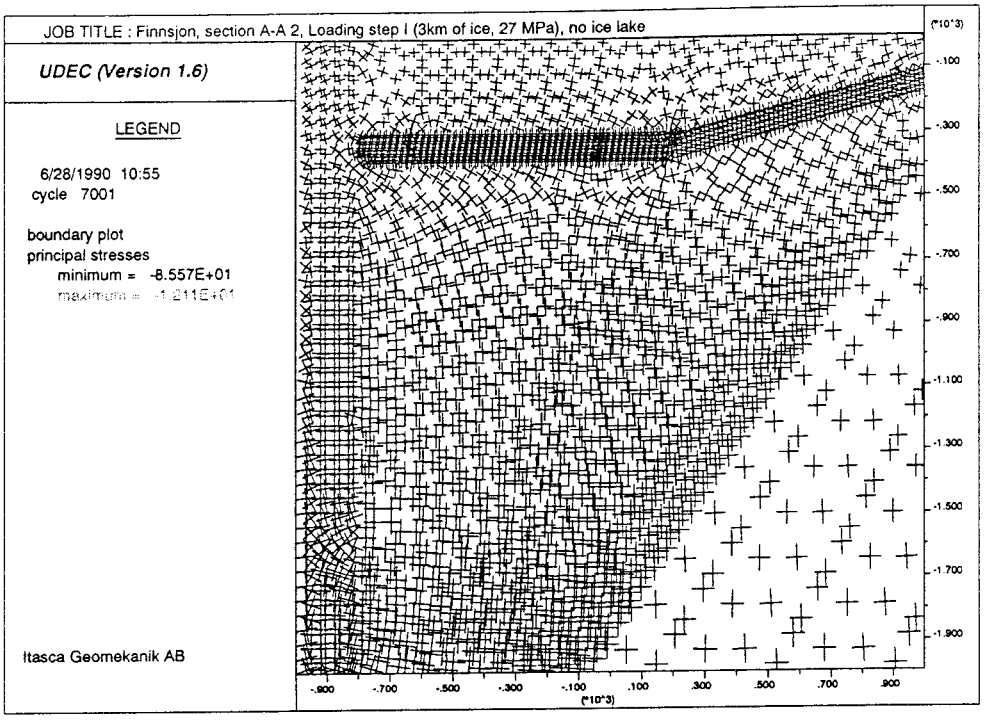

a)

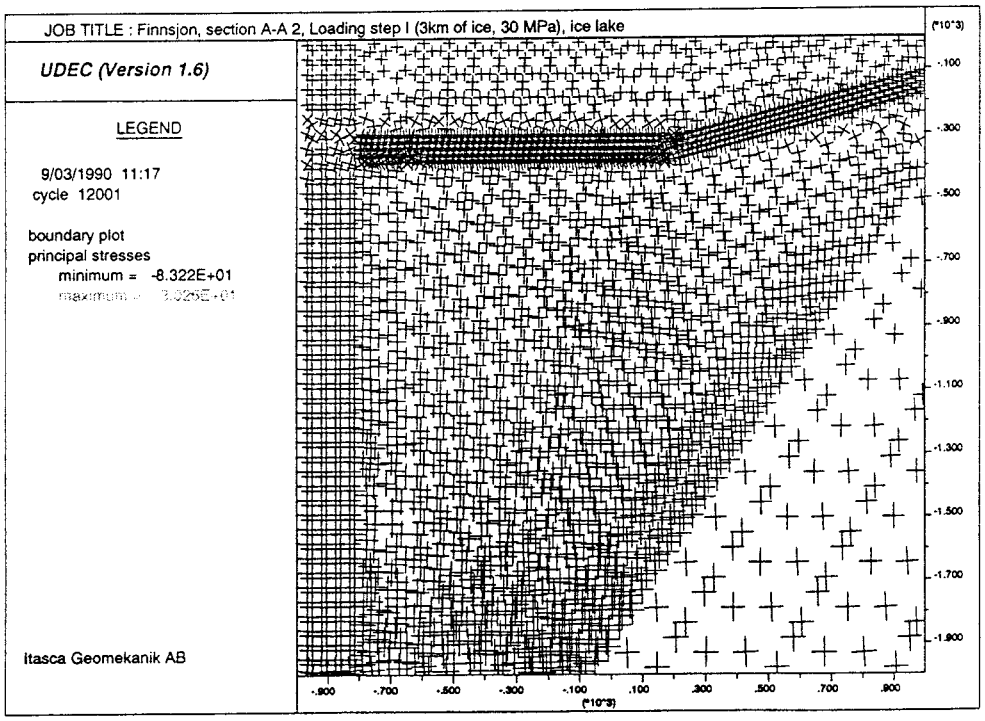

b)

Figure 6.4 Principal stress distribution, loading step I. a) Model 3, b) Model 4.

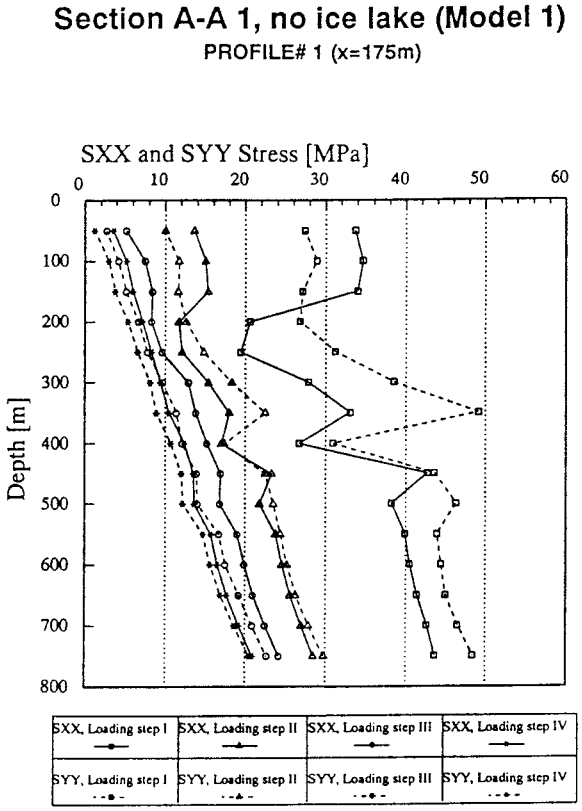

a)

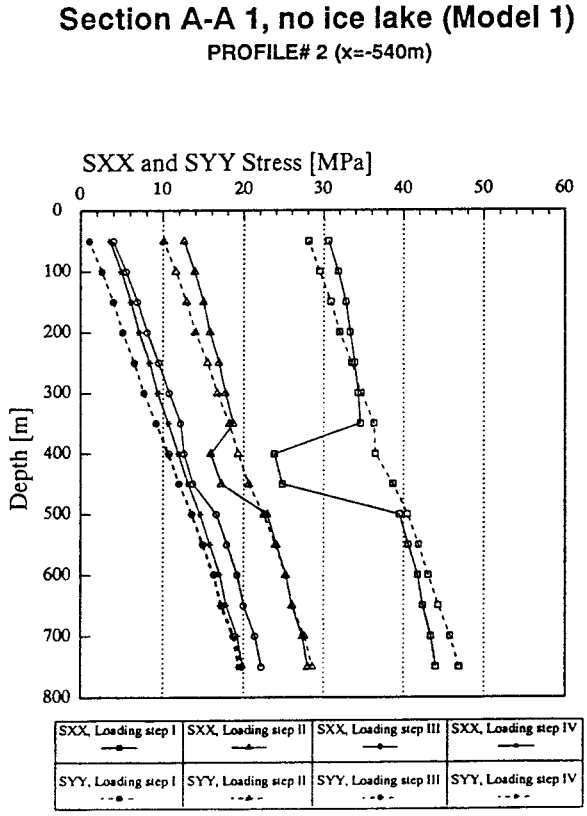

b)

Figure 6.5 Horizontal stress, SXX, and vertikal stress, SYY, versus depth, Model 1. a) profile # 1, b) profile # 2.

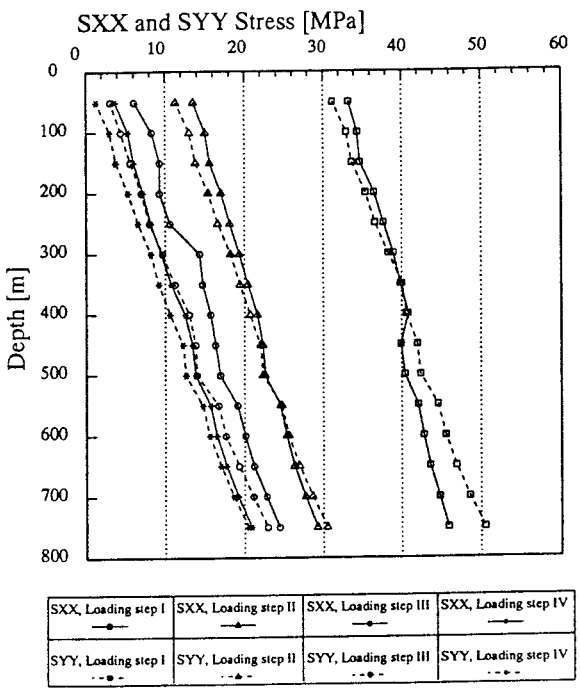

a)

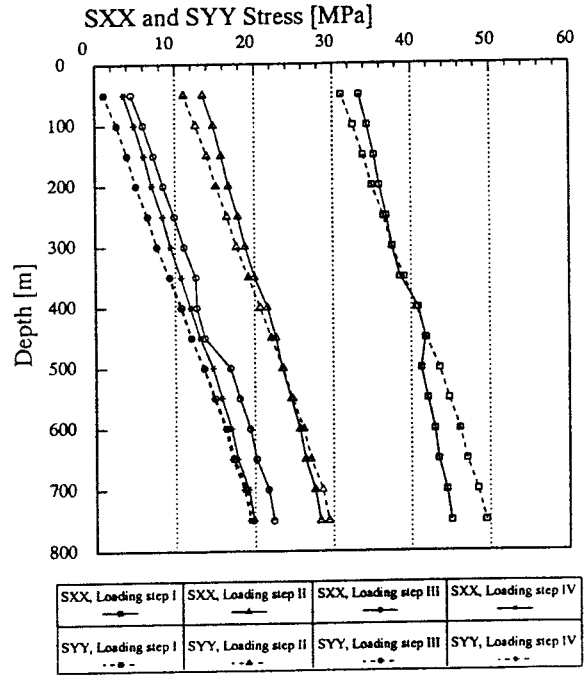

b)

Figure 6.6 Horizontal stress, SXX, and vertikal stress, SYY, versus depth, Model 2. a) profile # 1, b) profile # 2.

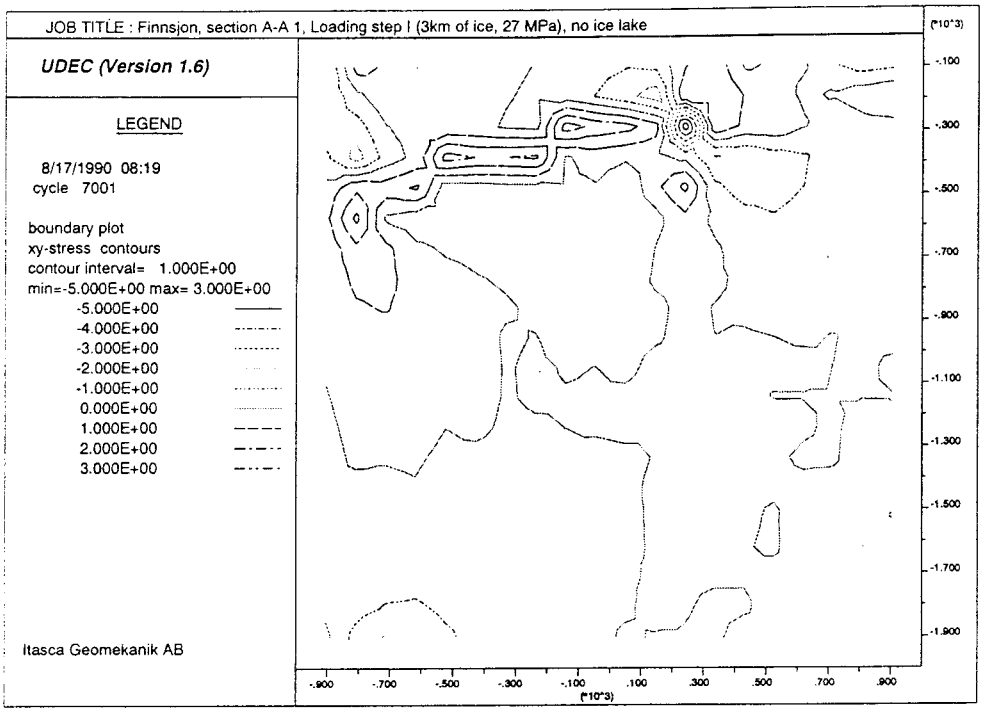

a)

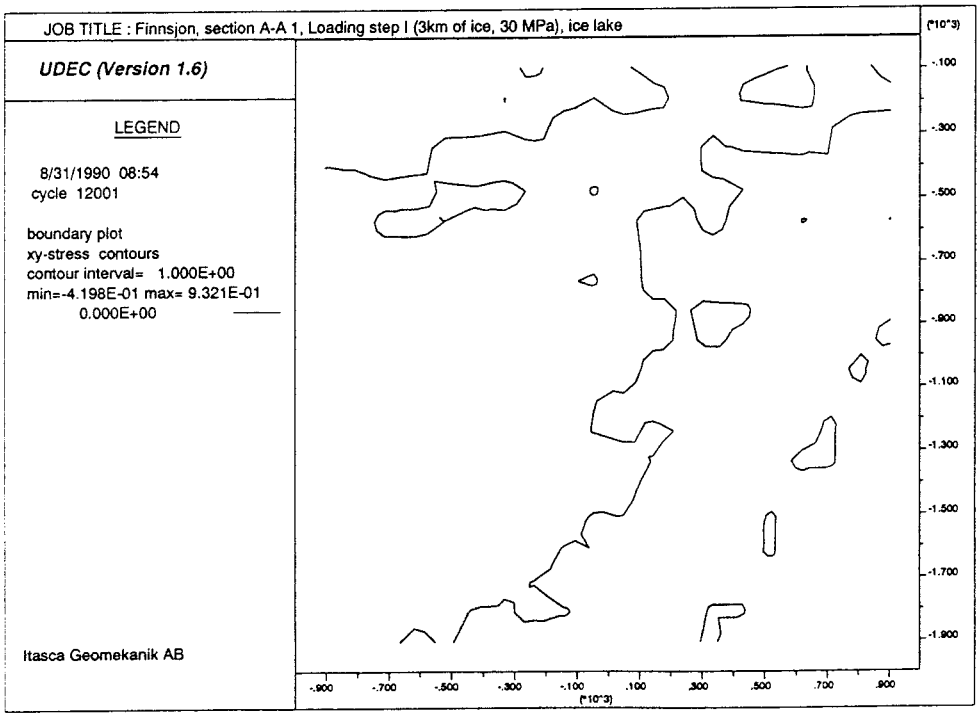

b)

Figure 6.7 Shear stress contours, loading step I. a) Model 1, b) Model 2.

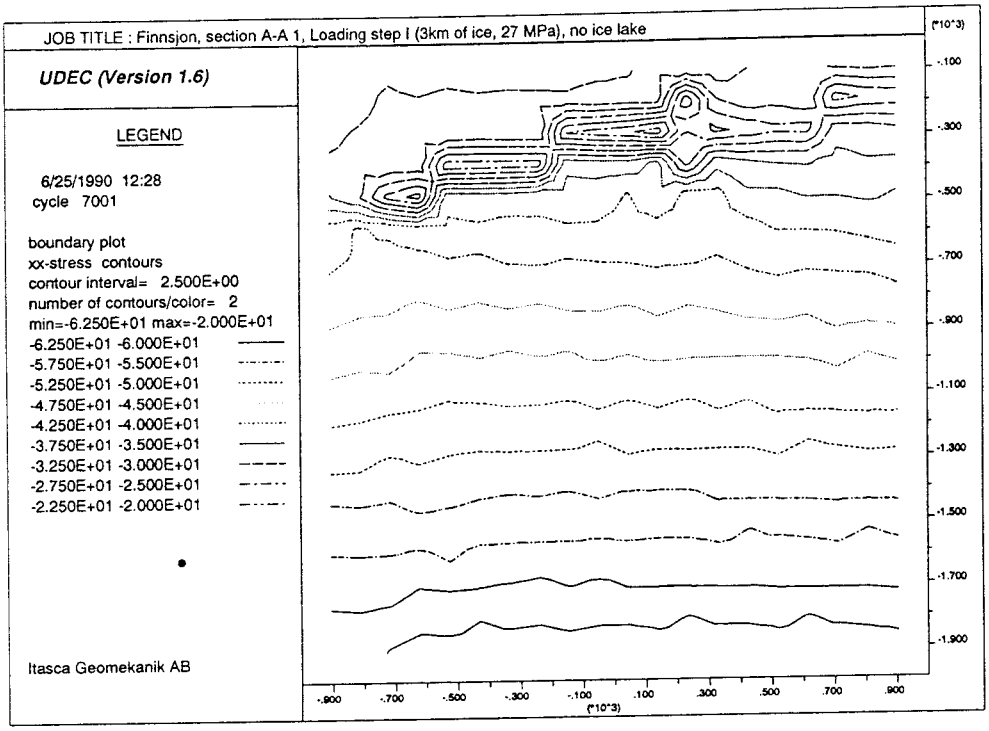

a)

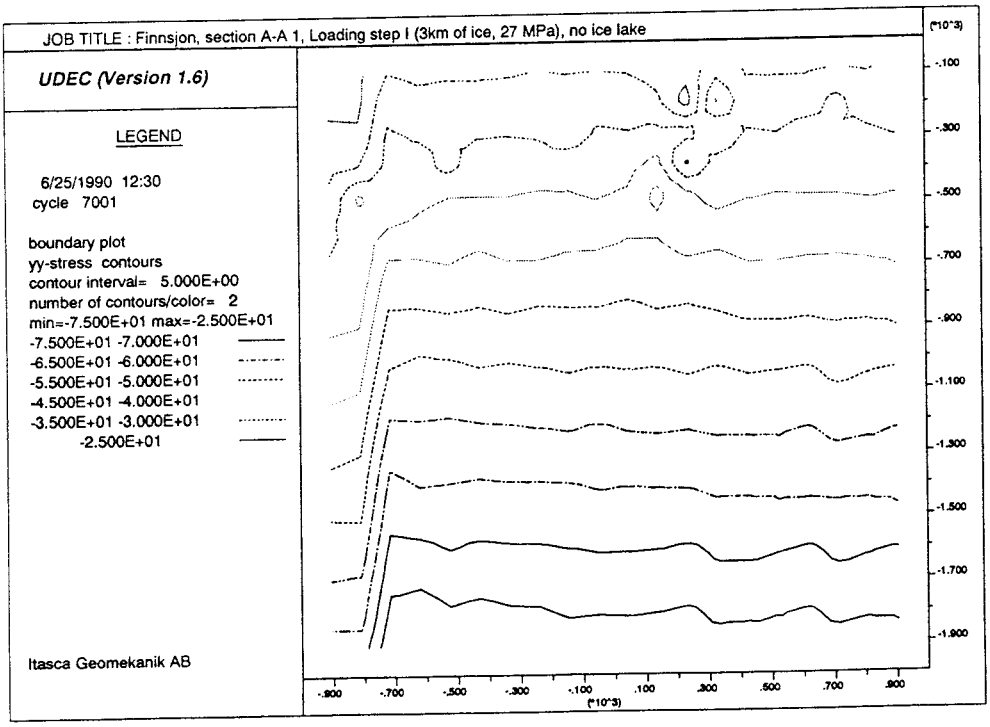

b)

Figure 6.8 Contours of horizontal and vertical stresses, Model 1, loading step I. a) horizontal stress, b) vertical stress.

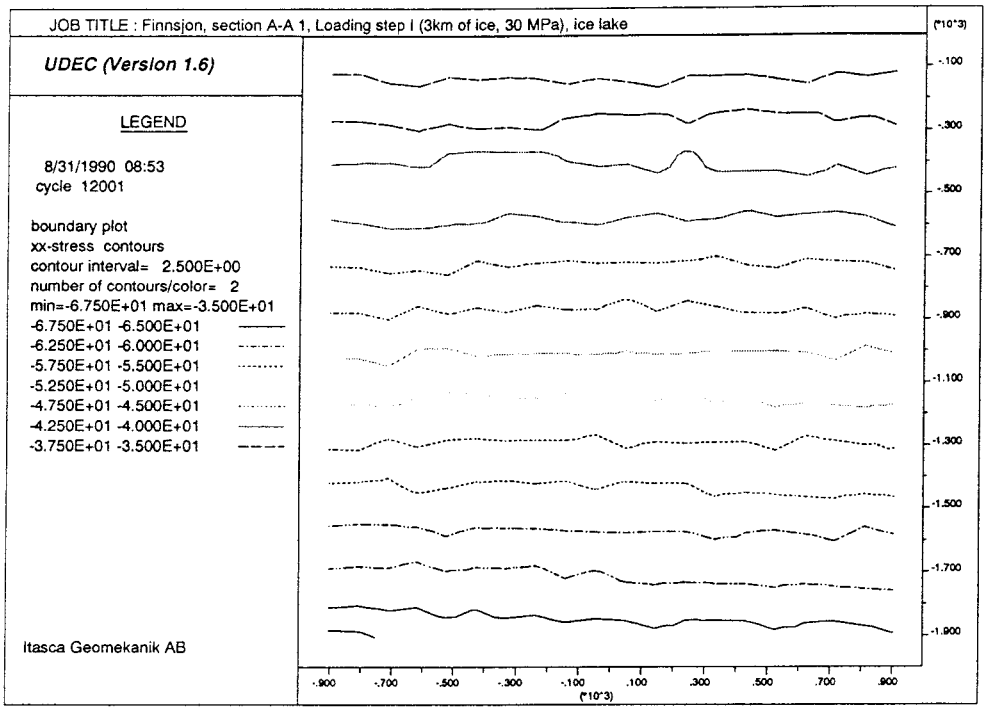

a)

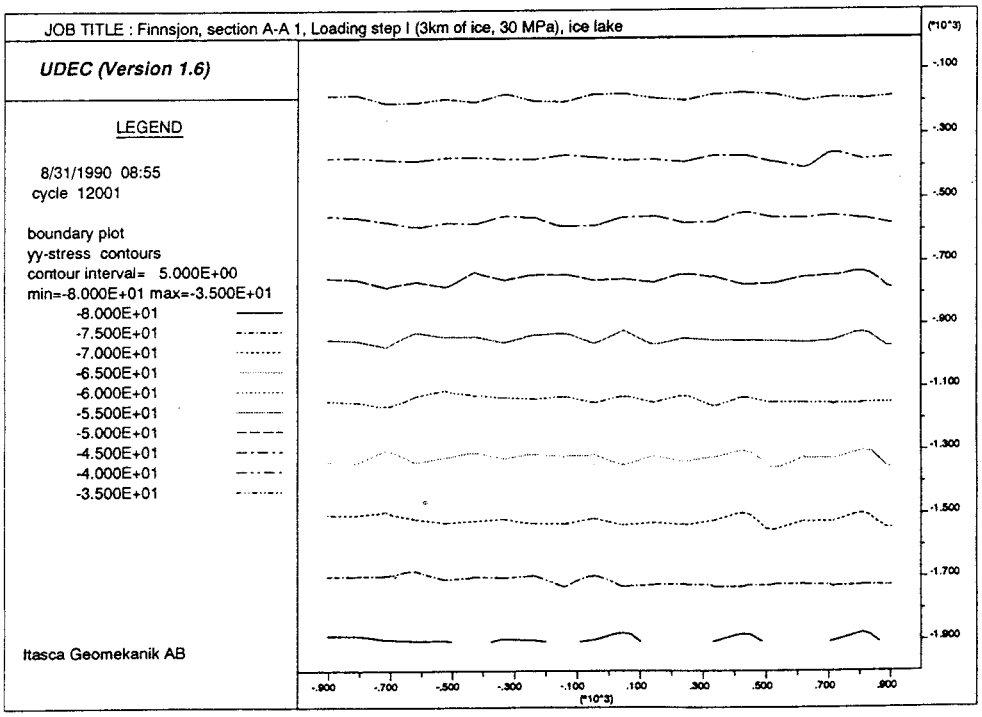

b)

Figure 6.9 Contours of horizontal and vertical stresses, Model 2, loading step I. a) horizontal stress, b) vertical stress.

Loading step II (1 km ice load) shows similar results for the different models as in loading step I, except that the stress magnitudes, stress concentrations and changes in the stress gradients are smaller. Stresses are very similar in models of section A-A1 and A-A2, i.e. the fault geometry has minor influence on the state of stress for loading step I and II.

Loading step III (ice wedge) shows an uneven loading at the surface and the principal stress trajectories incline with respect to the horizontal plane, Figure 6.10. The dip of the trajectories is maximum in the bottom right corner of the models, and decreases towards the upper left corner. Above fracture Zone 2, it appears that the dip of the zone determines the principal stress orientations for the ice lake cases, sections A-A1 and A-A2, cf. Figure 6.10. There is no noticeable difference in the stress state between models with and without ice lake. Contours of the horizontal and vertical stress show very small stress concentrations in the models for loading step III and the stress field is more or less equal to that for an elastic model.

The stress state at loading step IV (no load) is almost the same as that for the in situ condition (step 0).

6.2.2 Displacement

When evaluating displacements for Models 1-4, there is no relevance in presenting absolute displacement magnitudes for one specific model, since the magnitudes are dependent on the location of the fixed point of the models, cf. section 5.4. Also the loading condition due to the boundary elements affects the displacement field, e.g. the contours of vertical displacements are curved and the gradient of horizontal displacement exists for an infinite load. This situation is caused by the fact that the model is not capable at present of representing an infinite surface load, and bending takes place in the model. The results presented in this section is therefore focused on relative displacements.

There is no significant difference in the total displacement for models of section A-A1 and section A-A2. This means that the fault geometry of fracture Zone 2 has almost no influence on the displacements. Therefore only results of Models 1 and 2 (section A-A1) are presented.

Figure 6.11 shows the displacement vectors for Model 1 (no ice lake) and Model 2 (ice lake), at loading step I (3 km ice). The maximum displacement is somewhat smaller for the model of ice lake than without ice lake. Contours of vertical displacements are shown in Figure 6.12. Fracture Zone 2 is compressed in Model 1 (no ice lake) whereas the zone appears to be, more or less, uneffected by ice loading for the case of no ice lake, Model 2. This indicates that the displacements that occur in Model 2 are related to elastic strains of the intact rock blocks rather than movement along discontinuities. The average strain for a profile ranging between 250 and 750 m level below surface, in the center of the model, amounts to 0.4 and 0.28 mm/m for Models 1 and 2 respectively.

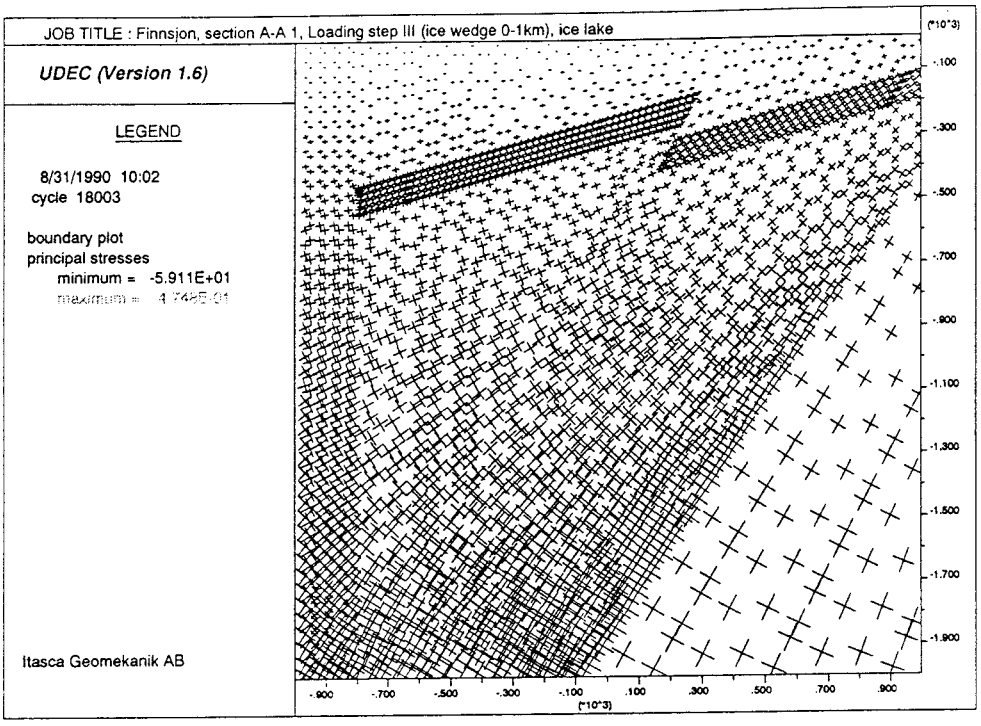

a)

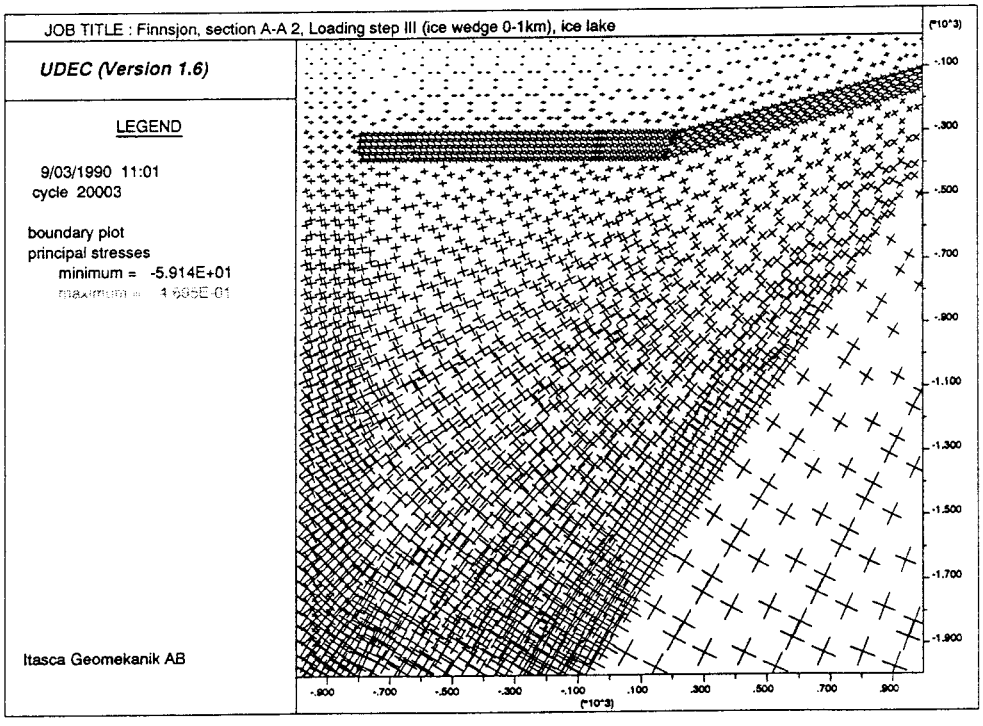

b)

Figure 6.10 Principal stress distribution, loading step III. a) Model 3, b) Model 4.

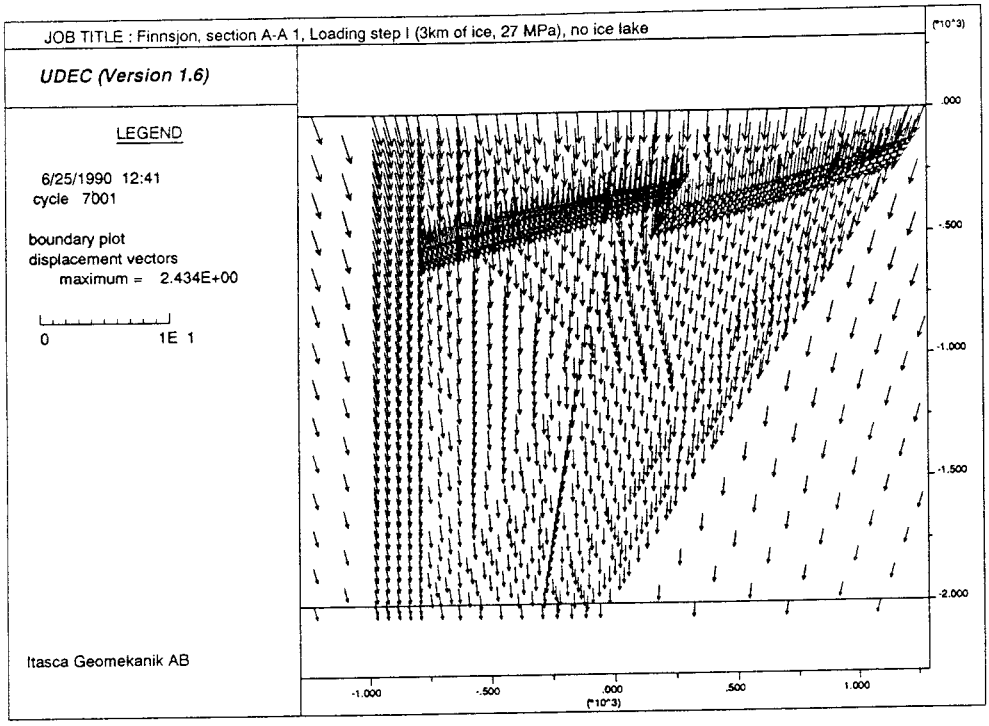

a)

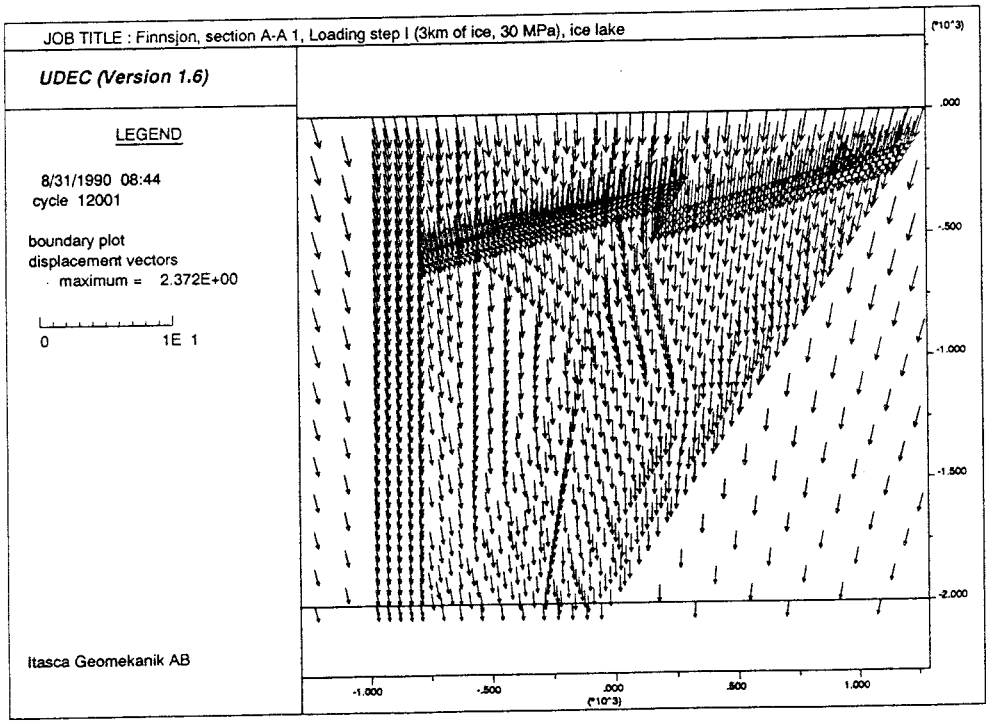

b)

Figure 6.11 Displacements vectors, loading step I. a) Model 1, b) Model 2.

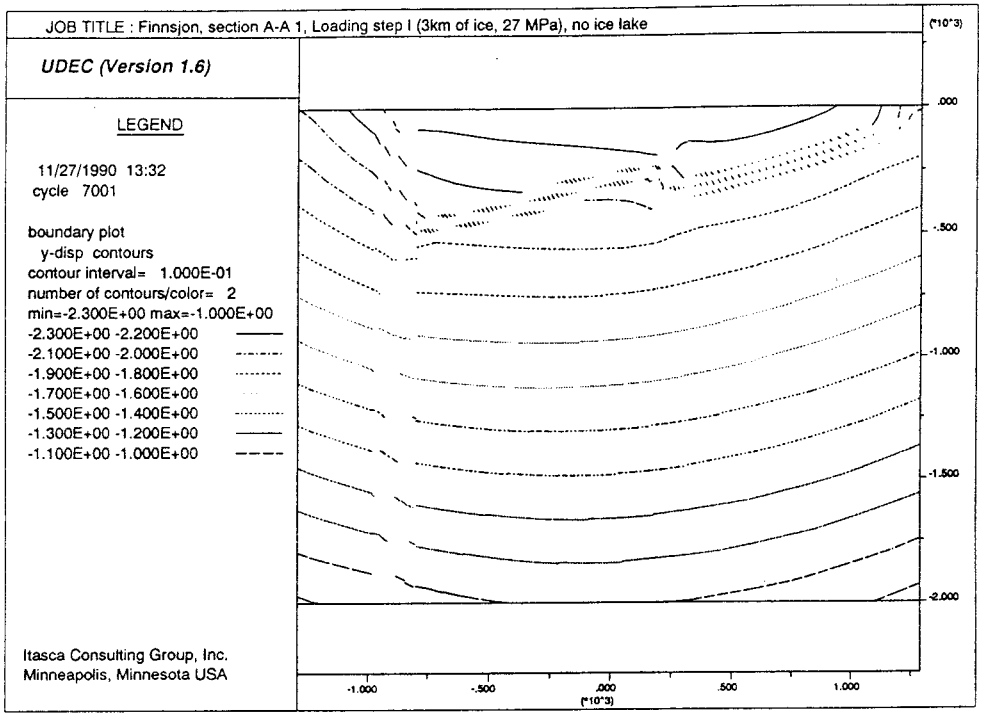

a)

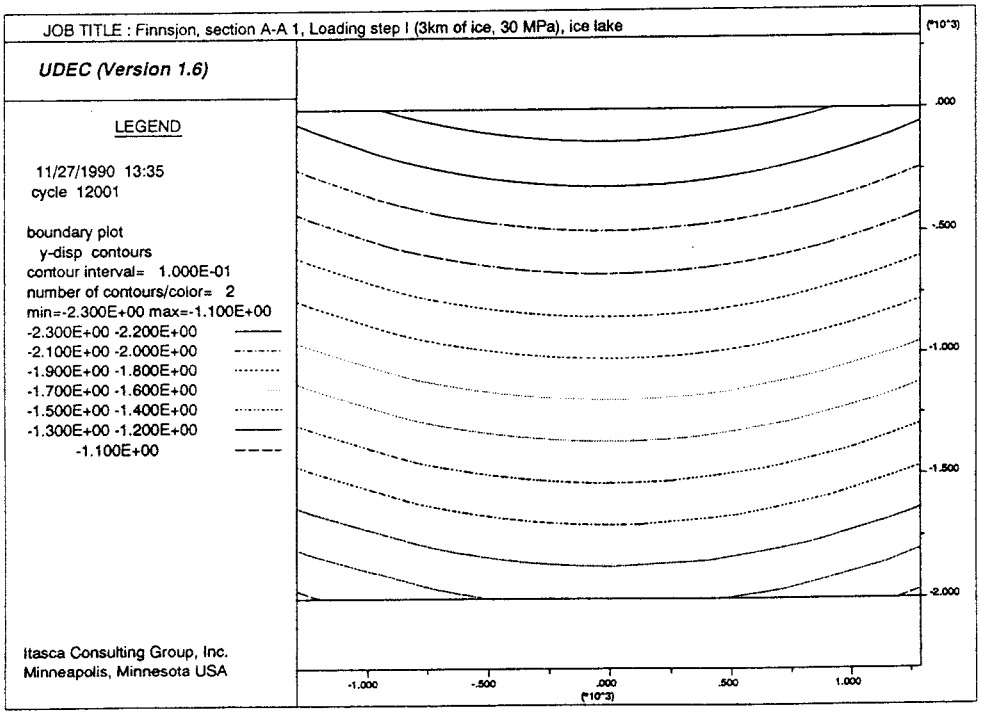

b)

Figure 6.12 Contours of vertical displacements loading step I. a) Model 1, b) Model 2.

To explore and explain the difference between the models it is worthwhile to study the difference in shear and normal displacements of the fracture zones. Let us take a closer look at the area in the models where Zone 2 is intersected by Zone 6. Figures 6.13 and 6.14 show the shear displacements and joint closures caused by loading step I. The thickness of the lines in these plots are directly proportional to the actual movement. Notice that different scales are used.

Model 1 (no ice lake) causes much larger shear displacement and closure of Zone 2. The major shearing occurs on subvertical fractures in Model 1 whereas it is the subhorizontal joints in Model 2 that constitute the major shearing. The maximum shear displacement, for the area studied in both models, takes place along a small segment of Zone 6. The maximum shear displacement in Model 1 is about seven times larger than that for Model 2.

The difference in joint closure within the studied area can be explained by the difference in pore pressure. The pore pressures in loading step I is 30 MPa higher for Model 2 compared with Model 1 and this inhibits compression of the joints.

Figure 6.15 shows the joint separation for Model 2 (ice lake). Model 1 does not display any joint separation, since no forces are imposed on the joints by the pore pressure.

Loading step II gives similar results of absolute displacements, vertical displacement contours, and shearing behavior in the rock mass for Model 1 and Model 2. However, for Model 2 the maximum shear displacement does not decrease when changing from loading step I to loading step II.

For loading step III (ice wedge), there are no significant differences in the displacement field between the two models, except that fracture Zone 2 compresses more beneath the ice wedge in Model 1 relative to Model 2. This is, again, a result of the difference in pore pressure. Figure 6.16 shows the displacement vectors and contours of the horizontal displacements for Model 1 (no ice lake). It appears that the rock mass moves upwards in the left part of the model and down in the right part. This produces shear strains and shear stresses in the model. The vertical shear strain along a horizontal line through the model, from the right edge of fracture Zone 14 to fracture Zone 4, at 500 m depth, amounts to about 0.3 mm/m. The corresponding horizontal strain is about 0.06 mm/m. The shear displacements of fractures are shown in Figure 6.17. Here it is seen that the shear displacements occur not only in the upper part of the model, but also in Zone 14 in the lower parts. A similar response was obtained for Model 2.

The final loading step (IV) shows very minor residual displacements for all four models. This indicates that elastic behavior is the main response of the models to glaciation.

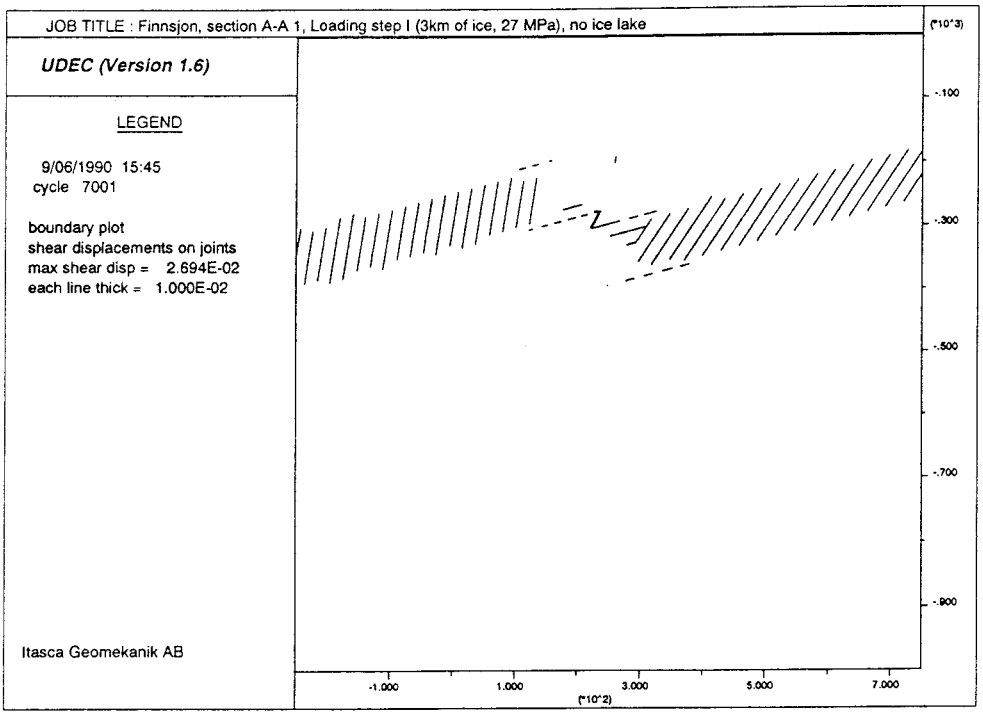

a)

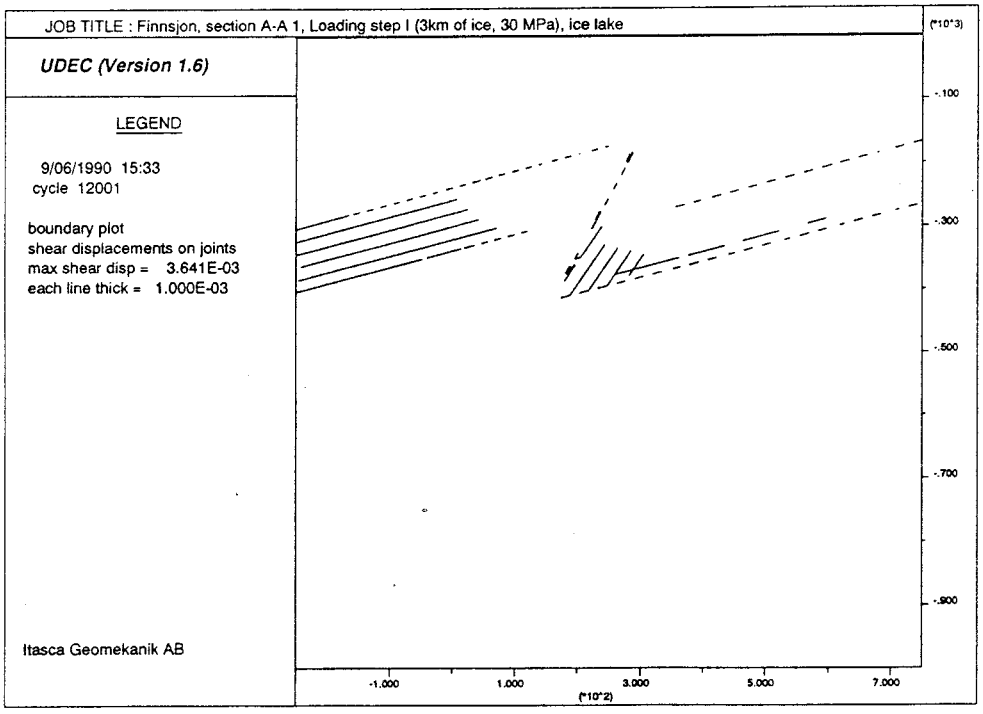

b)

Figure 6.13 Detail of shear displacements on joints in the vicinity of fracture Zone 2, loading step I. a) Model 1, b) Model 2.

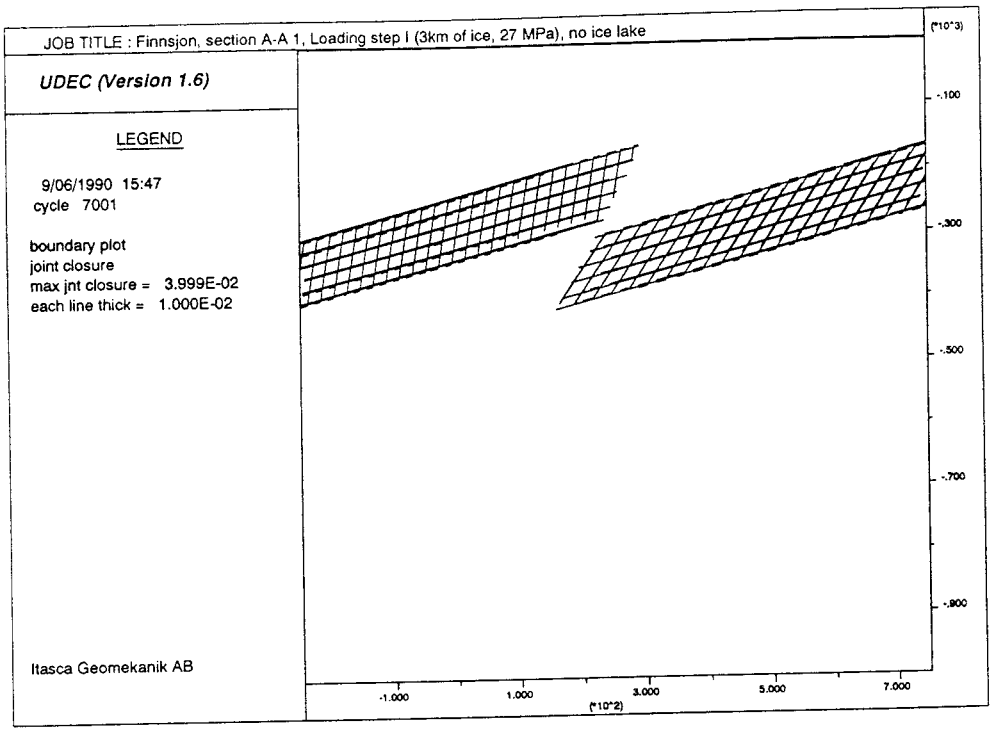

a)

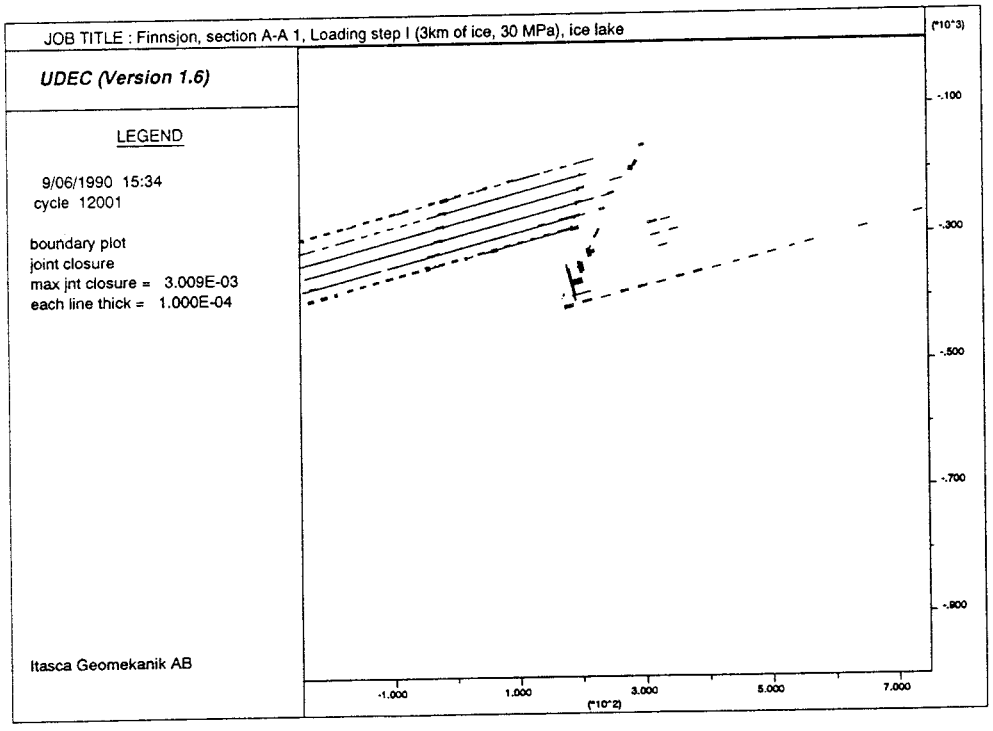

b)

Figure 6.14 Detail of joint closure in the vicinity of fracture Zone 2, loading step I. a) Model 1, b) Model 2.

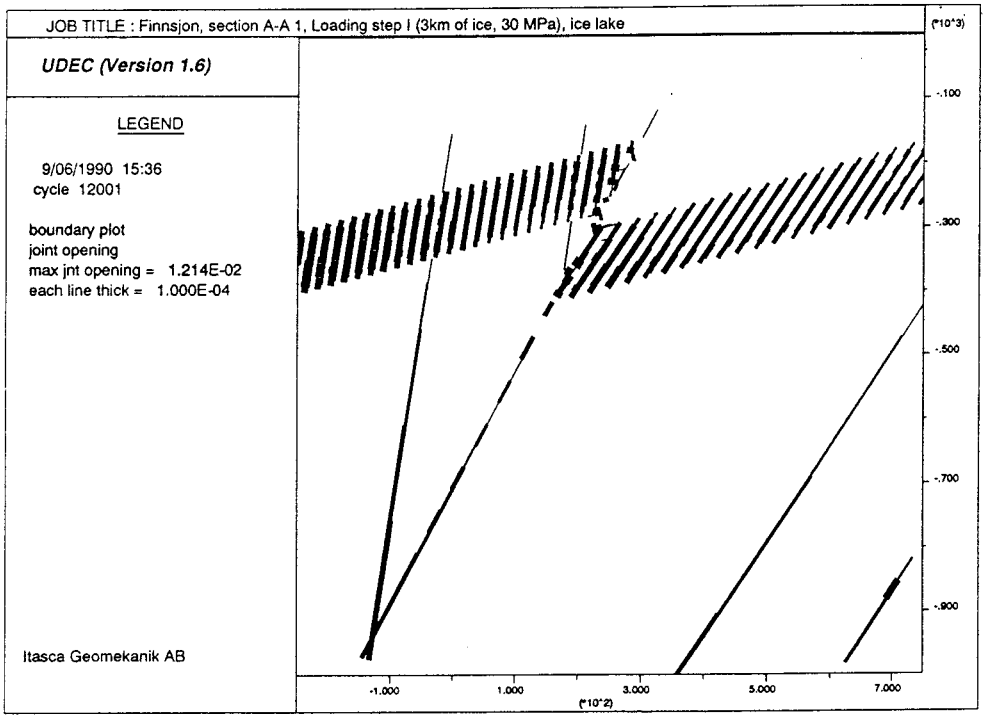

Figure 6.15 Detail of joint separation, loading step I, Model 2.

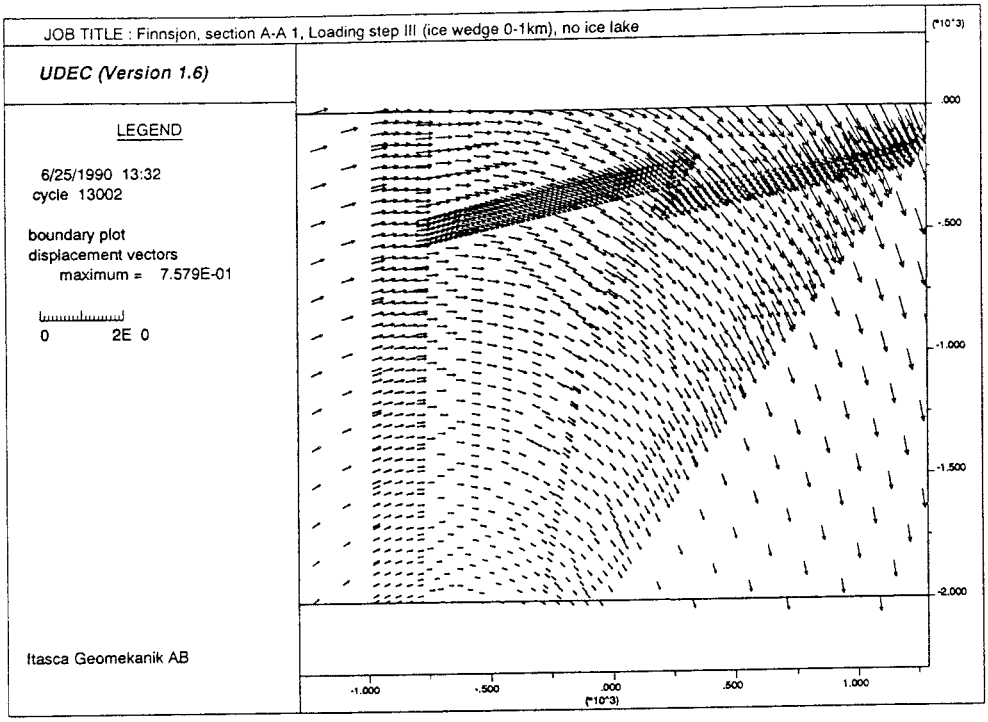

a)

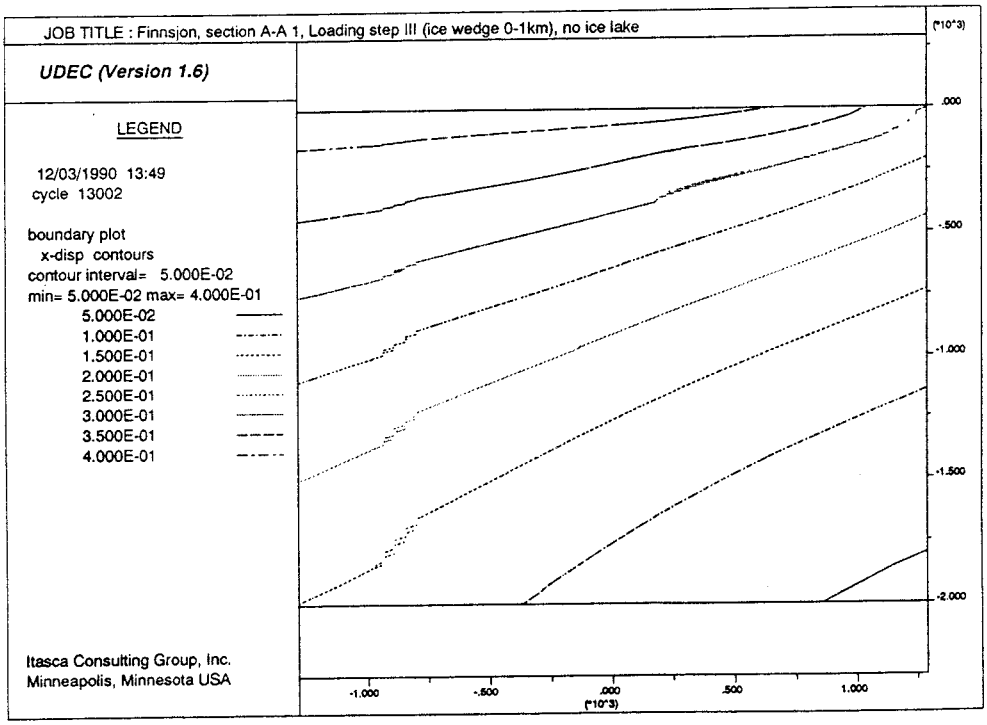

b)

Figure 6.16 Displacement field, loading step III, Model 1. a) displacement vectors, b) contours of horizontal displacement.

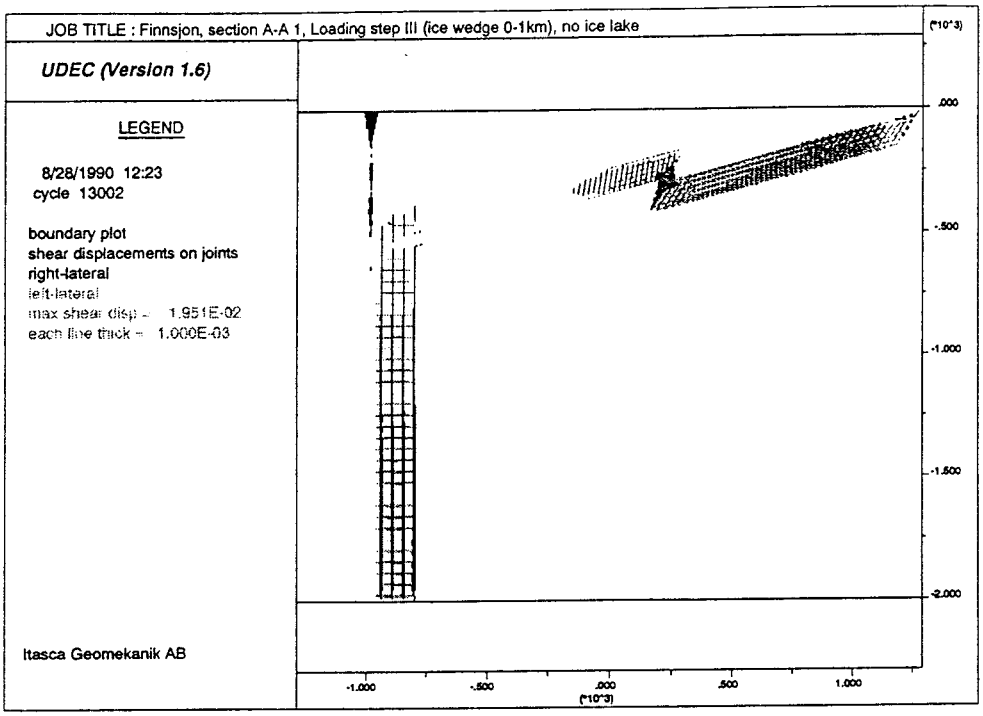

Figure 6.17 Shear displacements on joints, loading step III, Model 1.

6.2.3 Failure of fracture zones

When the shear or tensile strength of a fracture zone is exceeded, the zone fails. The constitutive model for the fracture used in this study makes it possible to plot these failed fracture zones. When looking at the following plots it is important to keep in mind that once a zone or a segment of a zone is failed, its failure remains. Although the stress state acting on the fracture surface may not correspond to that which caused the failure, the plots will still show the fractured zone for subsequent calculation cycles.

Like the displacements in the models, there is no significant difference in fracture zone failure for sections A-A1 and A-A2. Therefore section A-A 1 for Models 1 and 2 were selected to present the results.

Figures 6.18 and 6.19 show the extent of fractured joints and fracture zones in loading step I (3 km ice) and IV (no ice load) respectively. Figure 6.18 shows that Model 1 with the ice lake produces just slightly more failure than Model 2 with the ice lake. This was not expected since the shear capacity of the joints are controlled by the effective normal stress acting on the joint surface according to the following equation:

$$\tau = C + \sigma_n' \tan\phi \qquad (6.1)$$

where, τ = shear capacity, C = cohesion, σ_n' = effective normal stress, $\tan\phi$ = friction coefficient.

The effective normal stress is defined by the total normal stress minus the pore pressure. Therefore the shear capacity in the joints is lower in the ice lake models. More fracturing of joints can be expected for these models, since the loading on the rock surface was about the same as for models with hydrostatic pore pressure.

In order to give a reasonable explanation to the results, we consider the two rigid blocks and a discontinuity shown in Figure 6.20. For Case I, the applied vertical stress at the top of the model exceeds the total stress (existing joint pore pressure and effective normal stress). Consequently, the top of the model must displace downward to increase the effective normal stress in the discontinuity. However, problem kinematics requires that some shear displacement take place. Shear displacements cause shear stresses. If the shear stresses exceed the shear strength, the discontinuity fails. In Case II the applied vertical stress at the top of the model equals the existing total stress. Consequently, little if any displacement is required, since the problem is almost in equilibrium. As a result, the effective normal stresses in Case II should be less than in Case I. However, shear stresses should also be lower. Therefore, it is possible that the structure in Case II has lower effective normal stress than that in Case I, but no more failure.

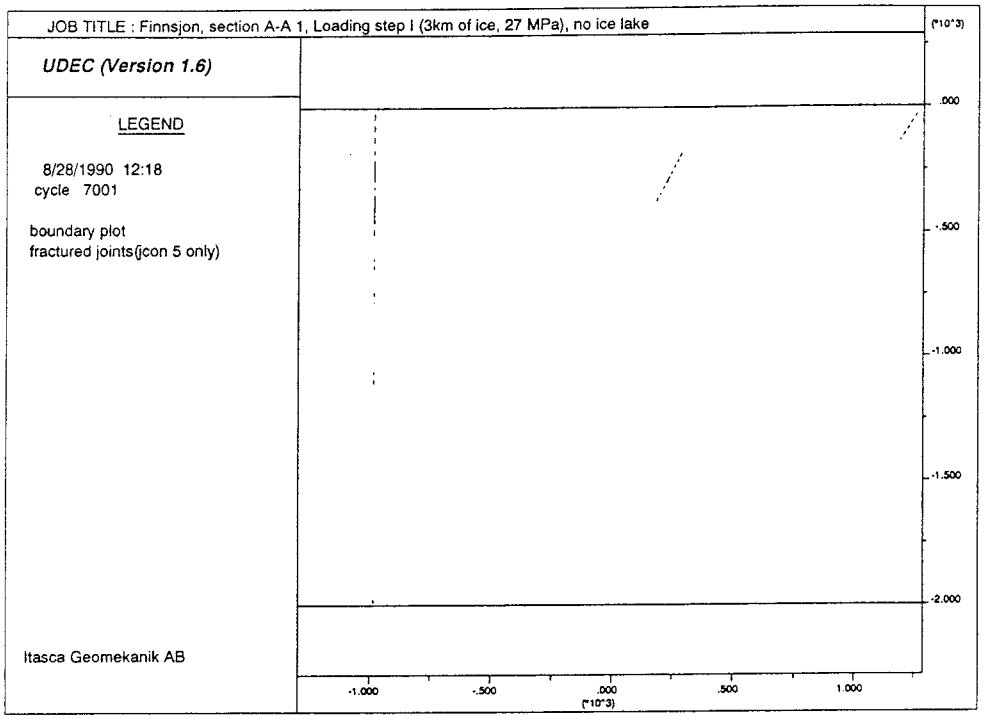

a)

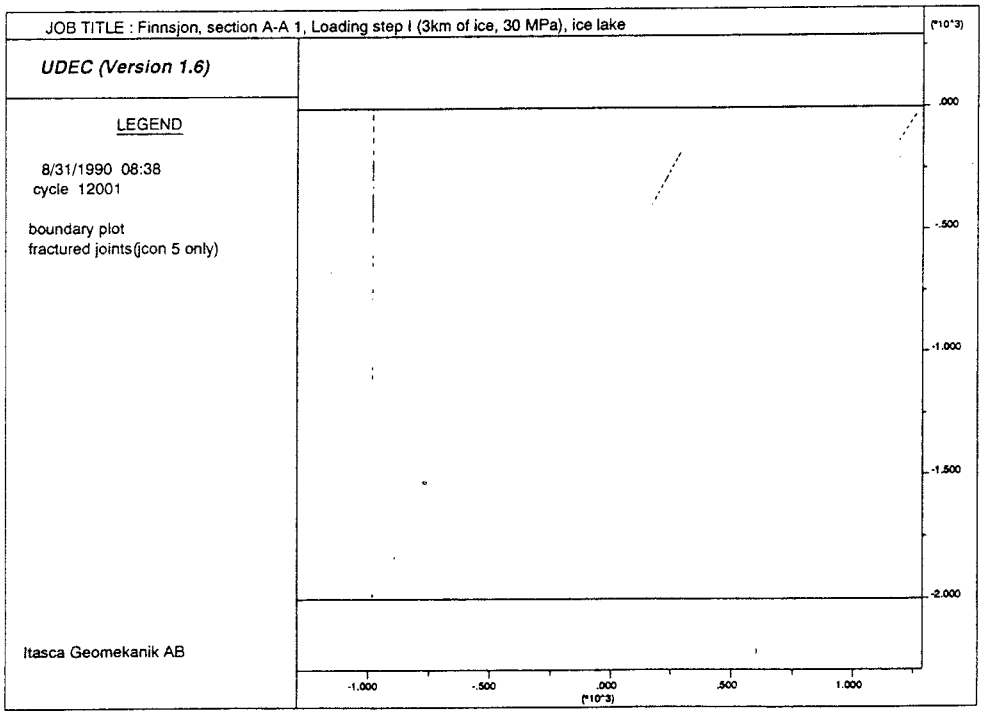

b)

Figure 6.18 Fractured joints, loading step I. a) Model 1, b) Model 2.

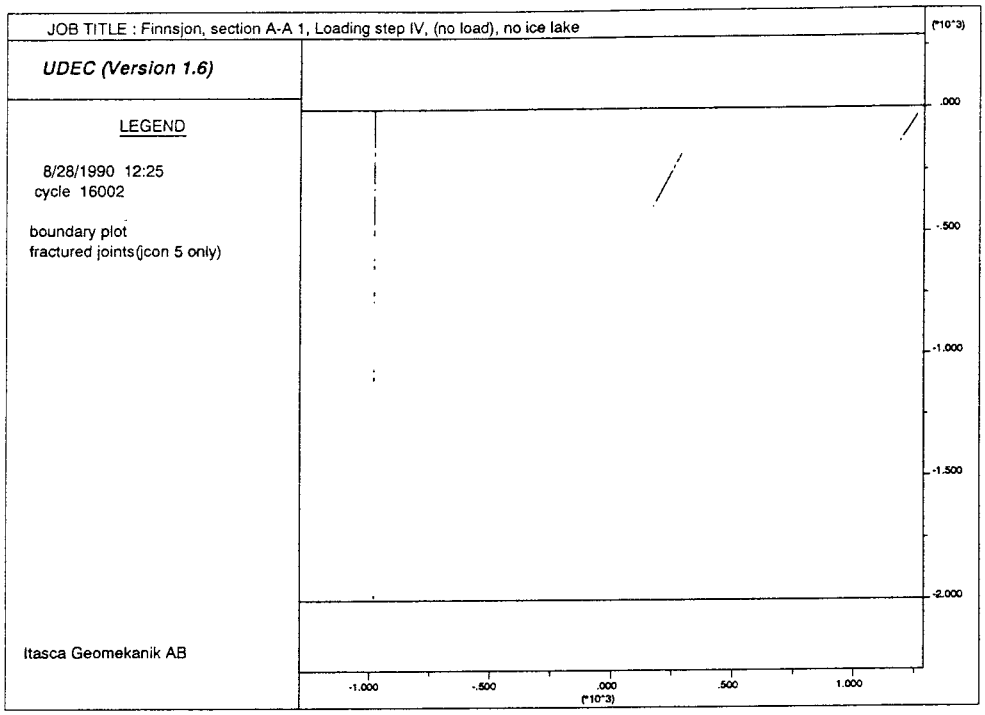

a)

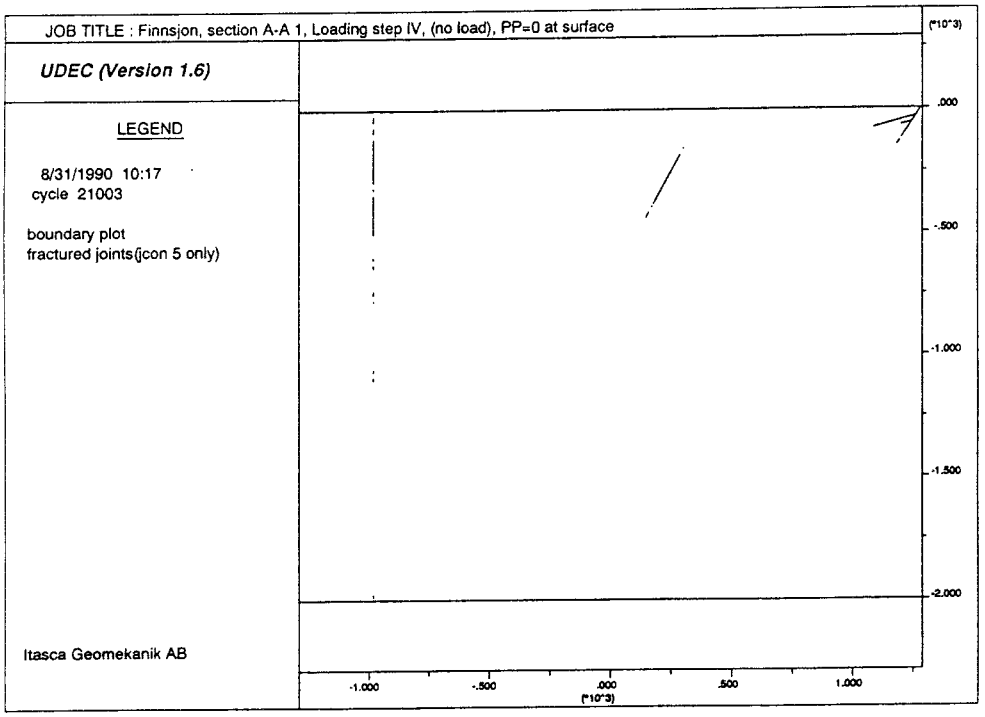

b)

Figure 6.19 Fractured joints, loading step IV. a) Model 1, b) Model 2.

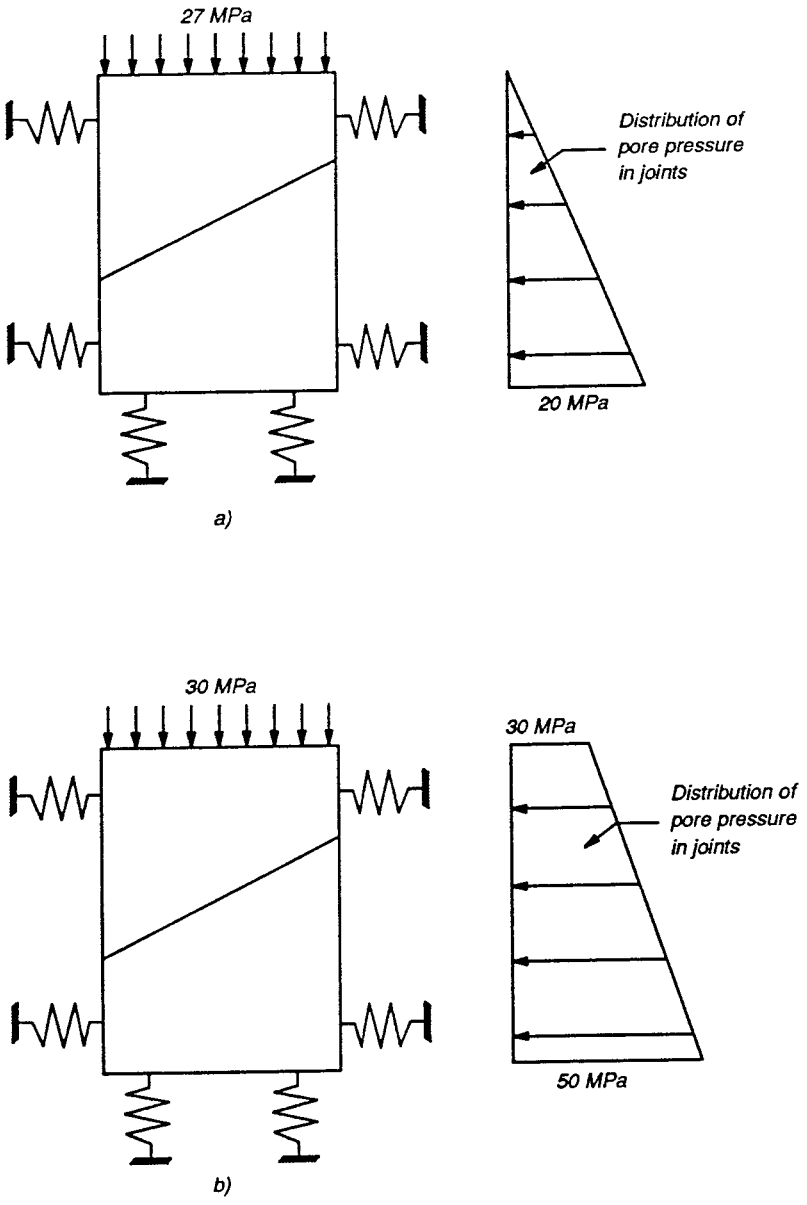

Figure 6.20 Simplified rigid block model. a) Case I (no ice lake), b) Case II (ice lake)

6.3 MODEL 5

6.3.1 Stress

The purpose of Model 5 was to simulate the subsidence and uplift of the earths crust synchronous with the ice loading and melting. Loading and boundary conditons for Model 5 are presented in Figure 5.8.

The loading of 3 km ice causes an excess of the stress in the model (Figure 6.21a) and above fracture zone 2. The fracture zone causes some minor changes of stress orientation, particularly at the off-set in the central part of the model. Notice the difference in state of stress for the

two boundary conditions in Model 1 and Model 6, cf. Figures 6.3 and 6.21a. After removal of the ice and glacial rebound to a final state of equilibrium (Figure 6.21b) the horizontal stresses become in excess of the vertical stress and with minor stress reorientation in the vicinity of fracture Zone 2. Also notice the almost isotropic state of stress at 500 m depth in the central part of the model.

Vertical stress, SYY, versus depth along profile no. 1 (X = 175 m) gave two interesting results, Figure 6.22. Firstly, only minor changes in vertical stress are due to the vertical displacements along the right boundary of the model, cf. loading steps I and II, and, II and IV. Secondly, the ice loading from 3 km ice causes a stress concentration in the vicinity of fracture Zone 2. Notice that the stress distribution is different from that obtained for Model 1 with boundary elements, cf. Figures 6.5a and 6.22. The maximum stress magnitudes are about the same, i.e. ~ 50 MPa. As melting takes place and the uplift reaches a stage of equilibrium the stresses at the fracture zone become less than that for the surrounding rocks. Glacial rebound can lead to a slight increase in the horizontal stress, SXX, (Figure 6.21b) as demonstrated for loading steps I and II, and steps III and IV. The tendency for stess changes in the vicinity of major fracture zones still remains, although the magnitudes are moderate.

6.3.2 Displacement

Loading of Model 5 with 3 km of ice and no ice lake gives a maximum vertical displacement of about 1.5 m (Figure 6.23a). A deeper model in the vertical direction and the same material properties will cause even larger displacements. Hence, the absolute displacements are of minor interest. After completing a glaciation cycle and associated crustal movements, remaining displacements of the order of 2.4 decimeter appear in the model, Figure 6.23b. The displacement pattern is also rather complicated with maximum displacement adjacent to the major fracture zone.

6.3.3 Failure of fracture zone

Of major interest for waste isolation is the failure and displacement of the major fracture zones. When loading the model with 3 km of ice only minor failure develops along the steep dipping fracture zones, Figure 6.24a. Subsidence of the crust results in only minor additional failure. The major change in failure appears as melting starts. Both some of the steep dipping fracture zones and the shallow dipping fracture Zone 2 fail and the failure takes place in the uppermost 1000 m of the crust, cf. Figure 6.24b. The failure of the fracture zones proceeds as melting continues and the situation for the last two loading steps are presented in Figure 6.25.

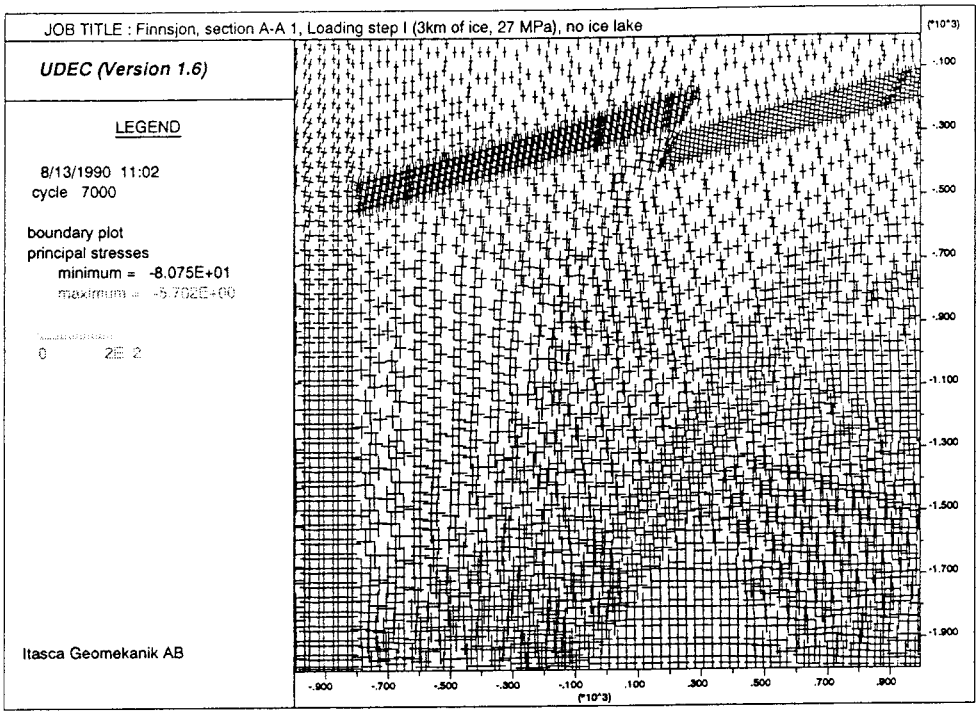

a)

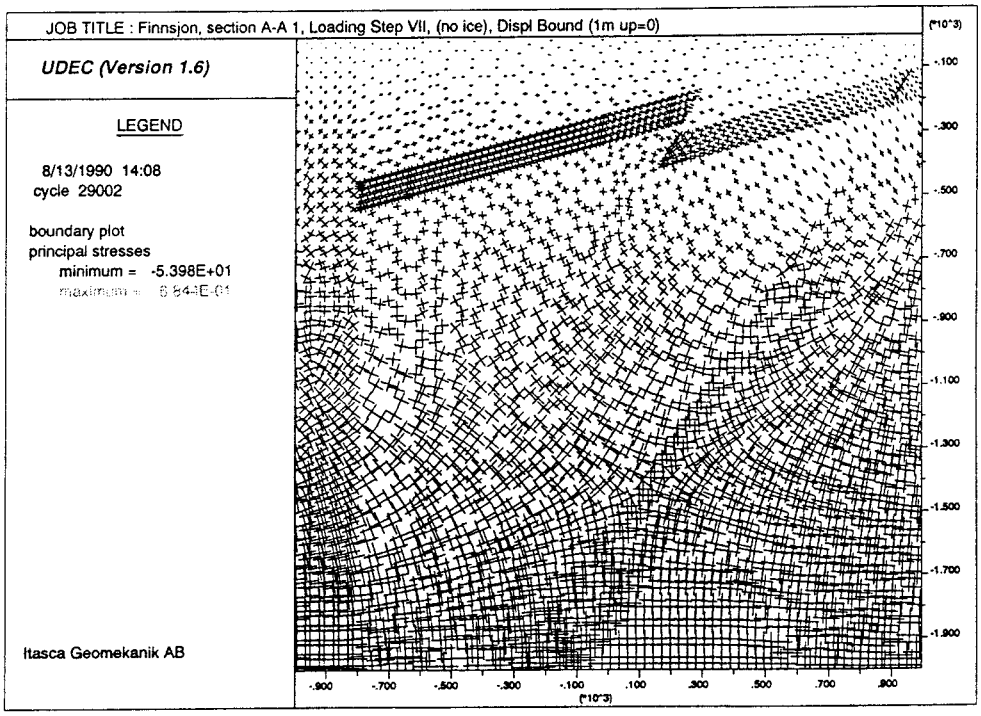

b)

Figure 6.21 Principal stresses for Model 5 without ice lake. a) loading step 1 with 3 km of ice, b) remaining stress after melting and complete glacial uplift.

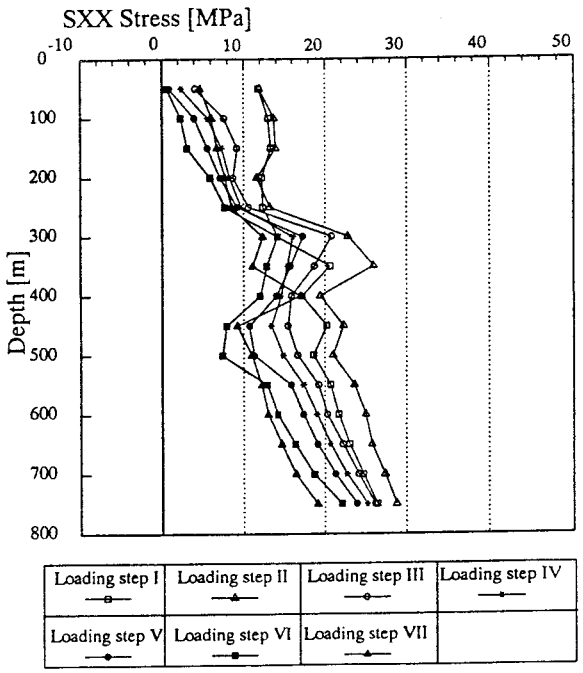

a)

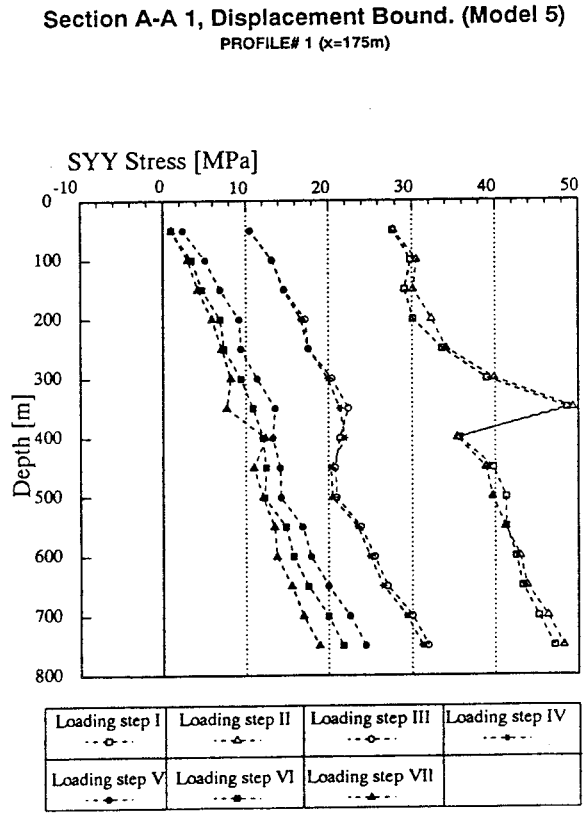

b)

Figure 6.22 Stresses versus depth along profile # 1, Model 5.
a) horizontal stress, SXX, b) vertical stress, SYY.

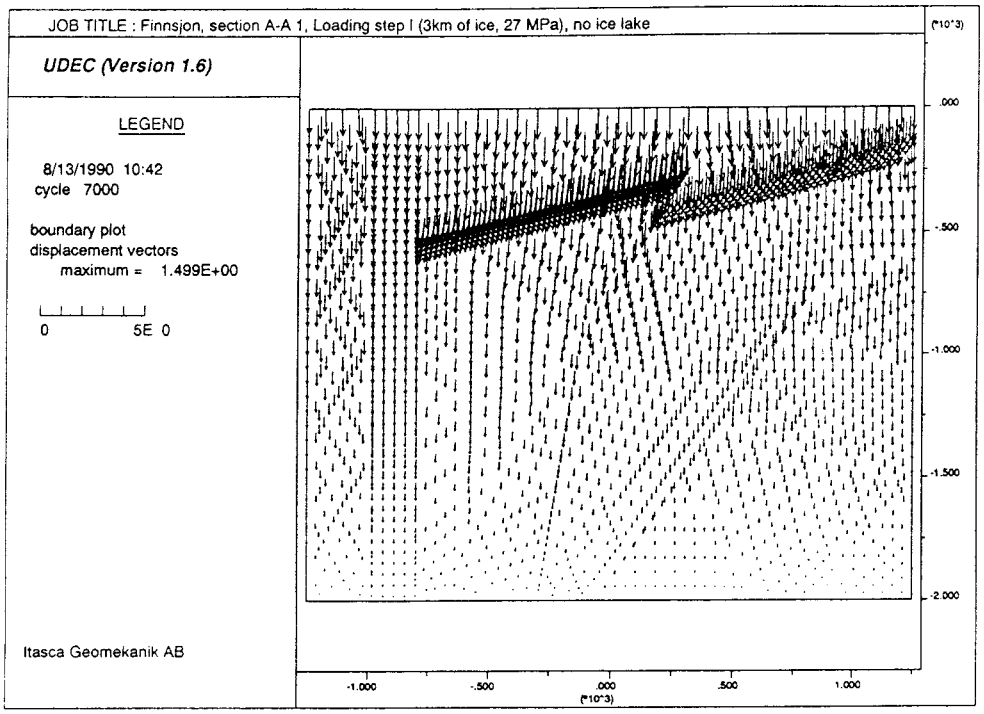

a)

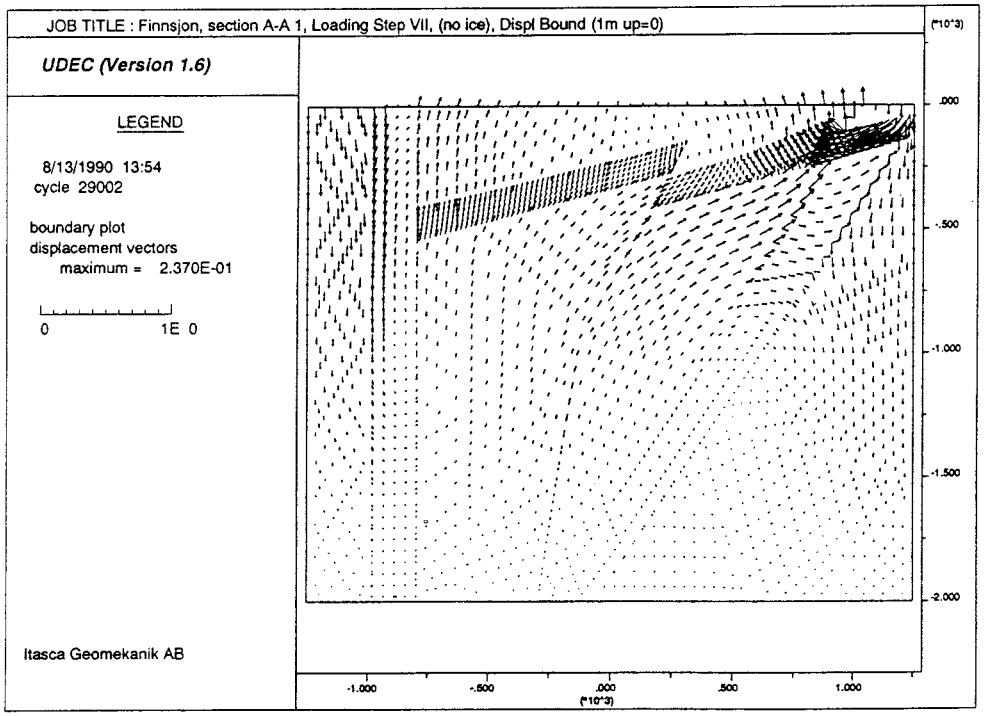

b)

Figure 6.23 Displacement vectors for Model 5. a) loading step I, 3 km of ice, b) loading step VII no ice load and equilibrium.

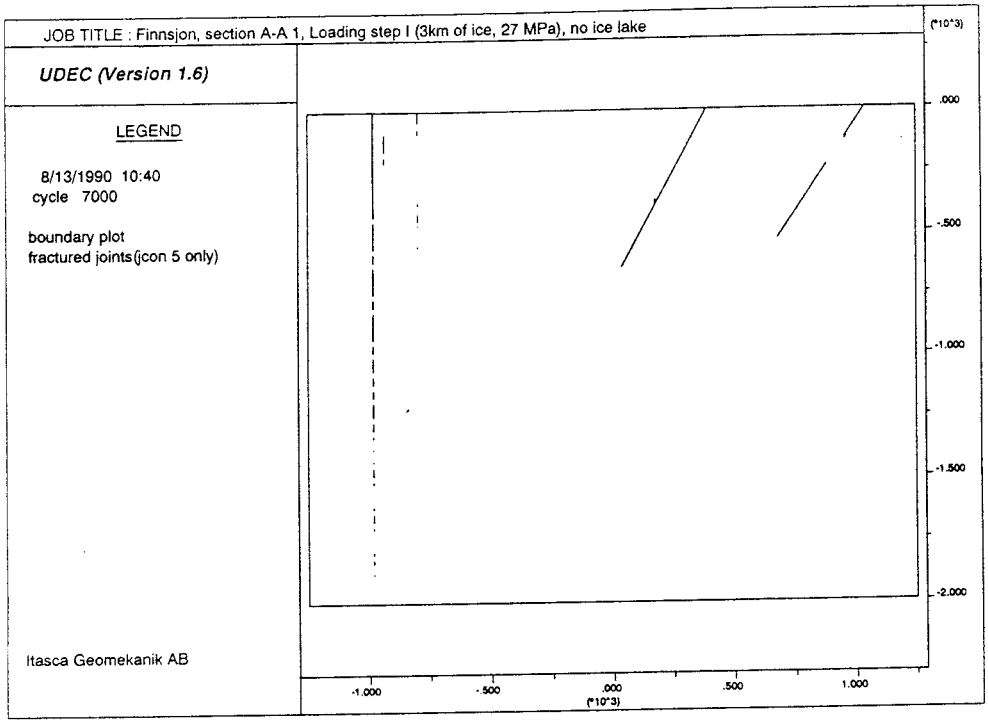

a)

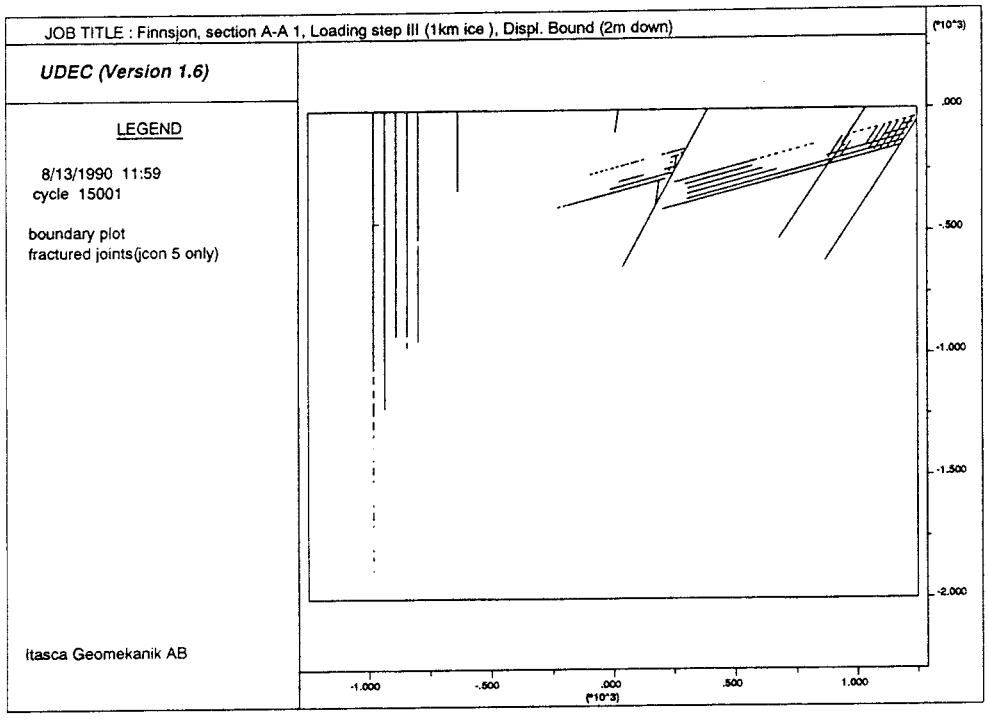

b)

Figure 6.24 Failure of fracture zones for Model 5. a) loading step I, b) loading step III. Notice the major increase in failure of fracture Zone 2 due to ice melting.

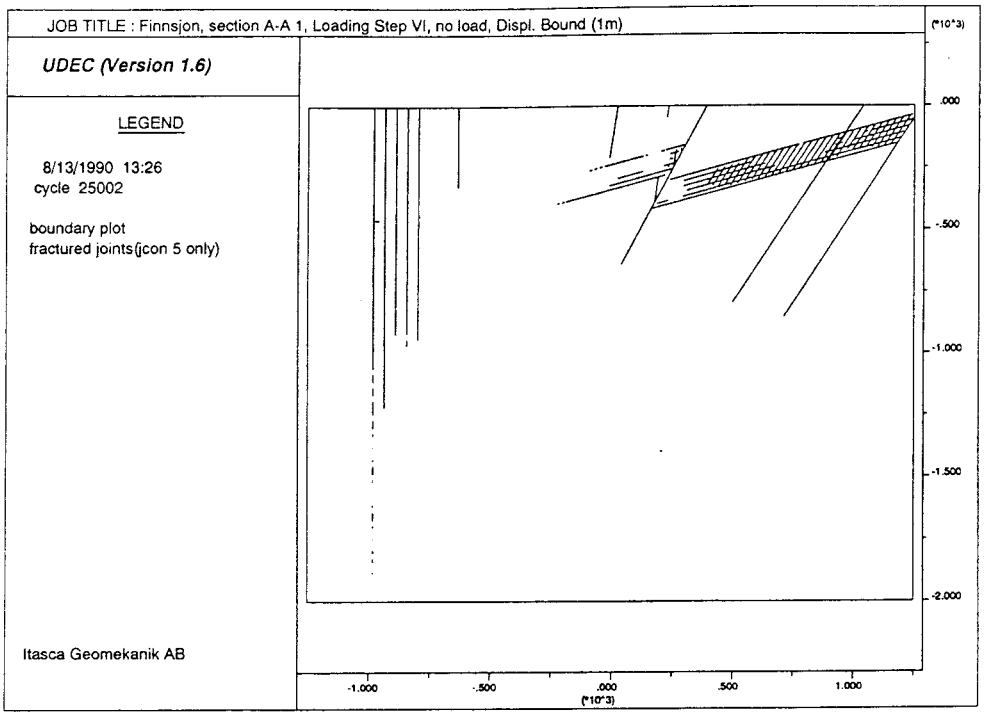

a)

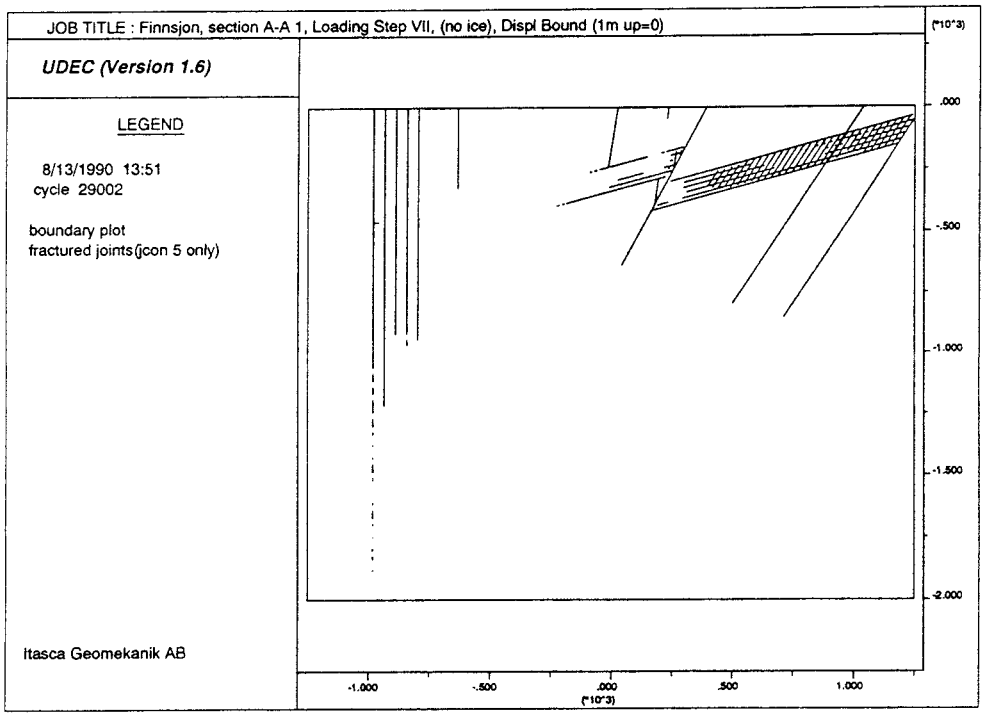

b)

Figure 6.25 Failure of fracture zones for Model 5. a) loading step VI, b) loading step VII. Notice the extensive failure of fracture Zone 2 due to a glaciation cycle.

6.4 MODEL 6

This analysis was added to the previous ones at a late stage of the study in order to explore in more detail the influence of different boundary conditions. Model 6 simulates the four loadig steps as prestented in Figure 5.7. In that respect it is identical with Model 1 and Model 3 (no ice lake). In Model 6 the displacement across the bottom boundary and the two vertical boundaries of the model is restricted, i.e. the model has rollers along the boundaries.

6.4.1 Stress

Horizontal and vertical stress versus depth for profiles No. 1 and 2 of Model 6 are shown in Figure 6.26. Here we notice a gentle stress increase with depth except for the disturbance along profile No. 1 at the intersection with fracture Zone 2. This disturbance is less pronounced than for the case with boundary elements in Model 1. The vertical stress SYY versus depth is almost identical for Model 1 and Model 6, cf. Figure 6.27. However, the horizontal stress SXX for the two models show major differences. The reason for this will be explored in more detail in the discussion, Chapter 7. Here we can observe that the horizontal state of stress due to the ice loading is of the same magnitude as the vertical stress for Model 1 with boundary elements. Roller boundaries in Model 6 result in horizontal stresses that are about one third of the vertical stress from the ice load.

6.4.2 Displacement

Displacements from loading Model 6 with 3 km of ice and no ice load after a complete glaciation cycle are depicted in Figure 6.28. Notice the vertical displacements from ice loading and the restricted displacements to the area above fracture Zone 2 after ice melting.

6.4.3 Failure of fracture zone

When loading the model with 3 km of ice, failure appears preferentially along the steeply dipping fracture zones. Unloading does not cause any additional failure and fracture Zone 2 remains intact, Figure 6.29. These results demonstrate that most of the displacements and failure of fracture Zone 2 recorded in Model 5 are due to the imposed vertical displacement, cf. Figures 6.25 and 6.29.

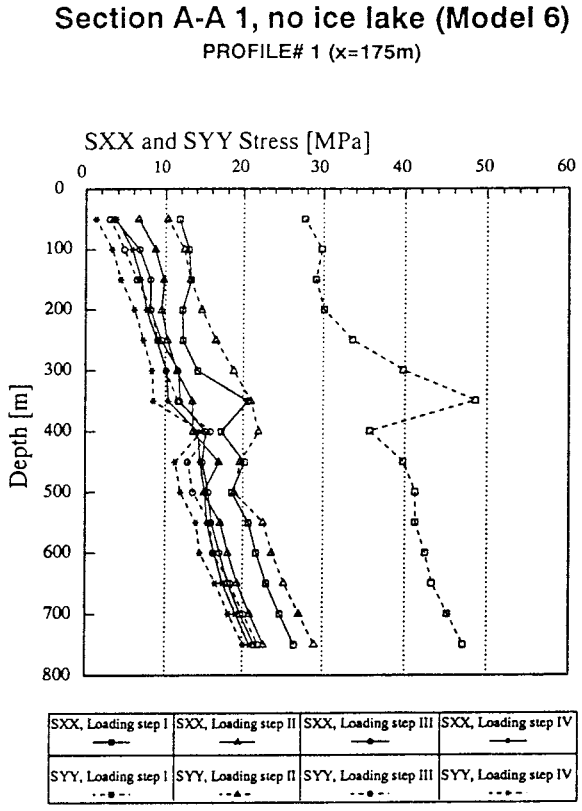

a)

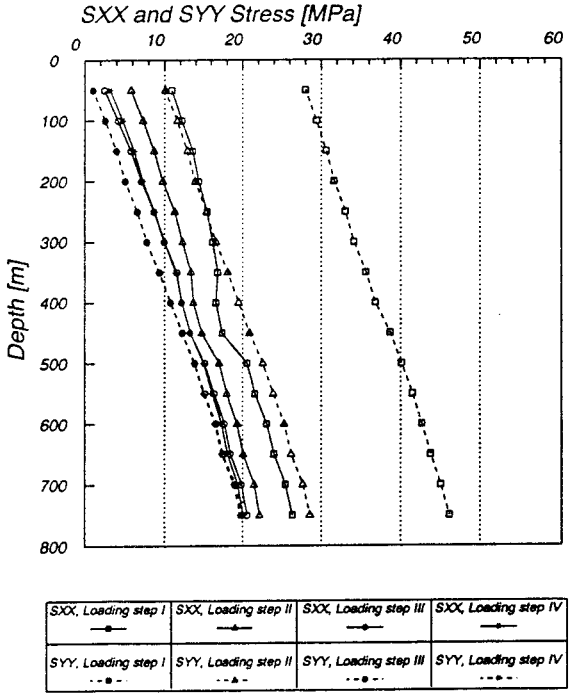

b)

Figure 6.26 Horizontal stress, SXX, and vertical stress, SYY, versus depth, Model 6. a) profile # 1, b) profile # 2.

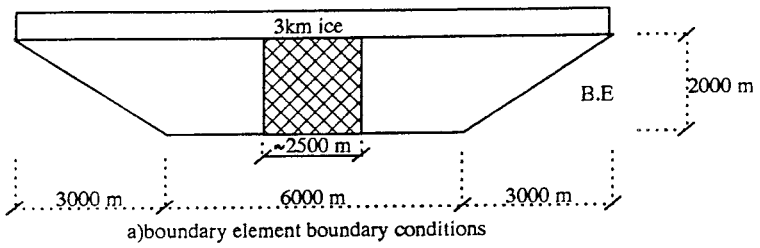

a)boundary element boundary conditions

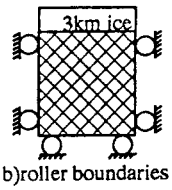

b)roller boundaries

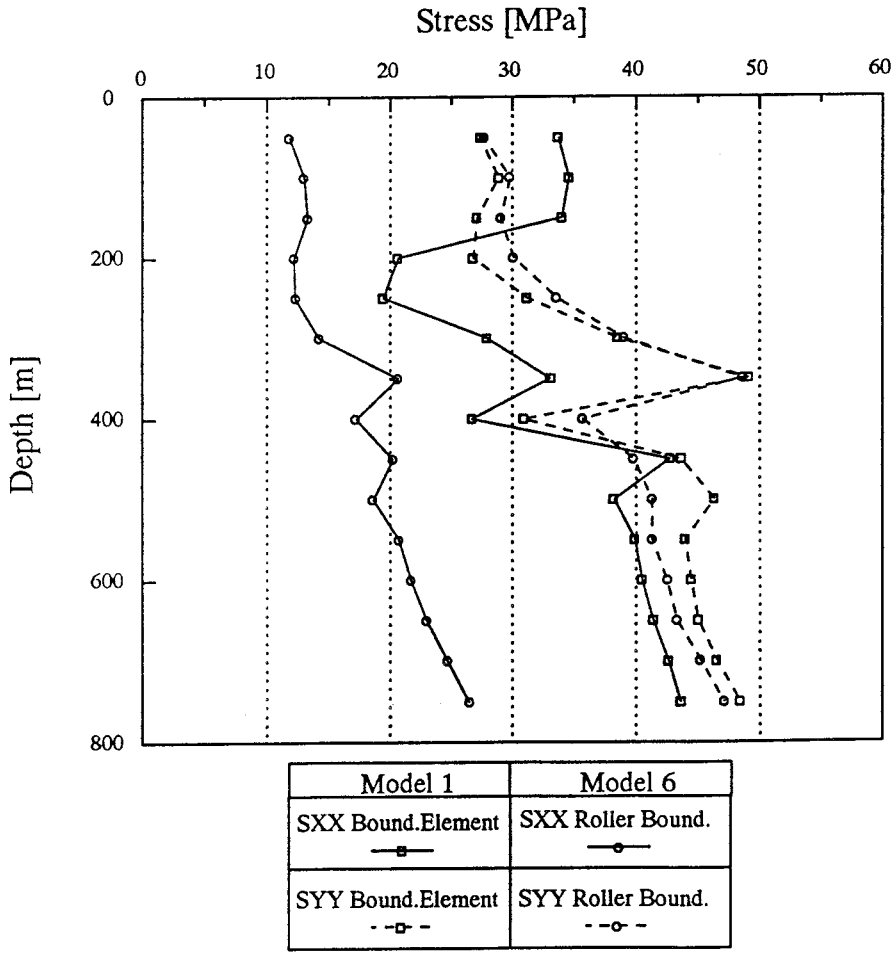

Figure 6.27 Comparison of stresses for Model 1 and Model 6, at profile # 1, loading step I.

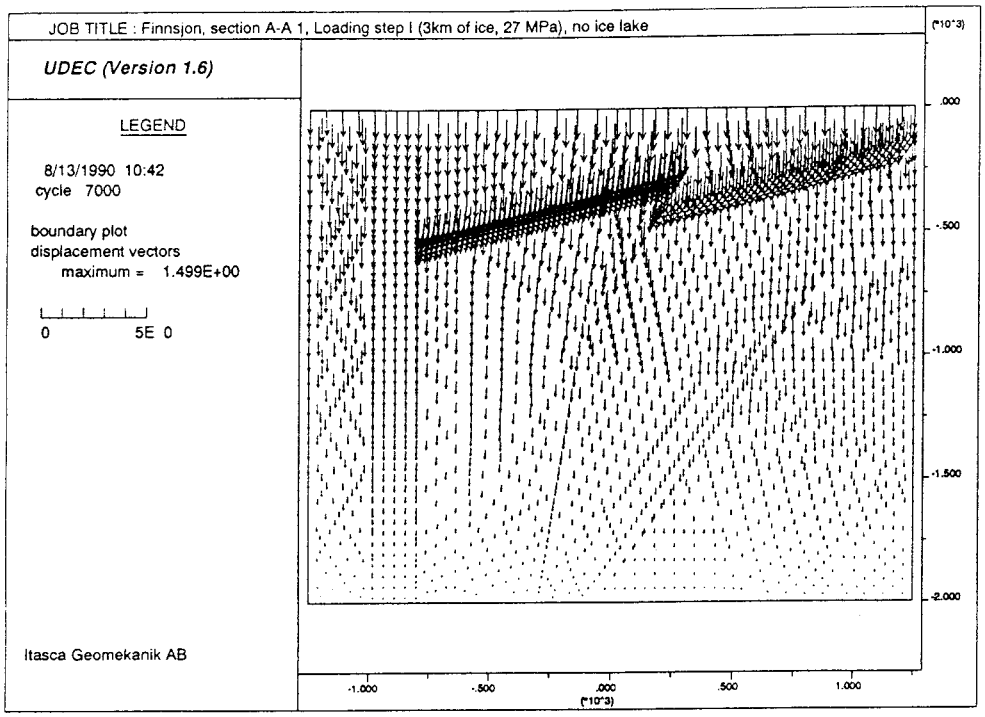

a)

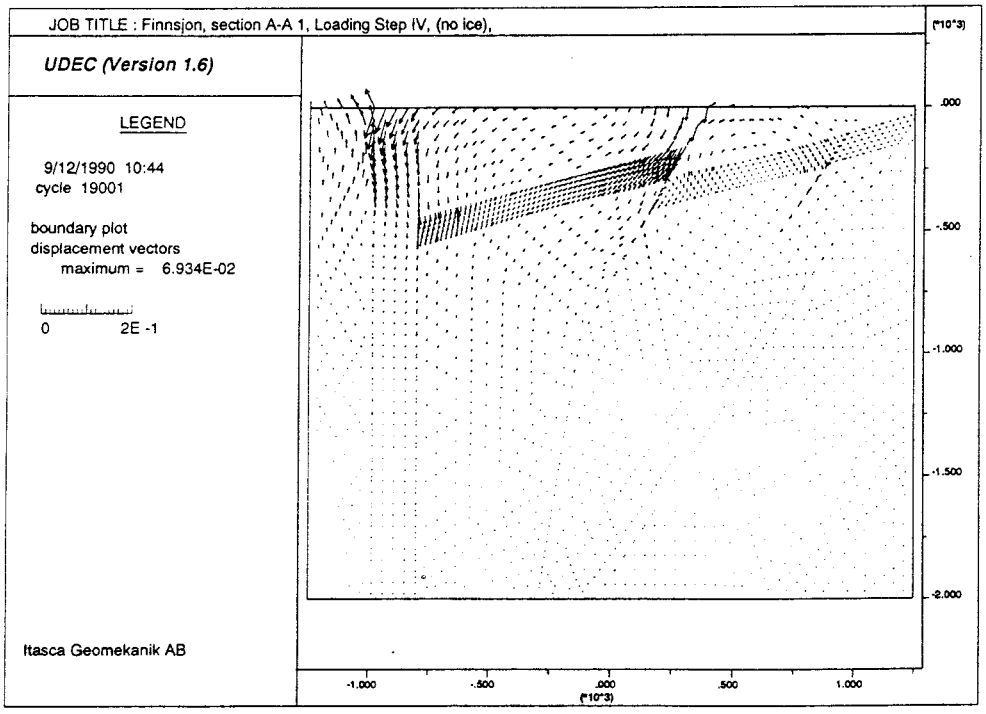

b)

Figure 6.28 Displacement vectors for Model 6, roller boundaries. a) loading step I, 3 km of ice, b) loading step IV, no ice load and equilibrium.

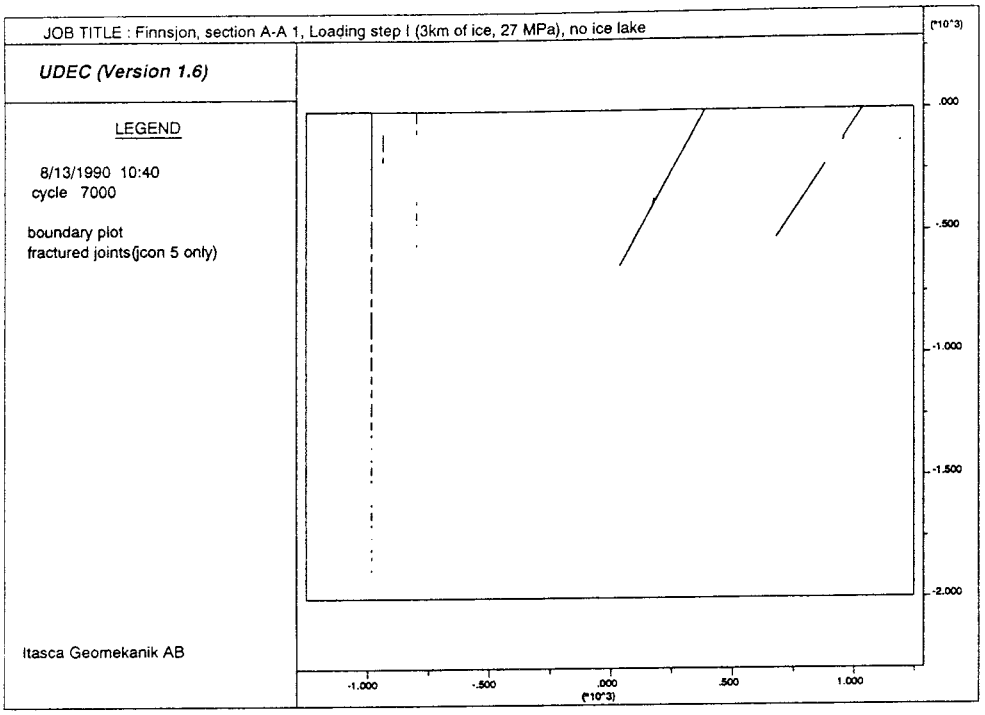

a)

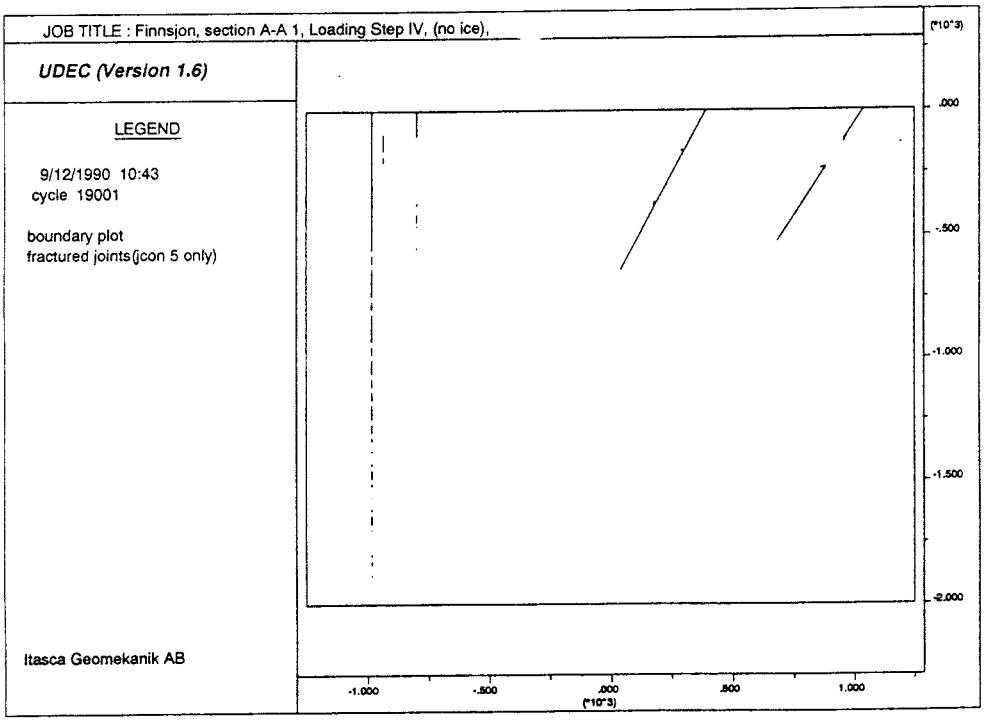

b)

Figure 6.29 Failure of fracture zones for Model 6. a) loading step I, b) loading step IV (no ice). Notice the minor change in failure for the two cases.

7 DISCUSSION

In the discussion of the results obtained in this study the following issues are of importance:

- Boundary conditions
- Geometry of fracture Zone 2
- Effects of an ice lake
- Location of a repository

7.1 BOUNDARY CONDITIONS

The major discrepancies in horizontal stresses for model with boundary elements (Models 1-4) and models with roller boundaries with isostatic displacements (Model 5) and without isostatic displacements (Model 6) clearly illustrate the importance of proper boundary conditions. This is a cardinal problem in rock mechanics modelling and needs to be explored. One way is to look for analytical solutions.

The analytical solution to the state of stress at an arbitrary point of an infinite halfspace of elastic material subjected to a two-dimensional (i.e. strip) loading, q (Figure 7.1), is given by the following equations:

$$\Delta\sigma_x=\frac{q}{2\pi}\left[2\left(\rho_1-\rho_2\right)-\left(\sin 2\rho_1-\sin 2\rho_2\right)\right] \qquad (7.1)$$

$$\Delta\sigma_y=\frac{q}{2\pi}\left[2\left(\rho_1-\rho_2\right)+\left(\sin 2\rho_1-\sin 2\rho_2\right)\right] \qquad (7.2)$$

where, $\Delta\sigma_x$ and $\Delta\sigma_y$ are the horizontal and vertical stress components, respectively, and 2a is the width of the load.

The analytical solution of the state of stress due to the loading has to be superimposed on the virgin rock stress as govern by eqs. (3.1) and (3.4). The calculated total horizontal stress, SXX, versus depth from the load of 3 km ice (27 MPa) for an ice sheet with the width a = 6 km and a = 500 km is shown in Figure 7.2. The analytical solution and the UDEC modelling with boundaries of boundary elements for the same width of a = 6 km the distributed load are almost identical. As the width of the ice sheet is increased to a = 500 km stress versus depth will increase. UDEC modelling with roller boundaries like Model 6 give much less horizontal stress for the same width of the ice load, Figure 7.2. This analysis illustrates the dilemma. When boundary elements are applied we obtain a result which is in agreement with the analytical solution according to eqs. (7.1) and (7.2).

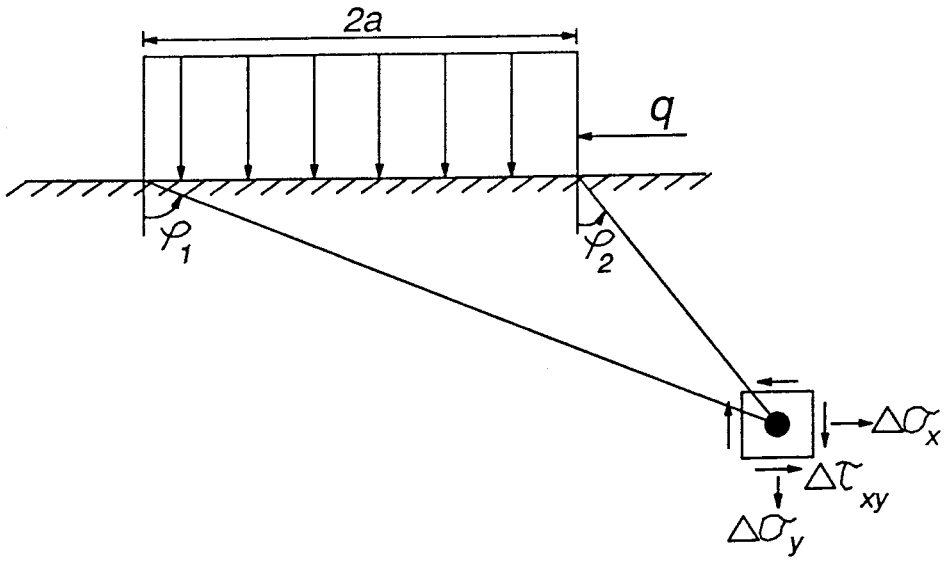

Figure 7.1 State of stress at a point of an infinite halfspace subjected to a finite uniformly distributed strip load, q.

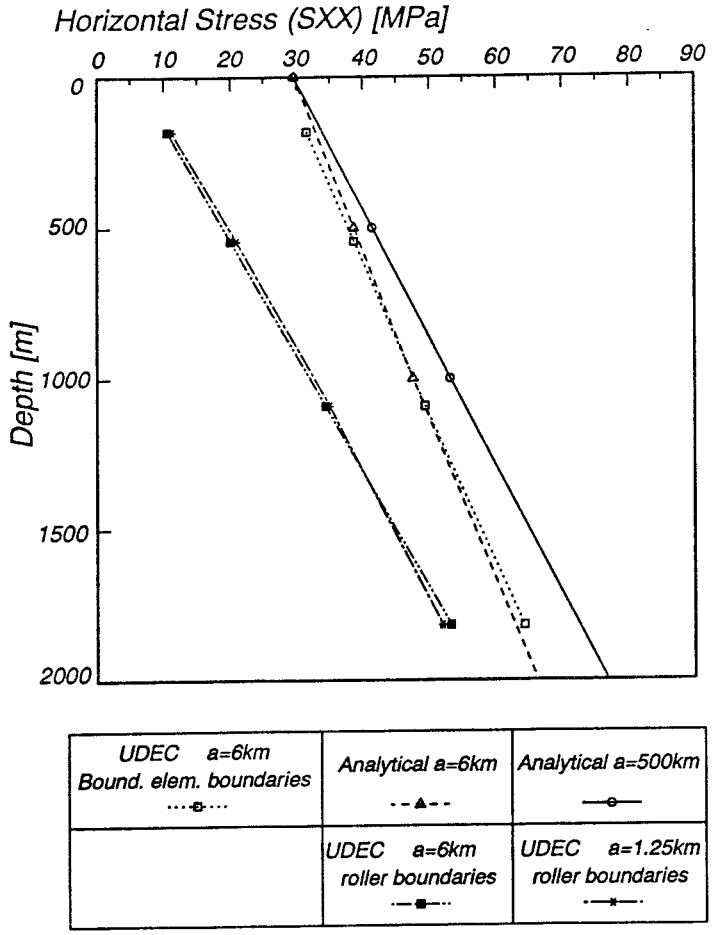

Figure 7.2 Analytical and numerical results of horizontal stress versus depth for a 3 km thick ice sheet assuming elastic conditions. Notice the good agreement between analytical solutions and UDEC models with boundary elements at the boundary of the models.

If we use roller boundaries and zero lateral displacements we only obtain the Poisson's effect which cause a lateral stress, σ_x, that is proportional to a function of Poisson's ratio of the rock material and the applied vertical stress

$$\sigma_X = \frac{\nu}{1-\nu}\sigma_Y \qquad (7.3)$$

where, ν is the Poisson's ratio.

We do not know for sure which of these assumptions is correct because no one has been measuring stresses beneath an ice sheet. It might well be that the most realistic state of horizontal stress underneath an ice sheet is an average between the two extremes depicted in Figure 7.2.

Except stress discontinuities adjacent to the major fracture zones the vertical stress, SYY, versus depth remain similar despite the boundary conditions, cf. Figures 6.5, 6.26 and 6.27.

7.2 GEOMETRY OF FRACTURE ZONE 2

In modelling the rock mass response to ice loading and melting a particular cross section of the Finnsjön site was chosen. Due to uncertainties in the interpretation of the diamond coring data two geometries of the sub-horizontal fracture Zone 2 have been modelled. Results from modelling the two geometries of fracture Zone 2 do not indicate any noticable differences in stresses, displacements and failure of fracture zones. There is no reason to believe that an application of another geometry of fracture Zone 2 to models with roller boundaries and displacement boundaries (Models 5 and 6) would cause any noticable difference in results.

7.3 EFFECTS OF AN ICE LAKE

In modelling the effect of an ice lake, the lake can be located on top of the ice sheet or be a subglacial lake located at the rock-ice interface. Models 2 and 4 simulate the effects of the ice lake. In Section 6.2.3 the importance of absolute stress and effective stress was discussed and the reduction in strength of a fracture zone was illustrated by means of a simple block model, Figure 6.20.

The results of models simulating an ice lake and high pore pressure in the fracture zones gave almost the same amount of failure of fracture zones as for models without ice lake. The influence of an ice lake has not been studied for models with roller boundaries and/or displacements along the boundaries. However, there is no reason to believe that the introduction of ice lake and pore pressure would drastically change the results.

7.4 LOCATION OF A REPOSITORY

Results from this study clearly demonstrates the stress discontinuities and stress concentrations adjacent to major fracture zones. This might

increase the stresses as high as 40-50 MPa at 300 m depth when an ice sheet is resting on the ground surface, cf. Figure 6.5. As pore pressure from an ice lake starts to act in the fracture zones the horizontal and vertical stresses tend to become equal and shear stresses are diminished, cf. Figure 6.6. Although shear stresses are diminish opening of fracture zones take plae, cf. Figure 6.15. Fracture zone opening and failure of fracture zones is most pronounced for models with roller boundaries and isostatic displacements (Model 5). Here we notice a major increase in failure of fracture Zone 2 due to ice melting and isostatic displacement (Figures 6.24 and 6.25). However, most of the failure is located to fracture Zone 2.

The state of virgin stress and the stress increase due to ice loading, normal and shear displacements of fracture zones, and the stress concentration and failure of fracture zones, demonstrates the need for a protection zone between the repository and the major discontinuities. Engineering judgement and the results of the modelling and in particular the stresses versus depth, a protection zone of 100 m width from the outer boundary of the discontinuity to the repository location is recommended. A repository located between fracture Zones 1, 5 and 14 at Finnsjön should be located at a depth of about 600-650 m in the case of section A-A1. This value will be reduced to 500-550 m in the case of section A-A2.

8 CONCLUSIONS AND RECOMMENDATIONS

Six models of a cross section of the Finnsjön test site have been simulated by means of distinct element analysis and the computer code UDEC. The rock mass response to glaciation, isostatic movements and water pressure from an ice lake have been simulated.

The conclusions presented here are of course only valid for the conditions and assumptions presented in Section 5. This means that if the modelling was preformed under different conditions and/or assumptions, the results might be different.

- The results of the modelling is sensitive to the selected boundary conditions. For four of the models (Models 1-4) a boundary condition with boundary elements was specified for the bottom and sides of the models. This gives a state of stress inside the model (under elastic conditions) which agrees very well with the analytical solution of the state of stress in an infinite halfspace subjected to a finite uniformly distributed load. This approach gives a stress state where the horizontal and vertical stress versus depth are of the same order of magnitude. Roller boundaries along the bottom boundary and the two vertical boundaries (Model 6) gave less horizontal stress. No stress measurements exist below large ice sheets to confirm which of the two approaches is correct. Isostatic movements corresponding to the expected magnitude from future glaciations were applied to the right and bottom boundary of the distinct element model (Model 5).

- Due to uncertainties in the interpretation of borehole data two geometries of the sub-horizontal fracture Zone 2 have been modelled. Results from modelling the two different geometries (Models 1-4) do not show any noticable differences in stresses, displacements and failure of fracture zones.

- Under normal pore pressure conditions in the rock mass, the weight of the ice load increases the vertical stress in proportion to the thickness of the ice sheet. The horizontal stresses differ depending on the selected boundary conditions (cf. Figures 6.5, 6.26 and 6.27). Major stress discontinuities exist in the vicinity of the fracture zones and these should be accounted for in siting of a radioactive waste repository, cf. Figure 6.5.

- A lake situated on top of the ice sheet and connected to the underlying rock mass or a lake at the rock/ice interface will increase the pore pressure in the fracture zones. The effective stresses acting in the models (Models 2 and 4) tend to make the state of stress more isostatic, cf. Figure 6.6 and the stress discontinuities in the vicinity of the fracture zones diminish.

- Most of the displacements of fracture zones in Models 1-4 are taken up by Zone 2 (cf. Figure 6.13 and 6.14). Zone 14, i.e. the vertical fracture zone at the left hand side of the model, showed the next most amount of shear and normal displacement.

- Future displacements due to glaciation and deglaciation is most likely to occur in existing fracture zones. The average vertical strain between

250 m and 750 m level below surface amounts to 0.3 mm/m from loading of 3 km of ice in Model 1-4.

- The strength of the fracture zones are given in accordance with the Coulomb slip criterion. Models with boundary elements (Models 1-4 show minor failure along the steeply dipping fracture zones (cf. Figures 6.18, 6.19 and 6.29).

- Calculated displacements and stresses are sensitive to selected parameters of joint stiffnesses, rock deformability and strength. The best estimated parameter values for Swedish bedrocks have been applied in this study. A sensitivity analysis for the most critical parameters in the modelling will enhance the understanding of the rock mass response to glaciation.

- Simulation of isostatic movements in combination with ice loading and ice melting (Model 5) gave several new and interesting results. Stress discontinuities and large displacement appear at the major fracture zones. Subsidence of the crust adds only minor failure of fracture zones compared to the situation with only ice loading. The major change in failure appears when melting simulation is initiated. The shallow dipping fracture Zone 2 and some of the steeply dipping zones fail and the failure is located to the uppermost ~ 1000 m of the crust.

- The state of virgin stress and the stress increase due to ice loading, deformation and failure of fracture zones prove the need for a protection zone between the repository and the major discontinuties. A protection zone of ~ 100 m width from the outer boundary of the discontinuity to the repository location is suggested. This value is based on results showing that the stress disturbance diminishes at this distance from the outer boundary of the discontinuity.

- A repository located between fracture Zones 1,5 and 14 and below fracture Zone 2 at Finnsjön is recommended to be located at a depth of about 600-650 m in the case of section A-A1. In the case of section A-A2 this value will be decreased to 500-550 m.

- The results of this study demonstrates the need for further development of the distinct element method and the UDEC code. The code should handle boundary elements at the boundary of the models and allow for synchronous displacements of the boundary in order to simulate isostatic movements of the crust. Further, it would be a great improvement if the code allowed for loading of the boundary element surface outside the distinct element domain.

9 ACKNOWLEDGEMENTS

Thanks are due to Loren Lorig of Itasca, Minneapolis, for stimulating discussions about the boundary conditions for models of this study and for the improving of the content in this report.

10 REFERENCES

Ahlbom, K. and Smellie, J.A.T. (Eds.) 1989. Characterization of fracture Zone 2, Finnsjön Study Site. SKB Technical Report 89-16, 6 parts. Swedish Nuclear Fuel and Waste Management Company, Stockholm.

Ahlbom, K. and Tirén, S. 1989. Overview of geologic and hydrogeologic character of the Finnsjön Site and its surroundings. Technical Report IRAP 89206, Swedish Geological, Uppsala.

Andersson, J-E., Ekman, L. Nordqvist, R. and Winberg, A. 1989. Hydrogeological conditions in the Finnsjön area. Compilation of data and conceptual model. SKB Working Report R & D 89-24, Swedish Nuclear Fuel and Waste Management Company, Stockholm.

Axelsson, K. 1983. Kontinuumsmekanik. Kompendium. Division of Structural Engineering, Luleå University of Technology, Luleå.

Bjarnason, B. and Stephansson, O. 1988. Hydraulic fracturing stress measurements in Borehole Fi-6 Finnsjön study site, Central Sweden. SKB Working Report R & D 88-54, Swedish Nuclear Fuel and Waste Management Company, Stockholm.

Board, M. 1989. UDEC (Universal Distinct Element Code) Version ICG 1.5. Software Summary. Prepared for U.S. Nuclear Regulatory Commission. NUREG/CR-5429, Vol. 1.

Bäckblom, G. and Stanfors R. (Eds.) 1989. Interdisciplinary study of post-glacial faulting in the Lansjärv area, Northern Sweden, 1986-1988. SKB Technical Report 89-31, Swedish Nuclear Fuel and Waste Management Company, Stockholm.

Cundall, P.A. 1971. A computer model for simulating progressive large scale movements in blocky rock systems. In: Proc. Symp. International Society for Rock Mechanics, Nancy, France, 1971, Vol. 1, Paper No. II-8.

Cundall, P.A. 1980. UDEC - A generalized distinct element program for modelling jointed rock. Peter Cundall Associates, Report PCAR-1-80. Report to U.S. Army, European Research Office, Contract DAJA 37-79-C-0548.

Eronen, M. and Olander, H. 1990. On the World's ice ages and changing environments. University of Helsinki. Report YJT-90-13, Nuclear Waste Commission of Finnish Power Companies, Helsinki.

Itasca. 1990. UDEC, Version ICG1.6, Vol. I, User's manual.

Itasca. 1990. UDEC, Version ICG1.6, Vol. II, Verification and example problems.

Jing, L. and Stephansson, O. 1988. Distinct element modelling of the influence of glaciation and deglaciation of the state of stress in faulted rock masses. SKB Arbetsrapport 88-12, Swedish Nuclear Fuel and Waste Management Company, Stockholm.

Kakkuri, J. 1986. Newest results obtained in studying the Fennoscandian land uplift phenomenon. Tectonophysics, Vol. 130, pp. 317-331.

Koerner, F.M. 1984. Conditions at the ice/rock interface of large ice sheets. In: W.F. Heinrich (Ed.) Workshop on Transitional Processes. Whiteshell Nuclear Research Establishment, Pinawa, Manitoba, Canada, pp. 200-211.

Lemos, J. 1987. A distinct element model for dynamic analysis of jointed rock with application to dam foundations and fault motion. Ph.D. Thesis, University of Minnesota, Minneapolis.

Muir Wood, R. 1989. Extraordinary deglaciation reverse faulting in Northern Fennoscandia. In: S. Gregersen and P.W. Basham (Eds.) Earthquakes at North-Atlantic passive Margins: Neotectonics and postglacial rebound. Kluwe Academic Publishers, pp. 141-173.

Mörner, N. 1979. The Fennoscandian uplift and Late Cenozoic geodynamics: Geological evidence. Geol. Journal, 3.3, pp. 287-318.

Rosengren, L. 1989. Numerical modeling of stress distribution and joint behaviour around the ventilation drift at Stripa Mine. Stripa Project, Phase B. IGAB Report for Clay Technology AB, Lund.

Stephansson, O., Särkää, P. and Myrvang, A. 1986. State of stress in Fennoscandia. In: O. Stephansson (Ed.) Proc. Int. Symp. on Rock Stress and Rock Stress Measurements, Centek Publishers, Luleå, pp. 21-32.

Stephansson, O. 1987. Modelling of crustal rock mechanics for radioactive waste storage in Fennoscandia - Problem definition. SKB Technical Report 87-11, Swedish Nuclear Fuel and Waste Management Company, Stockholm.

Stephansson, O. and Shen, B. 1990. Rock mass response to glaciation and thermal loading from nuclear waste. In: K. Andersson (Ed.) GEOVAL'90. (in press)

Swedish Nuclear Fuel and Waste Management Company. 1986. Final storage of nuclear fuel. Research and Development Program 1987-1992. SKB R & D Program 86. Swedish Nuclear Fuel and Waste Management Company, Stockholm.

Swedish Nuclear Fuel and Waste Management Company. 1989. SKB R & D Program 1989. Program for research and development and other measures. Swedish Nuclear Fuel and Waste Management Company, Stockholm.

Vonhof, J.A. 1984. Potential hydrodynamic effects of glaciation on the Canadian Shield. In: W.F. Heinrich (Ed.) Workshop on Transitional Processes. Whiteshell Nuclear Research Establishment, Pinawa, Manitoba, Canada, pp. 212-228.

List of SKB reports

Annual Reports

1977-78
TR 121
KBS Technical Reports 1 – 120
Summaries
Stockholm, May 1979

1979
TR 79-28
The KBS Annual Report 1979
KBS Technical Reports 79-01 – 79-27
Summaries
Stockholm, March 1980

1980
TR 80-26
The KBS Annual Report 1980
KBS Technical Reports 80-01 – 80-25
Summaries
Stockholm, March 1981

1981
TR 81-17
The KBS Annual Report 1981
KBS Technical Reports 81-01 – 81-16
Summaries
Stockholm, April 1982

1982
TR 82-28
The KBS Annual Report 1982
KBS Technical Reports 82-01 – 82-27
Summaries
Stockholm, July 1983

1983
TR 83-77
The KBS Annual Report 1983
KBS Technical Reports 83-01 – 83-76
Summaries
Stockholm, June 1984

1984
TR 85-01
Annual Research and Development Report 1984
Including Summaries of Technical Reports Issued during 1984. (Technical Reports 84-01 – 84-19)
Stockholm, June 1985

1985
TR 85-20
Annual Research and Development Report 1985
Including Summaries of Technical Reports Issued during 1985. (Technical Reports 85-01 – 85-19)
Stockholm, May 1986

1986
TR 86-31
SKB Annual Report 1986
Including Summaries of Technical Reports Issued during 1986
Stockholm, May 1987

1987
TR 87-33
SKB Annual Report 1987
Including Summaries of Technical Reports Issued during 1987
Stockholm, May 1988

1988
TR 88-32
SKB Annual Report 1988
Including Summaries of Technical Reports Issued during 1988
Stockholm, May 1989

1989
TR 89-40
SKB Annual Report 1989
Including Summaries of Technical Reports Issued during 1989
Stockholm, May 1990

Technical Reports
List of SKB Technical Reports 1990

TR 90-01
FARF31 –
A far field radionuclide migration code for use with the PROPER package
Sven Norman[1], Nils Kjellbert[2]
[1]Starprog AB
[2]SKB AB
January 1990

TR 90-02
Source terms, isolation and radiological consequences of carbon-14 waste in the Swedish SFR repository
Rolf Hesböl, Ignasi Puigdomenech, Sverker Evans
Studsvik Nuclear
January 1990

TR 90-03
Uncertainties in repository performance from spatial variability of hydraulic conductivities –
Statistical estimation and stochastic simulation using PROPER
Lars Lovius[1], Sven Norman[1], Nils Kjellbert[2]
[1]Starprog AB
[2]SKB AB
February 1990

TR 90-24
The Poços de Caldas Project: Summary and implications for radioactive waste management
N. A. Chapman[1], I. G. McKinley[2], M. E. Shea[3], J. A. T. Smellie[4]
[1]INTERRA/ECL, Leicestershire, UK
[2]NAGRA, Baden, Switzerland
[3]Battelle, Chicago
[4]Conterra AB, Uppsala

TR 90-25
Kinetics of UO_2(s) dissolution reducing conditions: numerical modelling
I. Puigdomenech[1], I. Casas[2], J. Bruno[3]
[1]Studsvik AB, Nyköping, Sweden
[2]Department of Chemical Engineering, E.T.S.E.I.B. (U.P.C.), Barcelona, Spain
[3]Department of Inorganic Chemistry, The Royal Institute of Technology, Stockholm, Sweden
May 1990

TR 90-26
The effect from the number of cells, pH and lanthanide concentration on the sorption of promethium on gramnegative bacterium (Shewanella Putrefaciens)
Karsten Pedersen[1], Yngve Albinsson[2]
[1]University of Göteborg, Department of General and Marine Microbiology, Gothenburg, Sweden
[2]Chalmers University of Technology, Department of Nuclear Chemistry, Gothenburg, Sweden
June 1990

TR 90-27
Isolation and characterization of humics from natural waters
B. Allard[1], I. Arsenie[1], H. Borén[1], J. Ephraim[1], G. Gårdhammar[2], C. Pettersson[1]
[1]Department of Water and Environmental Studies, Linköping University, Linköping, Sweden
[2]Department of Chemistry, Linköping University, Linköping, Sweden
May 1990

TR 90-28
Complex forming properties of natural organic acids. Part 2. Complexes with iron and calcium
James H. Ephraim[1], Andrew S. Mathuthu[2], Jacob A. Marinsky[3]
[1]Department of Water in Environment and Society, Linköping University, Linköping, Sweden
[2]Chemistry department, University of Zimbabwe, Harare, Zimbabwe
[3]Chemistry Department, State University of New York at Buffalo, Buffalo, NY, USA
July 1990

TR 90-29
Characterization of humic substances from deep groundwaters in granitic bedrock in Sweden
C. Pettersson, J. Ephraim, B. Allard, H. Borén
Department of Water and Environmental Studies, Linköping University, Linköping, Sweden
June 1990

TR 90-30
The earthquakes of the Baltic shield
Ragnar Slunga
Swedish National Defence Research Institute
June 1990

TR 90-31
Near-field performance of the advanced cold process canister
Lars Werme
Swedish Nuclear Fuel and Waste Management Co (SKB)
September 1990

TR 90-32
Radioclide transport paths in the nearfield – a KBS-3 concept study
Roland Pusch
Clay Technology AB and Lund University of Technology
July 1990

TR 90-33
PLAN 90
Costs for management of the radioactive waste from nuclear power production
Swedish Nuclear Fuel and Waste Management Co (SKB)
June 1990

TR 90-34
GEOTAB: User's guide – Version 1.8.2
Ergodata
October 1990

TR 90-35
Dose conversion factors for major nuclides within high level waste
Ulla Bergström, Sture Nordlinder
Studsvik Nuclear
November 1990

TR 90-36
Sensitivity analysis of groundwater flow Licentiate thesis
Yung-Bing Bao
Royal Institute of Technology, Department of Land and Water Resources, Stockholm, Sweden
December 1990

TR 30-37
The influence of fracture mineral/ groundwater interaction on the mobility of U, Th, REE and other trace elements
Ove Landström[1], Eva-Lena Tullborg[2]
[1]Studsvik AB, Nyköping
[2]SGAB, Gothenburg
December 1990

TR 90-38
Solute transport in fractured rock – Applications to radionuclide waste repositories
Ivars Neretnieks
Department of Chemical Engineering,
Royal Institute of Technology, Stockholm
December 1990

TR 90-39
Modelling of the movement of the redox front in the uranium mine in Poços de Caldas, Brazil
Leonardo Romero, Luis Moreno, Ivars Neretnieks
Royal Institute of Technology, Stockholm
June 1990